UNIVERSITY OF CALIFORNIA, SAN DIEGO

Functional and Structural Study of Vpu from HIV-1 by Nuclear Magnetic Resonance Spectroscopy

A dissertation submitted in partial satisfaction of the
requirements for the degree Doctor of Philosophy

in

Chemistry

By

Hua Zhang

Committee in Charge:

Professor Stanley J. Opella, Chair
Professor Seth M. Cohen
Professor John C. Guatelli
Professor Akif Tezcan
Professor Elizabeth Villa

2015

The Dissertation of Hua Zhang is approved, and it is acceptable in quality and form for publication on microfilm and electronically:

_____

_____

_____

_____

_____

Chair

University of California, San Diego

2015

DEDICATION

For my parents, Min Zhang and Zheming Tang

without them, I will not be here.

TABLE OF CONTENTS

LIST OF ABBREVIATIONS

^{1}H	Proton
^{13}C	Carbon - 13
^{15}N	Nitrogen – 15
AMS	Ammonium sulfate
BST2	Bone marrow stromal antigen 2
CCR7	C-C chemokine receptor type 7
CD4	*Cluster of differentiation 4*
CNBr	Cyanogen bromide
CP	cross-polarization
CSA	Chemical shift anisotropy
CSI	Chemical shift index
CXCR1	C-X-C chemokine receptor type 1
Cyto	Cytoplasmic
Da	Dalton
DCP	double-cross-polarization
DEC	Decoupling
DHPC	1,2-dihexanoyl-*sn*-glycero-3-phosphocholine
DMEPC	1,2-dimyristoyl-sn-glycero-3-ethylphosphocholine
DMPC	1,2-dimyristoyl-sn-glycero-3-phosphocholine
DMTAP	1,2-dimyristoyl-3-trimethylammonium-propane
DPC	Dodecylphosphocholine

DTT	Dithiothreitol
DNA	deoxyribonucleic acid
EDTA	Ethylenediamine tetracetic acid
ER	Endoplasmic reticulum
gp120	Envelope glycoprotein GP120
gp160	Envelope glycoprotein GP160
GPCR	G-protein coupled receptor
HETCOR	Heteronuclear correlation
HEPES	4-(2-hydroxyethyl)-1-piperazineethanesulfonic acid
HFIP	1,1,1,3,3,3-Hexafluoro-2-propanol
HIV-1	*Human immunodeficiency virus, type 1*
HIV-2	*Human immunodeficiency virus, type 2*
INEPT	Insensitive Nuclei Enhanced by Polarization Transfer
IPAP	In-phase/anti-phase
IPTG	Isopropyl □-thiogalactoside
KSI	Ketosteroid isomerase
LB	Luria-Bertani
LG	Lee-Goldberg
LP	Linear prediction
MAS	Magic-angle-spinning
MTSL	S-(2,2,5,5-tetramethyl-2,5-dihydro-1H-pyrrol-3-1)methyl methansulfonthiate
NCACX	^{15}N chemical shift / ^{13}Ca chemical shift / ^{13}C chemical shift

NCOCX	^{15}N chemical shift / ^{13}CO chemical shift / ^{13}C chemical shift
NK-cell	Natural killer cell
NKG2D	Natural killer group 2, member D
NMR	Nuclear magnetic resonance
NOE	Nuclear overhauser effect
NTB-A	NK-cell, T-cell and B-cell antigen
OS	Oriented sample
PDB	Protein data bank
PDSD	proton-driven spin diffusion
PRE	paramagnetic relaxation enhancement
RA	Rotationally aligned
SDS	Sodium dodecyl sulfate
SDS-PAGE	Sodium dodecyl sulfate-polyacrylamide gel electrophoresis
RDC	Residual dipolar coupling
RMSD	Root mean squared deviation
RF	Radiofrequency
S/N	Signal-to-noise
SLF	Separated-local-field
SPINAL-16	small phase incremental alternation, with 16 steps
t1	Incremented time interval in a two-dimensional experiment
t2	Signal acquisition interval in a two-dimensional experiment
TFE	2,2,2-Trifluoroethanol
TGN	trans-Golgi network

TM	Transmembrane
TOCSY	Total correlation spectroscopy
TROSY	Transverse relaxation optimized spectroscopy
Vpu	Viral protein U

LIST OF FIGURES

LIST OF TABLES

ACKNOWLEDGEMENTS

First and foremost, I would like to thank my thesis advisor, Prof. Stanley Opella. I have very little knowledge of biochemistry, structural biology, and NMR when I joined the lab; however, he gave me the opportunity to learn a variety of new techniques and conduct exciting research in his laboratory. None of my thesis work would be possible without his guidance, and more importantly, he always tell me to keep optimistic. I also would like to thank the other members of my thesis committee, Prof. Seth M. Cohen, Prof. John Guatelli, Prof. Akif Tezcan, and Prof. Elizabeth Villa.

Many thanks are given to Dr. Yan Wang for teaching me all the biochemical and NMR techniques, and leading me to the Vpu project when I first joined the group. Special thanks are given to Dr. Eugene Lin for giving me endless support both professionally and personally. We joined the Opella lab at same time, and work together on the very challenging Vpu project during the last few years of our PhD periods. I would also like to thank Dr. Sang Ho Park, who shares his experience with me and provides me with stimulating discussion to help solving tremendous problems. Acknowledgments must be given to other members who have worked on Vpu project, and they are Dr. Leon Cheung and undergraduate research assistants Christa Lam, Da Shi and Willi Cheung. I would also like to thank Dr. Ye Tian for helping on structure calculation and docking. In addition, I would also like to give many thanks to present and past members of the Opella research group. They are Dr. Gabriel Cook, Dr. Henry Nothnagel, Dr. Fabio Casagrande, Dr. Dongtao Cui, Dr. Anna De Angelis, Dr. Andreea-Cristina Balaceanu, Dr. Hanna Pavlova, Dr. Ratan Rai, Lindsay Dawson, Sabrina Berkamp, Mignon Chu, Jasmina Radoicic, Zheng Long, Vivan Wang, Mitchell Zhao and Leah Cho.

Many thanks must be given to Dr. Xuemei Huang and Dr. Anthony Mrse who gave me training on solution NMR spectroscopy. Additional thanks are given to Dr. Chin Wu, Dr. Chris Grant, and Dr. Yuan Yang who taught me a tremendous amount of knowledge of solid-state NMR spectroscopy. Special thanks are given to Dr. Bibhuti Das for sharing with me expertise of solid-state NMR spectroscopy and working on VpuTM together.

I would like to thank Prof. John Guatelli, Dr. Mary K. Lewinski and Moein Jafari, at UCSD School of Medicine for the collaboration on Vpu-BST2 project. I would also like to thank Prof. Edward Barker and Dr. Bharatwaj Sowrirajan in Department of Immunology- Microbiology at Rush University for the collaboration on Vpu-NTB-A project. By discussing with them, I gained tremendous biological knowledge.

In addition, I am very grateful to my undergraduate research advisor Prof. Vivian Wing-Wah Yam at University of Hong Kong. She is always my example as a female scientist.

Chapter 2, in full, is currently being prepared for submission for publication of the material. Zhang, H., Lin, E. C., Tian, Y., Das, B. B., and Opella, S. J. The dissertation author was the primary investigator and author of this material.

Chapter 3, in full, is a reprint of the material as it appears in the Journal of Biological Chemistry 2015. Lewinski, M. K., Jafari, M., Zhang, H., Opella, S. J., and Guatelli, J. The dissertation author was the co-first author of this paper.

VITA

2008 Bachelor of Science, University of Hong Kong, Hong Kong

2015 Doctor of Philosophy, University of California, San Diego

PUBLICATIONS

M. K. Lewinski*, M. Jafari*, **H. Zhang***, S. J. Opella, J. Guatelli, Membrane Anchoring by a C-terminal Tryptophan Enables HIV-1 Vpu to Displace BST2 from Sites of Viral Assembly, J. Bio. Chem., 290 (2015) 10919-10933. * Contributed Equally

B. B. Das, **H. Zhang**, S. J. Opella, Dipolar assisted asignment protocol (DAAP) for MAS sold-state NMR of rotationally aligned membrane proteins in phospholipid bilayers, J. Magn. Reson., 242 (2014) 224-232.

W. S. Son, S. H. Park, H. J. Nothnagel, G. J. Lu, Y. Wang, **H. Zhang**, G. A. Cook, S. C. Howell, S. J. Opella, 'q-titration' of long-chain and short- chain lipids differentiates between structured and mobile residues of membrane proteins studied in bicelles by solution NMR spectroscopy, J. Magn. Reson., 214 (2012) 111-118.

G. A. Cook, **H. Zhang**, S. H. Park, Y. Wang, S. J. Opella, Comparative NMR studies demonstrate profound differences between two viroporins: p7 of HCV and Vpu of HIV-1, Biochimica Et Biophysica Acta-Biomembranes, 1808 (2011) 554-560.

ABSTRACT OF THE DISSERTATION

Functional and Structural Study of Vpu from HIV-1

by Nuclear Magnetic Resonance Spectroscopy

by

Hua Zhang

Doctor of Philosophy in Chemistry

University of California, San Diego, 2015

Professor Stanley J. Opella, Chair

Viral protein U (Vpu) is an 81-residue membrane protein encoded by HIV-1. It has two distinct domains, a hydrophobic transmembrane domain, which has been well studied, and a cytoplasmic helical domain with two conserved phosphorylation sites, which has proven to be more difficult to study in large part because of its dynamics. The two domains are associated with different biological activities that contribute to the pathogenicity of HIV-1 infections in humans. Vpu removes CD4 receptor from ER and causes its subsequent degradation to enhance viral infectivity. Vpu enhances release of newly formed virus particles from infected cells by antagonize human immune restriction factor BST-2. Recently, Vpu has also been discovered to interact with NK cell receptor NK-cell, T-cell

and B-cell antigen (NTB-A) to induce down-modulation of NTB-A, and prevent HIV-Infected cells from degranulation and lysis by NK cells.

A combination of solution and solid-state NMR experiments are used to determine the structure of cytoplasmic domain (VpuCyto) and full-length of Vpu in micelles and liposomes environment. Both constructs have a U-shape cytoplasmic domain that associated with the lipid environment. The second section describes the membrane anchoring property of W76 in the C-terminus of Vpu. Biological study found that W76 is specifically important for the enhancement of virion release, and NMR data suggests that W76 might function by interacting directly with the lipid bilayer. Significant intensity change and chemical shift perturbation were observed for W76 upon addition of liposomes to VpuCyto; in addition, paramagnetic relaxation enhancement (PRE) indicates that the residue is embedded in the interior of micelles. The last section describes the interaction between transmembrane domains of Vpu and NTB-A base on a combination of biological, NMR spectroscopic and computational methods. The knowledge about the transmembrane domain of Vpu (VpuTM) enables detailed studies of its interactions with NTB-A. NMR spectral changes demonstrate that specific residues in VpuTM interact with specific residues in the transmembrane domains of NTB-A. A model of the complex is generated by docking, with the input of interaction faces base on NMR and biological results.

Chapter 1 General Introduction

1.1 Introduction to membrane proteins

Approximately 30% of the expressed genes in prokaryotic and eukaryotic genomes encode membrane proteins (1) (1,2), which are involved in a wide range of critical biological functions such as transport, signal transduction, metabolism, enzyme catalysis, etc. The mutation or abnormal expression of MPs that lead to misfolding, conformational change and dysfunction can cause a variety of diseases including cancer, heart disease, Alzheimer's disease, etc (3-6). Therefore, MPs are highly desirable drug targets, and 60% of drugs in current pharmaceutical industry already target membrane proteins, where G protein-coupled receptors (GPCR) and ion channels form the two major groups of drug targets(5,7). To better understand the functions of MPs, knowledge about the structures, molecular dynamics and environments need to be carefully investigated, and these three key factors are mutually dependent and jointly dictate the functions of MPs.

Two prominent structural architectures of MPs are helix bundles and β-barrels. Helical membrane proteins, containing 1 to 20 transmembrane domains (TMD), are more ubiquitous and represent 70-85% of all MPs. β-barrel MPs are mainly found in bacteria.

1.2 Structural biology of Membrane Proteins

Despite the importance of MPs, structural characterization of MPs still remains a big challenge, and MP structures at atomic resolution only account for around 1% of the total number of structures deposited in the Protein Data Bank (PDB). The difficulties of

MP characterization result from protein engineering, protein reconstitution, instrumentation for data collection and methods for data processing and analysis.

Firstly, the expression and purification of sufficient amount of MPs for structural studies are not as straightforward as that of soluble proteins. Decade back, MPs for structural study were mainly obtained from endogenous sources, and were highly limited to proteins with abundant copies in the cells. With the advent of recombinant DNA technology, heterologous expression of MPs in *E. coli* has become the most widely used expression system due to simple techniques, high efficiency and inexpensive cost (8). During expression, the hydrophobic MPs tend to insert into cell membranes and hamper cell growth; thus, many strategies were designed to circumvent this obstacle and maximize yield of MPs. *E. coli* C41 (DE3) and C43 (DE3) strains with higher cytotoxic tolerance were developed for MPs over-expression (9). An alternative approach relies on a fusion partner expressed together with the MP, which forms inclusion bodies to prevent the insertion into cell membrane and enable cell growth. As a prokaryotic expression system, *E. coli* system has always been critiqued as lacking proper lipids, folding chaperons and/or post-translational modifications to enable proper folding of eukaryotic MPs, and alternatives as yeast (10), insect (11), mammalian cells (12), and the *in vitro* cell free (CF) system (13)have been be used to produce well behaved MPs as well. One of them to be highlighted here is the CF expressing system, not only because it allows the addition of complex eukaryotic protein synthesis machinery into extracts from E. coli or wheat germ to facilitate posttranslational modifications such as glycosylation, it can also directly incorporate de novo synthesized membrane protein into the native lipid bilayer like environment such as nanodiscs or even biological membranes (14,15). Importantly, all

occur in a cell independent micro system where no cytotoxicity problem occurs, and much simpler purification process is needed. In addition to the optimized system for protein production, the appropriate membrane environment to correctly fold MPs is critical for the structure and function of MPs. The activity of MPs is dependent on a variety of factors including lipid composition, fluidity, membrane curvature, pH, temperature, etc. In order to provide a biologically relevant membrane environment, scientists have built a number of lipid models including micelles, lipid cubic phase (LCP), bicelles (1,16,17), nanodiscs (18), liposomes (19,20), etc.

Besides the sample preparation, developments in biophysical techniques for MPs structure determination are also crucial for tackling the challenges. X-ray crystallography, electron microscopic (EM) and nuclear magnetic resonance (NMR) spectroscopy have been the three major techniques for solving the structure of MPs.

X-ray crystallography requires high-quality crystals of MPs to get strong diffraction patterns for analysis; however, crystallization of MPs remains a significant obstruction due to 1) the hydrophobic nature of MPs which requires detergent or lipids for solubilization 2) the flexible nature of terminal region and loops hinders the formation of well-ordered 3D crystals; and 3) the dynamic properties of MPs which favors more than one conformation. To overcome each obstacle of crystallization, crystallographers developed the lipid cubic phase (LCP) (21), and many chemically synthesized detergents (22) to facilitate MPs solubilization and crystallization in a lipid environment. In addition, sequence modifications including mutations, deletion of flexible regions and insertion of stable and crystallizable fusion partner (1,23,24) are frequently used to improve the thermal stability and packing of protein to get good crystals. Furthermore, agonists (25) or

nanobodies (26) have been added to lock MPs into one stable conformation that favors crystallization. The development of synchrotron beamlines exemplified as microfocus beamlines, serial femtosecond crystallography (SFX) (27) using X-ray free-electron laser (XFEL) radiation (27), etc. enabled data collection with crystals with lower criteria. Despite the difficulties, X-ray crystallography is still the method to solve the most MPs structures due to the advantages including the mature methodology, high resolution, and convenient accessibility

Electron microscopic (EM) only requires two-dimensional (2D) crystals, and allows studying MPs in large complexes; however, so far the best structure resolution obtained from 2D crystals is about ~4 Å (28).

However, both X-ray crystallography and EM require preparation of the sample in a cryogenic environment, and lack the ability to study MPs structure and dynamics in their native lipid bilayer environment. On the other hand, NMR spectroscopy is a complementary technique to X-ray crystallography and cryo-EM; it not only provides structure information but also dynamics characterization of MPs in native lipid bilayer environments with or without their interaction partners. Moreover, recent strategies in protein labeling schemes (29-32), and the development of new pulse sequences in both solution (33,34) and solid-state NMR (35,36) have overcome the size limit obstacle to facilitate MPs study in lipid environments.

1.3 NMR can characterize membrane proteins in various lipid environments

In 1973, Singer and Nicolson proposed the “fluid mosaic model” (37) of cell membranes, a lipid bilayer environment in which MPs are embedded and function with

motions. Therefore, it is important to mimic biological membranes for structural and functional study of MPs. In order to do that, many parameters need to be adjusted including lipid composition, phase, fluidity, curvature, charge, etc. Membrane models as micelles, isotropic bicelles, nanodiscs and liposomes have been widely applied in NMR spectroscopy to study MPs.

For Solution NMR spectroscopy, resonance linewidth is inversely proportionate to the tumbling rate and the size of the complex under investigation. So it is essential to incorporate MPs in a hydrophobic membrane mimic environment to maintain correct folding, while keeping the total complex small in size to yield well-resolved spectra. The most commonly used system for solution NMR study of MPs is the isotropic detergent forming micelle, which is a compromise between the need for a hydrophobic environment and fast tumbling rate. To obtain the optimized MP behavior for solution NMR, screening of detergents and conditions is required, and the most extensively used detergents are sodium dodecyl sulfate (SDS), n-dodecylphosphocholine (DPC) and short-chain phosphatidylcholines (C_6- or C_7-DHPC) with double acyl chains and phosphatidyl choline head group that is the closest mimic to biological phospholipids. Bicelles, a lipid bilayer disc, formed by the mixture of long chain lipids like 1,2-dimyristoyl-sn-glycero-3-phosphocholine (DMPC) and short chain lipid/ detergent such as DHPC in aqueous media, is an alternative membrane system used in NMR experiments. The size of the bicelle can be adjusted by changing the ratio of long chain lipid to short chain lipid/detergent, characterized as q value. Bicelles can vary in sizes from small discs with fast isotropic tumbling motion to large discs with anisotropic motion to allow MPs study by both solution NMR spectroscopy and solid-state NMR (16,38,39). Examples of MPs incorporated into

bicelles with fully functions have been shown. Nanodiscs, assembled by phospholipids wrapped by membrane scaffold protein (MSP) derived from human serum apolipoprotein, has emerged as a popular membrane mimicking system with the advantage of non-detergent characteristic(18). Detergents are known to interfere with the folding of MPs especially the extra cellular domains. The major drawback of using nanodiscs for solution NMR spectroscopy is the relatively large size (8 nm diameter) resulting in the slow reorientation time. Recently, the development of truncated MSP enabled the formation of nanodiscs with reduced size (4 nm diameter), which favors the study of MPs in solution NMR (40).

Solid-state NMR allows studying MPs in their native phospholipid bilayer environment, since the resonance linewidth is not affected by the increasing molecular size. Structural study of MPs by solid state NMR is usually accomplished by two methods, either the orientated sample (OS) NMR with uniaxial alignment of the protein-containing bicelle sample (41,42) or magic angle spinning (3) NMR of unoriented proteoliposome sample (36,43,44).

When q =3.2, bicelles will self-assemble and align the bilayer normal perpendicular to the external magnetic field. On the other hand, proteoliposome, formed by reconstitution of MPs with phospholipid bilayers (liposomes) directly is one of the closest bilayer systems to biological membrane. To make proteoliposomes, MPs and designated lipids are mixed together with either organic solvents or detergents. Organic solvents are usually removed under nitrogen gas followed by lyophilization. The dried protein-lipid films are then rehydrated. The sizes of proteoliposomes are manipulated by extrusion through membranes with different pore size or sonication. For the detergent methods, proteoliposomes are

formed upon removal of detergent either by dialysis or addition of bio-beads. To obtain concentrated liposomes for NMR spectroscopy, samples are usually spun down by ultracentrifugation. Notify that for both protein containing bicelles and proteoliposomes, a broad spectrum of lipids with different chain lengths and head groups, or even cholesterol can be incorporated. Additionally, pH, charge and hydration levels can be readily mediated to make the bilayer system more physiological.

1.4 Structural and dynamics study of membrane proteins by solution NMR

NMR spectroscopy requires ^{15}N and/or ^{13}C isotopic labeling of MPs to perform multi-dimensional experiments, ^{2}H perdeuteration, and selective labeling to obtain spectra with better resolution. Once the isotopically labeled protein is purified and incorporated into the micelles or bicelles, a ^{1}H-^{15}N heteronuclear single quantum correlation (HSQC) solution NMR spectrum is acquired to determine if the sample is homogeneous and well behaved. For protein complexes with larger sizes (>20kDa), transverse relaxation optimized spectroscopy (TROSY)-based HSQC is an alternative starting point (45). Each resonance peak on the 2D HSQC spectrum corresponds to a backbone amide site in the protein, and can be assigned with a series of triple resonance “backbone walk” 3D experiments such as HNCA, HN(CO)CA, HNCACB, HN(CO)CACB, etc. In addition to the backbone resonances, side-chain resonances are also important in protein structure characterization and dynamics study, and can be measured and assigned with 3D experiments as HCCCONH, CCCONH, TOCSYHSQC, etc.

A variety of NMR experiments can be applied to determine the secondary structure of the protein including chemical shift index (CSI) plot (46), deuterium/hydrogen

experiments, and residual dipolar coupling (RDC) measurements (47). The chemical shift is dependent on the local electrochemical environment, and as a result, is highly influenced by the secondary structure of the site. CSI, chemical shift deviations from random coil values of amino acid residues at $^{13}C'$, ^{13}Ca, ^{1}Ha, are indicative of the (47) secondary structure of the site, and can be used empirically to estimate phi and psi angles of the peptide plane. H/D exchange experiments provide insight into the topology of the membrane proteins, for the residues in the structured and membrane embedded region exchange slower than those exposed in loop regions (48). Similarly, resonance intensity plots are effective method of providing dynamics information. With decreasing tumbling time of the site, the linewidth of resonances are broadened, resulting in decreasing in the peak intensity. As a result, residues in mobile region tend to have stronger peaks than those in the structured regions. Furthermore, Heteronuclear ^{1}H-^{15}N NOE measurements alone can probe the backbone dynamics by identifying the structured region and the mobile region (49). Since dynamics and motion are correlated with structure; with measurement of amide ^{15}N spin lattice relaxation (T_1), spin spin relaxation (T_2), NOE, and the subsequent calculation of order parameter base on modelfree formalism provides a reliable guide to backbone internal motion in fast time scale (ps-ns) and secondary structure

Using chemical shifts of CO, CA, CB, HA and HN site, backbone torsional angles can be predicted through programs as TALOS+ (50), and along with backbone dynamics data, an initial model of protein structure can be calculated based on programs such as Xplor-NIH (51,52) or CS-Rosetta (53). To further refine the structure to atomic resolution, additional angular restraints and distance restraints need to be incorporated.

Structure determination of globular protein by NMR spectroscopy used to rely on distance restraints obtained from inter proton NOEs observed in multidimensional spectra. However, for most MPs incorporated in micelles, the chemical shift spread for protons is small, and it is almost impossible to assign different protons unambiguously. Furthermore, to avoid homonuclear dipolar coupling between protons resulting in fast T_2 relaxation and broad linewidth, many MPs samples are perdeuterated and as a result lack NOEs. In order to overcome these problems, paramagnetic relaxation enhancement (PRE), which depends on the dipolar coupling between unpaired electron and nucleus, can be measured and converted to distance restraints, and serves as an alternative source of long-range distance restraints (54,55). The magnitude of PRE is proportional to inverse six order of distance between the electron and nucleus, which is similar to NOE effect. However, it significantly extends the distance range from 6Å based on NOE to 30Å, due to the large magnetic moment of electrons. To introduce a paramagnetic probe with unpaired electron to MPs for PRE measurements, residue of interest is mutated to cysteine by site-directed mutagenesis, followed by covalent attachment of spin label containing paramagnetic reagent such as S-(1-oxyl-2,2,5,5-tetramethyl-2,5-dihydro-1H-pyrrol-3-yl)methyl methanesulfonothioate (MTSL) or N-[S-(2-pyridylthio)cysteaminyl]EDTA-metal. The PRE effect can be easily measured by acquiring HSQC spectra of paramagnetic labeled sample and the reduced sample or corresponding diamagnetic labeled sample, followed by comparing the intensity changes of resonances. The intensity change can be further correlated to distance between the resonance residue and the paramagnetic center (56).

In addition to distance restraints, measurements of residue dipolar couplings (RDCs) provide orientation restraints for structural calculations (57). Dipolar coupling

between two spins is dependent on the vector connecting the two spins with respect to external magnetic field. Normally in solution NMR, dipolar couplings are averaged to zero due to the fast molecular reorientation rate; however, when molecules are incorporated into weakly aligned environment in which their tumbling are partially restricted, the orientation dependent dipolar couplings can be reintroduced. The resulting non zero value for dipolar coupling are named RDC, and can be measured for structure determination. There are multiple detergent resistant weakly aligned media suited for MPs as intact bacteriophage (58), stretched or compressed polyacrylamide gels (59,60), DNA nanotubes (61), lanthanide ions (62), bicelles (63), etc. Besides providing angular information, plot of RDC value with respect to residue number generates sinusoidal dipolar waves in the helical structured regions. And residues in the highly mobile region usually yield negligible RDC values.

1.5 Structural and dynamics study of membrane proteins by solid-state NMR

Although solution experiments give valuable information of MPs in micelles, bicelles and nanodiscs, in order to study the MPs in lipid bilayers, which is a more biologically relevant environment, solid-state NMR techniques are employed to study the structure of MPs. For OS NMR, MPs are incorporated into bicelles, which align in the magnetic field so that the bilayer normal is perpendicular to the external magnetic field. For protein incorporated in bicelles, good ^{1}H decoupled ^{15}N 1D spectra showed that proteins are uniaxially oriented and undergo rotational diffusion with respect to bilayer normal (42). Separate-local-field (SLF) experiments provide the angular-dependent measurements of dipolar couplings and chemical shift anisotropies (CSAs), which can be

converted to structural restraints. To complement the OS NMR and alleviate resolution problems caused from the homonuclear coupling in solid state, novel magic angel spinning (3) experiment schemes called the rotational aligned approach are being implemented to study MPs incorporated into unoriented liposomes (36,64). When temperature is low, MPs are rigid in the liposome, and a full powder pattern is observed for both dipolar coupling and chemical shift due to the anisotropy of the sample (Figure 1.1). However, when the temperature is above the transition temperature of lipid, MPs are undergoing fast rotational diffusion along bilayer normal, and the motion has an orientation dependent effect on the powder pattern, which can be extracted and converted to orientation restraints (65-67) (Figure 1.1). With MAS experiments, ^{15}N, ^{13}C anisotropic chemical shift, ^{1}H-^{15}N, ^{1}H-^{13}C dipolar couplings, as well as ^{15}N, ^{13}C isotropic chemical shift can be measured and translated to structural restraints. Moreover, experiment based on J coupling transfer enables seeing the mobile regions of MPs, which were invisible in conventional ssNMR experiments, and provides dynamics information of MPs in liposomes.

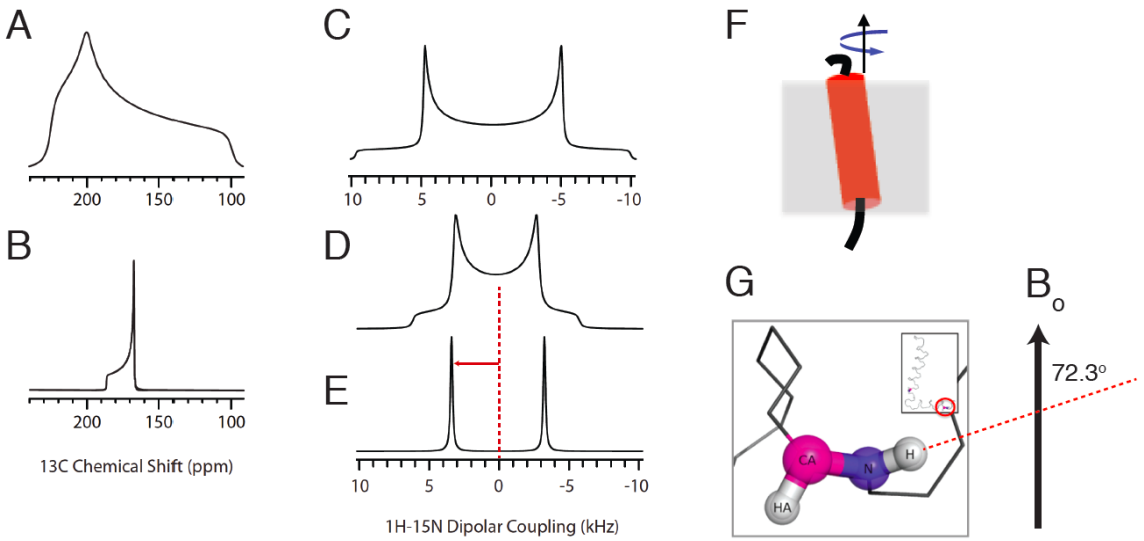

Figure 1.1 Rotational diffusion has an orientation dependent effect on the powder patterns.

A, ^{13}C Chemical shift powder pattern on C' site when protein is rigid. B, Reduced ^{13}C Chemical shift powder pattern on C' site when protein is undergoing fast rotational diffusion. C, ^{1}H-^{15}N dipolar coupling powder pattern when protein is rigid. D, Reduced ^{1}H-^{15}N dipolar coupling powder pattern when protein is undergoing fast rotational diffusion. E, Parallel edge extracted from D. F, Cartoon representation of a helix undergoing fast rotational diffusion in lipid bilayers. G, A residue in helix showing 72.3° amide vector with respect to external magnetic field.

1.6 NMR studies of protein interactions

Interactions of MPs with ligands, which can be small molecules or macromolecules, are crucial for many biological functions. One major advantage of NMR is to study MPs interactions in a dynamic membrane mimic environment at molecular level, even if the interactions are weak. The simplest method is to measure chemical shift perturbations induced by addition of unlabeled ligand to ^{15}N labeled protein (68,69). If protein-protein interaction is being studied, then each protein can be labeled individually, giving information about both interaction partners. Binding site can be readily determined since peaks corresponding to residues directly involved in binding have more significant chemical shift change due to a change in local conformation and environment. The gradual

change can be traced by titration of ligand into the protein, and the dissociation constant can be fitted.

In addition, both NOE and PRE experiments can be applied to elucidate protein interactions, since they measure inter spin distances. PRE is particularly suited for interaction study since it covers a wider distance up to ~30Å, and is applied to reveal protein-protein (70), protein-nucleic interaction (71).

Saturation transfer difference (STD) experiment is able to investigate interaction between ligands and macromolecule at large size (72). The STD experiment is carried out on mixture of macromolecules and ligands. Signals of macromolecules are saturated by selective irradiation of a spectrum region that contains only signals from macromolecules. When a ligand is bound to the macromolecule, saturation effect transfer from macromolecule to the ligand through NOE, and as a result, signal reduction can be detected on the ligand, especially on the binding site. The advantages of STD experiment are 1) it is very sensitive, and only requires low concentration of macromolecules 2) it is fast 1D experiment and can be applied to high throughput screening experiments(73).

1.7 Vpu is a small viroproin with multiple biological functions

The virus protein U (Vpu) is a type 1 integral membrane protein encoded by one of the accessory genes of human immunodeficiency virus type 1 (HIV-1) (74-76). It has also been found in a subset of simian immunodeficiency viruses (SIVs) (77,78), but is not detected in HIV-2. Vpu protein, contains approximately 80 amino acids, has a short N-terminal luminal tail, a single α□helix transmembrane (TM) domain (~20 amino acids) and an amphipathic cytoplasmic (Cyto) domain. VpuCyto contains two α-helices connected by

a short loop where a highly conserved sequence DSGXXS is coded as phosphorylation sites (Figure 1.2)(79). Vpu is associated with down-modulation of several cellular proteins to contribute to the pathogenicity of HIV-1 infections in humans (Figure 1.3).

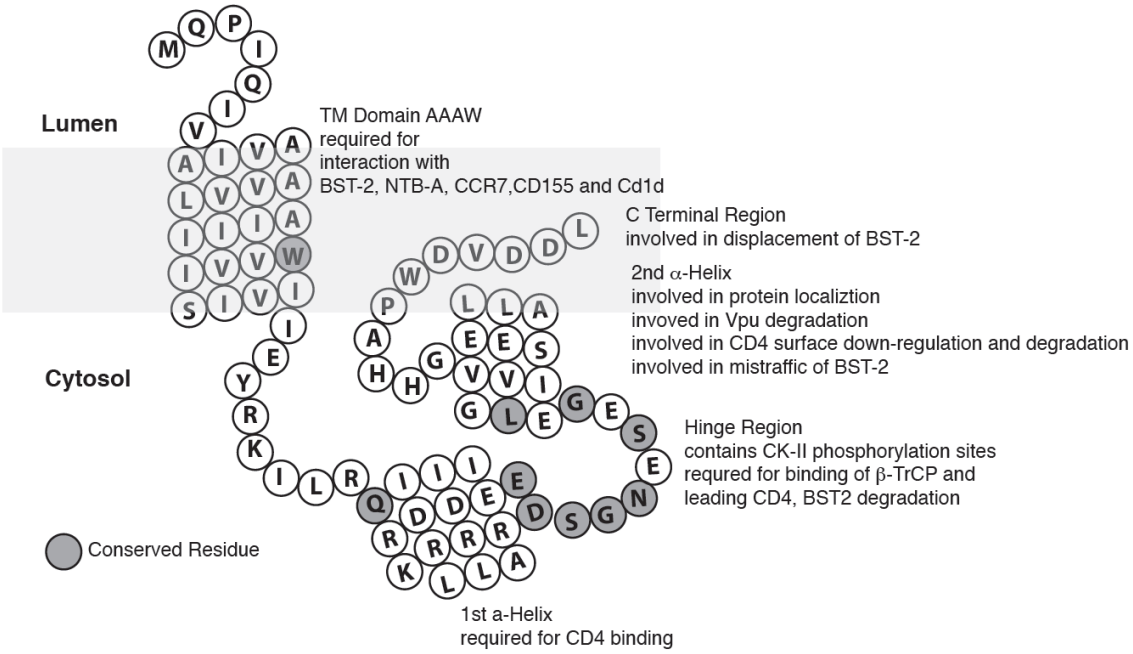

Figure 1.2 Schematic diagram of subtype B, strain NL4-3 Vpu in membrane bilayers (80).

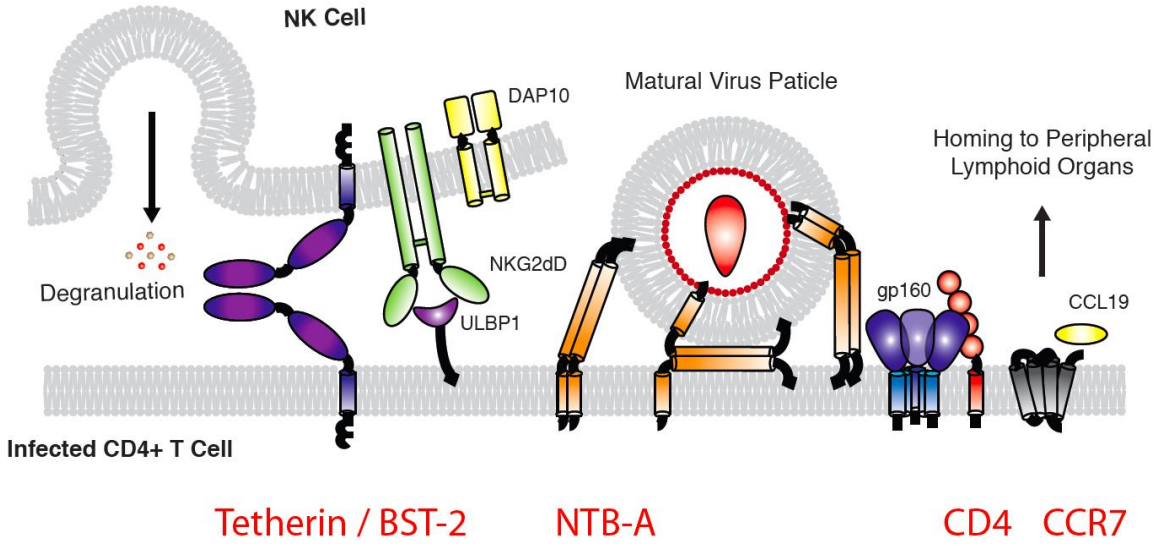

Figure 1.3 Vpu downmodulates and degrades several host cell proteins (81).

One of the major functions of Vpu is to down-regulate CD4 (82). Although CD4 acts as the host cell receptor during virus entry, the presence of CD4 on the cell surface disturbs virion release and decreases viral infectivity through binding to viral envelope (Env) precursor gp160 and subsequently interfering packaging of Env into virions (83-85). In addition, down-regulation of CD4 prevents superinfection, which can lead to apoptosis(86). Vpu induces CD4 degradation by retaining the newly synthesized CD4 in the endoplasmic reticulum (ER), and subsequently targeting CD4 to the ER- associated protein degradation (EARD)-pathway(87). In this process Vpu acts as a molecular adaptor; it first binds CD4 through its first □-helix within Cyto and then recuirts β-TrCP through phosphoserines in the loop of VpuCyto, linking CD4 to β-TrCP /SCF E3 ubiquitin ligase complex for degradation (88-90).

Secondly, Vpu enhances HIV-1 virion release by antagonizing the restriction factor BST-2/CD317 (also known as tetherin), which counteracts HIV viruses by tethering newly

formed viral particles to the infected cell surface and preventing their release(91,92). The underline mechanism of how Vpu disables BST-2 function is still under investigation. Vpu and BST-2 were found to interact within the trans-Golgi network (TGN) and endosomes, mainly through the TM region of both proteins, and this interaction is dependent on the A10, A14, A18 and W22 helix face in Vpu TM (90,93,94). The direct interaction between Vpu and BST-2 enables Vpu to downregulate BST-2 from cell surface and cause BST-2 degradation through the β-TrCP dependent pathway (95,96); however, both surface downregulation and degradation seems to be dispensable for the ability of Vpu to enhance virus release. Researchers has shown that Vpu displaces BST-2 from the virion assembly site, and mapped the phenotype to the C-terminal domain of VpuCyto, especially the W76 reside(97,98). The mutation of Vpu W76G severely impairs antagonizing effect of Vpu to BST-2, and is believed to account for the ability of Vpu to enhance virus release.

Recently Vpu has also been discovered to downmodulate the surface expression of the natural killer (7) cell receptor NK, T-cell, B-cell antigen (NTB-A) and to prevent HIV-Infected cells from degranulation and lysis by NK cells(99). The interaction of Vpu and NTB-A has also been mapped to the TM domains of both protein, and the same A10, A14, A18 and W22 helix face is associated in the interaction. In addition to downmodulation of NTB-A, Vpu also downmodulates CD1d from cell surface to evade CD1d-restricted NK cell responses(100). Neither downregulation of NTB-A nor CD1d rely on the β-TrCP dependent degradation pathway, but rather interfere with intercellular trafficking of the proteins(99,100).

Vpu also downregulates the chemokine receptor CCR7 from the cell surface, and subsequently disables the migration of $CD4^+$ T cells into the lymph noes, where the

triggering ligands of CCR7, CCL19 and CCL21, are present(101). As a result, it disables the activation of immune responses. In addition Vpu induces downregulation of CD155, a ligand for the DNAM-1 activating receptor of NK cell and CD8+ T cells from cell surface, and to help infected cells to evade NK cell mediated immune response(102). Both downmodulation of CCR7 and CD155 is associated with A10, A14 and A18 in the TM domain of Vpu. And neither of them involves degradation (101,102).

Chapter 2 Structural determination of Vpu from HIV-1 by NMR in membrane environments

2.1 Abstract

Viral protein U (Vpu) from HIV-1, a small membrane protein composed of an α-helix in the transmembrane domain and two α-helices in the amphipathic cytoplasmic domain, downmodulates several cellular proteins, including CD4, BST-2/CD317/tetherin, NTB-A, and CCR7. It interferes with the immune system, and enhances viral release. It is essential to characterize the structure and dynamics of Vpu in order to understand the mechanisms of protein-protein interactions, and potentially to discover antiviral drugs. In this article, we describe the investigations of cytoplasmic domain of Vpu and full-length Vpu in several lipid environments by NMR spectroscopy. Results from constructs suggest that results from the two helices in the cytoplasmic domain form a U-shape, although the length of inter-helical loop in the cytoplasmic domain and the orientation of the third helix vary with the lipid composition. The C-terminal helix is relatively flexible and provides accessibility for potential interaction partners.

2.2 Introduction

Viral protein U (Vpu) is one of the "accessory" proteins encoded by HIV-1. Although it is dispensable for viral replication *in vitro*, it has multiple biological functions that are crucial for viral infectivity *in vivo (82,103,104).* Vpu removes newly synthesized CD4 receptors from the endoplasmic reticulum (ER), and causes their subsequent degradation. As a result, it prevents CD4 receptors from binding to the viral envelope (Env)

precursor gp160 enhancing viral infectivity. Vpu also enhances the release of newly formed virus particles by antagonizing the human immune restriction factor BST-2/CD317 (tetherin), which otherwise prevents their release (91,92,96). Recently Vpu has been shown to induce down modulation of natural killer (NK) cell receptor NK, T-cell, B-cell antigen (NTB-A) from the cell surface, and prevent HIV-Infected cells from degranulation and lysis by NK cells (99,105). Vpu also down regulates the chemokine receptor CCR7 from the cell surface, and subsequently reduces the ability of $CD4^+$ T cells to migrate into the lymph nodes, where it helps with priming and assembly of immune responses (101).

Vpu is a small 81-residue type I membrane protein that has two distinct domains, a hydrophobic transmembrane (TM) domain with helix-1 and an amphipathic cytoplasmic (Cyto) domain with helix-2 and helix-3. Loop-1 connects TM and Cyto domain and the loop-2 connects the two helices in the Cyto domain, and contains two conserved phosphorylation sites. These two domains are individually associated with biological activities mentioned above that contribute to the pathogenicity of HIV-1 infection. The structures and properties of three polypeptide constructs are discussed in the article: TM domain (residues 2-31) of Vpu (VpuTM), Cyto domain (residues 28-81) of Vpu (VpuCyto), and full-length Vpu (VpuFull) (residues 2-81).

The interactions of Vpu with BST-2, NTB-A and CCR7 have been mapped to the TM domains of each of the polypeptides. VpuTM is shown to employ the A10, A14, A18 and W22 helix face in its protein-protein interactions with both biological and spectroscopic studies (94,101,105). Also, the single site mutation W22L is shown to inhibit the ability of Vpu to down regulate CD4; however, sequence scrambling of the TM domain, including the change of the position of the Trp position didn’t appear to affect the Vpu-

induced CD4 down regulation (106). Helix-2 in Vpu, which is in the cytoplasmic domain is required for CD4 binding (88); the conserved DSGXXS phosphorylation site in loop-2, which connects helix-2 and helix-3, acts as a molecular adaptor to recruit β-TrCP, linking CD4 and/or BST-2 to the β-TrCP /SCF E3 ubiquitin ligase complex for degradation (96,103,107-112). The tryptophan in the C-terminal helix of VpuCyto has been identified as a key residue for virus release enhancement, primarily due to the ability of Vpu to displace BST-2 from the virus assembly site (97,98,113).

It is essential to mimic the properties of biological membranes for structural, dynamic and functional studies of membrane proteins. Micelles, isotropic bicelles, nanodiscs and liposomes have been widely applied in both solution NMR and solid-state NMR studies. The isotropic micelle is the most widely used lipid media for solution NMR, since it reorients fast enough to give narrow line widths and at the same time provide a hydrophobic interior environment to solubilize and stabilize the membrane proteins. On the one hand, large lipid vesicles, such as, proteoliposomes, are more closely mimic membrane bilayers. They have slow tumbling rates because of their overall size, and therefore, require the techniques of solid-state NMR in order to obtain high resolution spectra. In addition, all the lipid systems can be further modified by changing lipid composition; pH, charge and hydration levels can be readily adjusted to make the bilayer system more physiological.

Solution NMR is well established as a method to characterize the structures and dynamics of proteins. Isotropic chemical shifts provide the empirical torsional angle restraints for the structure refinements, and residual dipolar couplings (RDCs) are available from samples in weakly aligned media as angular restraints. Distance restraints can be

derived from homo-nuclear Overhauser effects (NOEs) and paramagnetic relaxation enhancements (PREs).PRE provides an alternative source of long-range distance restraints for structure determination of helical membrane protein, which usually lack "long-range" ^{1}H-^{1}H NOE in micelles environment. For PRE measurements, first a paramagnetic probe is incorporated into the protein. Then the coupling of the electron to the nuclear spins contributes to the relaxation of the nuclear spin, which is inversely proportional to the distance between the electron and nuclear spin. (1-oxyl-2,2,5,5-tetramethyl-3-pyrroline-3-methyl) methanesulfonate (MTSL) is a widely used nitroxide spin label. It is covalently attached to the thio group of cysteine residue in the protein. The dynamics of local motions (usually within the range from picosecond to nanosecond) can be monitored by T_1 and T_2 relaxation, and heteronuclear NOEs. Similarly, solid-state NMR can be applied to characterize structures of proteins with input of torsion angle restraints, angular restraints and distance restraints. In magic angle spinning (MAS) solid-state NMR, dipolar couplings are averaged when the samples are spinning at 54.7°, the magic angle, and as a result spectra with narrow resonance linewidths result. A complication is that MAS solid-state NMR requires recoupling pulse sequences to measure the dipolar couplings. The heteronuclear dipolar couplings measured from the unoriented proteins are uninformative, because the powder patterns and the bond lengths (amide bonds or C-H bond at Cα) are essentially identical for all sites. However, when the proteins are undergoing fast rotational diffusion about the bilayer normal, the tensors are partially averaged, resulting in "reduced powder patterns" (65,66,114), whose parallel edges reflect the magnitudes of the dipolar couplings. In order to measure the angular-dependent heteronuclear dipolar couplings, it is necessary find the condition of fast rotational diffusion for the proteins, and this technique

is known as rotationally aligned (RA) solid-state NMR. The symmetric pulse sequence, $R18^{7}_{1}$ can recouple heteronuclear dipolar couplings, which are used as angular restraints in the structure refinements, and long mixing of homonuclear correlation spectra and PREs provide the distance restraints.

While the three-dimensional structure of Vpu full-length has not been solved previously, the structure of the VpuTM has been well studied in various membrane systems including detergent micelles (115), lipid bicelles (116), lipid bilayers (115) by both solution NMR and solid-state NMR, whereas the Cyto domain has proven to be more difficult to study in large part because of its flexibility. Previously, the structure of Vpu39-81 from HIV strain HV1S1 has been studied in 50% TFE, aqueous solution (117) and DPC micelles (118) by solution NMR.

Even though several biological studies have found the interactions partners of Vpu or shown the key residues or motifs involving phosphorylation or protein interactions, the details of structure and corresponding mechanisms at the molecular level are of interest. For instance, the understanding the conformation of the Cyto domain is crucial for understanding the mechanism of phosphorylation and how it recruits other interaction partners. In addition, the conformation of full-length Vpu and its possible conformational changes upon interactions are of interest, since many interactions collectively utilize all structure domains, for example the down modulation of CD4 and the dysfunction of BST-2. Several key points need to be clarified in structure determination of Vpu: (1) what is the relative orientation of the TM domain and the Cyto domain; (2) what is the relative orientation of the two helices in the Cyto domain? Are they linear or forming a U-shape conformation. (3) How do the helices associate with lipids? Are they lying on the lipid

surface, partially or fully embed in the membrane, or exposed in the aqueous solution. (4) Is loop-2 structured or flexible? If it is flexible, how dynamic it is? (5) How do loop-2 and terminal region associate with lipids?

NMR spectroscopy has ability to answer questions, and in this article, we focus on solving the structure of full-length Vpu, and studying both the structure and dynamics of VpuCyto in order to provide more insights in the biological functions at the molecular level.

2.3 Results

The secondary structure of VpuFull in DHPC micelles and of VpuCyto in aqueous solution and DHPC micelles were characterized by CD spectroscopy. All of the CD spectra showed a maximum around 191nm, and local minima near 208nm and 222nm, which are indicative of the presence of a helical secondary structure. The CD spectrum of VpuCyto in aqueous media (Figure 2.1C) shows approximately 54% helical content. In contrast, in DHPC micelles, VpuCyto is estimated to have 71% helical content (Figure 2.1B). Thus, VpuCyto appears to be substantially more helical in the presence of DHPC micelles. This indicates that the cytoplasmic domain is affected by the lipid environment, and not freely soluble in the aqueous environment. The CD spectrum of VpuFull in DHPC micelles (Figure 2.1A) shows evidence of about 76% helical content, which arises from the inclusion of the helical TM region. Our CD spectra provide evidence of structure in VpuCyto, even in aqueous media, which differs from the findings of Wittlich et al, who found predominantly disordered Vpu38-81 in DPC micelles. The results are in agreement in showing an increase in secondary structure in the presence of micelles.

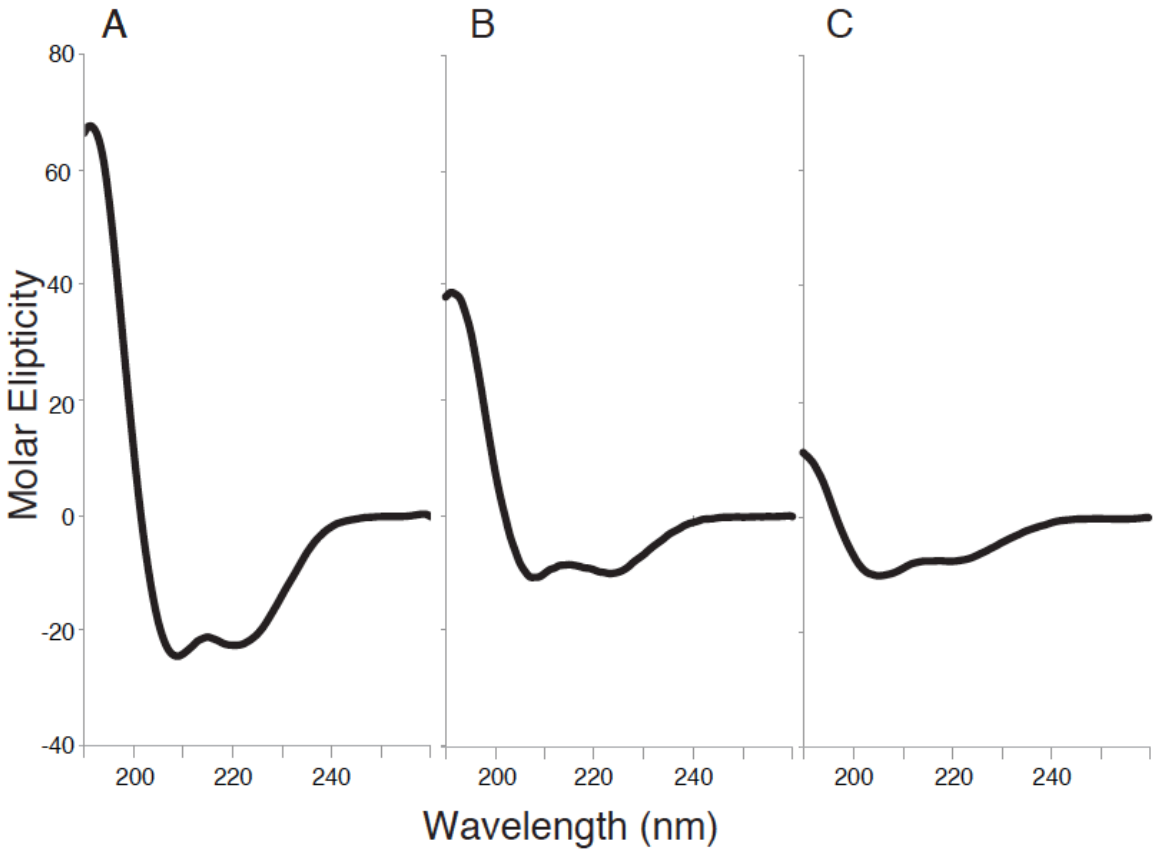

Figure 2.1 CD spectra of VpuFull and VpuCyto.

A, CD spectrum of VpuFull in 100 mM DHPC micelles. B, CD spectrum of VpuCyto in 100 mM DHPC micelles. C, CD spectra of VpuCyto in aqueous solution.

As shown in Figure 2.2, both uniformly ^{15}N labeled VpuCyto and VpuFull solubilized in DHPC micelles gave well-resolved two-dimensional HSQC spectra. The two spectra overlap to a large extent, indicating that the structure of VpuCyto alone is representative of the cytoplasmic domain in full-length Vpu. In addition, the spectra could be fully assigned to the residues in the polupeptides, as laveled in Figure 2.2A and B.

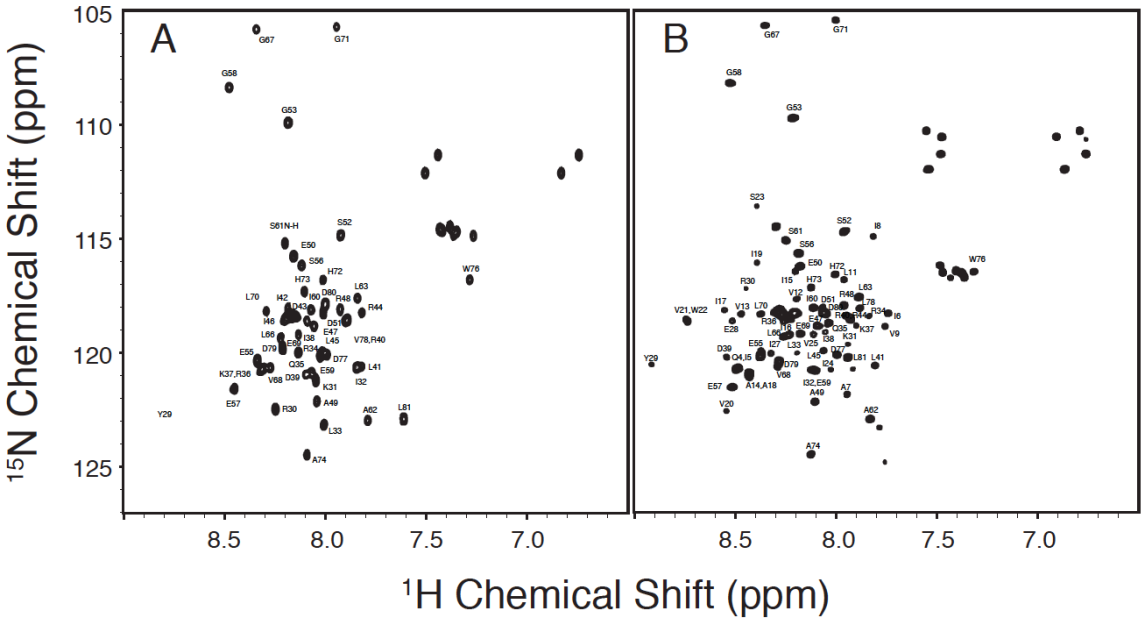

Figure 2.2 ^{1}H/^{15}N HSQC NMR spectra of VpuCyto and VpuFull.

A, Assigned ^{1}H/^{15}N HSQC spectrum of VpuFull in 100 mM DHPC micelles. B, Assigned ^{1}H/^{15}N HSQC spectrum of VpuCyto in 100 mM DHPC micelles.

The series of ^{13}C-detected cross-polarization solid-state NMR spectra shown in Figure 2.3 were acquired over a range of temperatures in order to characterize the rotational diffusion of three Vpu constructs in phospholipid bilayers. Relatively slow magic angle spinning, at 5K Hz, was used in order to observe the sideband patterns of the ^{13}C' signals. The results show that VpuTM undergoes fast rotational diffusion when the temperature is higher than 25°C (Figure 2.3A). By contrast, no powder pattern is found even when VpuCyto is at 5°C (Figure 2.3B). At high temperatures, the ratio of the first left sideband to the center band of the carbonyl carbon of VpuCyto is 0.5, which is relatively high comparing to VpuTM. The orientation effects were simulated under the conditions that the principal value of C', σ_{11}, is either parallel or perpendicular to bilayer normal, and the orientation of helix is roughly parallel to σ_{11} of C' (Figure 2.3D-G). Comparison of

simulated powder patterns of helices with different orientations with experimental spectra of VpuTM and VpuCyto shows that the orientation of the TM domain is approximately parallel to the bilayer normal, while the orientation of cytoplasmic domain is approximately perpendicular to the bilayer normal. By comparing the spectra of VpuTM, VpuCyto, and VpuFull, we find that the spectra of VpuFull are combinations of those from VpuTM and VpuCyto. The range of reduced dipolar powder patterns observed in ^{1}H-^{13}C/^{13}C and ^{1}H-^{15}N/^{13}C separated-local-field (SLF) experiments (Figure 2.4) provide direct evidence that Vpu is undergoing fast rotational diffusion at 25 °C.

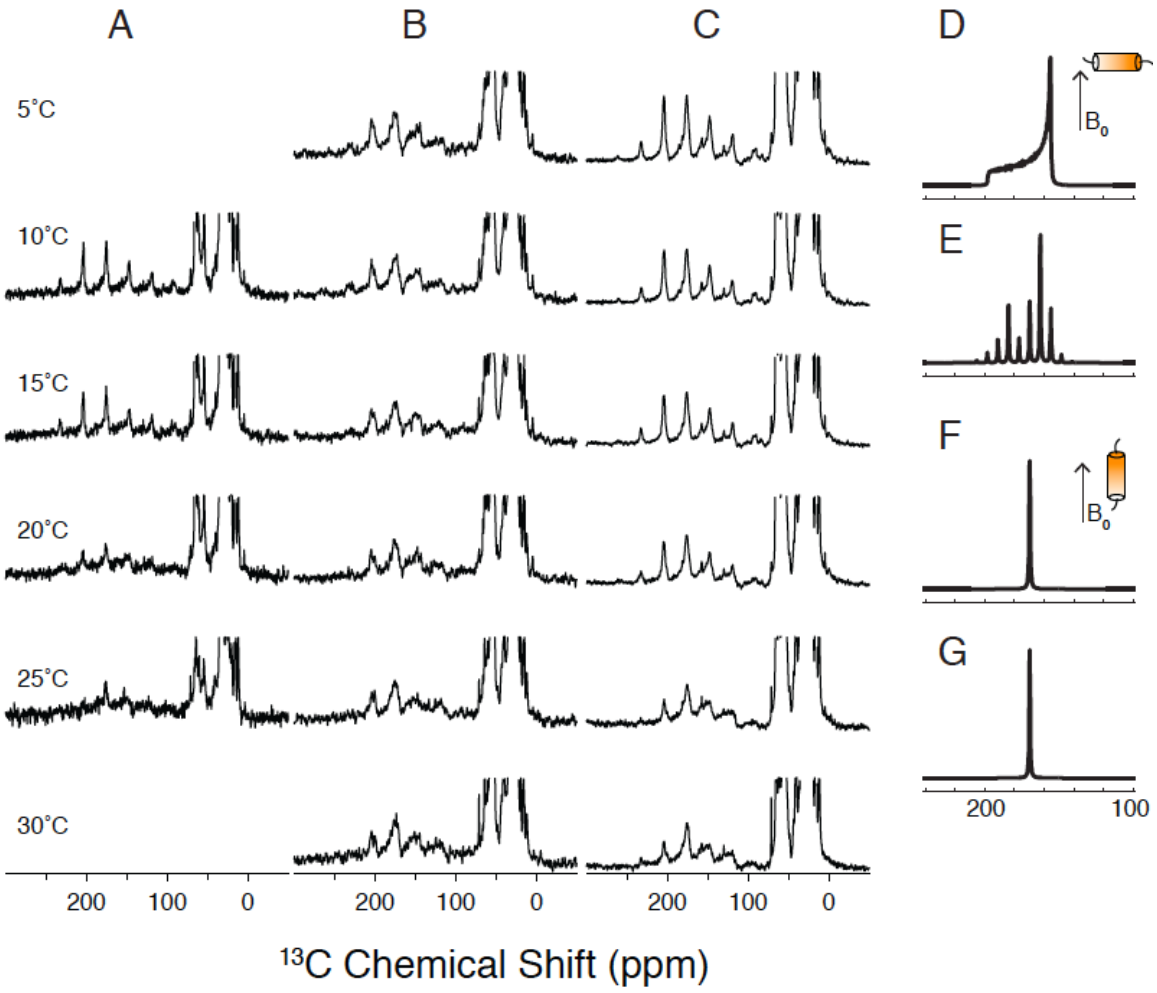

Figure 2.3 ^{13}C solid-state NMR spectra of three constructs of Vpu in DMPC proteoliposomes.

A, VpuTM. B, VpuCyto. and C, VpuFull. All the spectra were acquired at 5K Hz MAS at various temperatures. VpuTM is static below 15 °C and undergoing fast rotational diffusion above 25 °C. D, Simulated C' powder pattern of helix undergoing fast rotational diffusion with the helix axis perpendicular to the bilayer normal. E, Similated C' powder pattern of helix undergoing fast rotational diffusion with the helix axis perpendicular to the bilayer normal under 5K Hz MAS. F, Simulated C' powder pattern of helix undergoing fast rotational diffusion with the helix axis parallel to the bilayer normal. G, Similated C' powder pattern of helix undergoing fast rotational diffusion with the helix axis parallel to the bilayer normal under 5K Hz MAS.

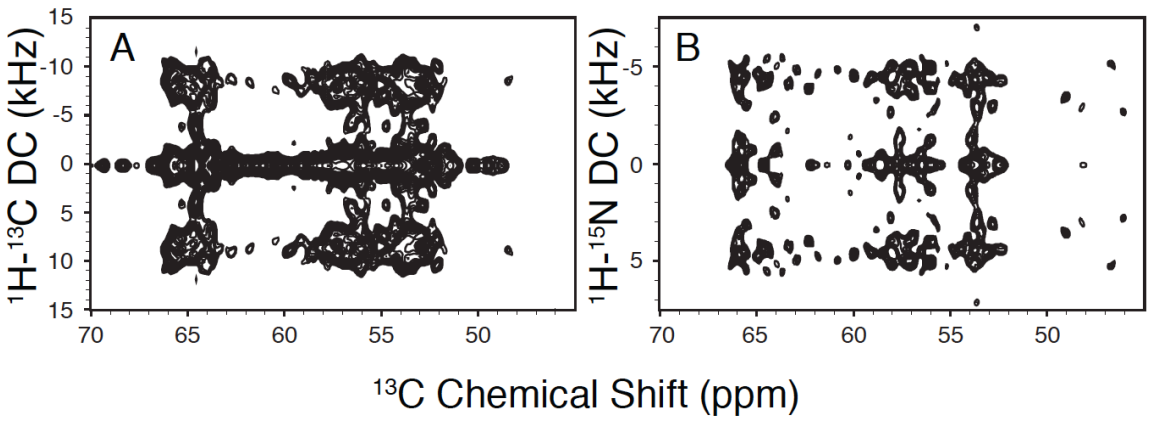

Figure 2.4 ^{1}H-^{13}C/^{13}C and ^{1}H-^{15}N/^{13}C SLF spectra of VpuFull in DMPC proteoliposomes.

A, ^{1}H-^{13}C/^{13}C SLF spectrum. B, ^{1}H-^{15}N/^{13}C SLF spectrum. The various dipolar couplings obtained from both experiments show that VpuFull is undergoing fast rotational diffusion, and single-site resolution is achievable when it is incorporated in proteoliposomes at 25 °C.

As shown in Figure 2.5, it is possible to obtain high-resolution ^{13}C/^{13}C and ^{13}C/^{15}N (two-dimensional) correlation spectra under these sample conditions. Spectral resolution is further improved in three-dimensional experiments. Importantly, the mobile regions of the Vpu polypeptide are determined by TOBSY (total through-bond correlation spectroscopy) (119,120) (Figure 2.5B). This J-coupling-based ^{13}C/^{13}C correlation experiment is only feasible for residues that are mobile enough to average out the dipolar couplings. Signals from about 30 residues are found in the TOBSY spectrum (Figure 2.5B) based on their chemical shifts. Partial assignments are available by considering dynamics studies of VpuCyto in micelles. Most of the mobile residues are found in loop-2 and both termini, suggesting these regions are highly dynamic in the lipid bilayer environment. Complementary dipolar based NCACX and NCOCX experiments identify the structured parts of VpuFull. This allows us to sequentially assign the chemical shifts of ^{15}N, ^{13}Cα and ^{13}C'. In these assignment experiments, the magnetization is transferred from amide protons

to ^{15}N with cross-polarization (CP), and then to $^{13}C\alpha$ or $^{13}C'$ by SPECIFIC-CP; the $^{13}C/^{13}C$ correlations are achieved with DARR mixing. Signals from 43 immobile residues were assigned with NCACX and NCOCX experiments (Figure 2.10), and their dipolar couplings are measured from ^{1}H-$^{15}N/^{15}N/^{13}C$ and ^{1}H-$^{13}C/^{15}N/^{13}C$ three-dimensional SLF experiments. The measured values of chemical shifts and heteronuclear dipolar couplings are listed in Table 2.1. Dipolar couplings provide valuable information on indicating secondary structure, especially α-helix of a protein. The resulting ^{1}H-^{15}N dipolar coupling values for the backbone amides in an ideal helix display a sinusoidal wave pattern referred to as a Dipolar Wave. Three Dipolar Waves are found in the plot of dipolar couplings versus residue numbers (Figure 2.6A), which indicates the existence of three helices in VpuFull. The tilt angles estimated according to the mean values and the amplitudes of dipolar waves, are 20°, 80° and 80° from bilayer normal for helices-1, -2 and -3, respectively.

Table 2.1 List of chemical shifts and dipolar couplings of VpuFull in proteoliposomes.

Residue	^{15}N CS (ppm)	^{13}Cα CS (ppm)	^{13}C' CS (ppm)	^{1}H-^{15}N DC (kHz)	^{1}H-^{13}C DC (kHz)
I8	119.52	65.30	175.90	8.5	
V9	119.93	66.80	176.69	8.5	18.1
A10	116.54	55.39	175.62		15.2
L11	119.26	58.53	176.15	7.7	17.7
V12	119.70	66.77	175.68	10.6	6.9
V13	120.64	66.66	175.57	4.5	12.9
A14	121.48	54.52	176.03	3.5	14.5
I15	115.91	63.85	176.20	7.4	17.6
I16	122.12	65.29	176.00	9.2	18.6
I17	121.84	65.05	176.14	4.3	16.4
A18	121.44	54.31	177.07	9.5	5.9
I19	116.00	64.61	176.98	10.3	18.3
V20	122.70	66.74	175.87	4.8	17.1
V21	120.20	66.56	175.67	4.5	14.6
W22	121.45	56.54	177.27	8.2	15.3
S23	118.8	60.19	175.99	9.1	15.0
I24	115.36	64.66	176.99		14.9
V25	121.10	66.96	176.59	6.0	16.9
I26	120.79	64.54	176.03	8.4	
I27	122.04	66.56	175.75	8.6	
Q35	120.84	60.81	174.68	7.6	

Table 2.1. List of chemical shifts and dipolar couplings of VpuFull in proteoliposomes, continued.

Residue	^{15}N CS (ppm)	^{13}Cα CS (ppm)	^{13}C' CS (ppm)	^{1}H-^{15}N DC (kHz)	^{1}H-^{13}C DC
I38	118.10	63.39	176.31		19.6
D39	119.20	56.44	176.81		
R40	121.63	54.80	177.05	7.8	14.8
L41	118.82	58.25	177.62	9.2	2.4
I42	118.20	63.42	176.63	8.5	
D43	119.59	56.96	176.55	6.3	13.5
R44	121.76	57.08	176.97	8.1	18.6
L45	120.35	57.78	175.88	8.6	16.6
I46	119.07	65.05	175.97	8.9	15.4
E47	122.35	60.12	177.29	8.0	7.3
R48	122.48	56.98	176.83	6.7	9.2
E59	117.57	58.99	177.28		
I60	119.07	65.55	176.01	7.4	16.2
S61	117.32	58.05	175.87	8.6	15.8
A62	120.23	52.83	175.95	5.9	3.4
L63	115.86	56.65	176.98		16.0
V64	119.73	66.96	176.86	8.6	17.8
E65	118.47	58.28	176.50	5.3	
L66	115.81	58.05	175.97	8.0	13.9
G67	103.05	46.51	173.83	1.3	
V68	115.55	66.44	175.66	6.5	
E69	120.24	59.42	176.01	7.2	18.2

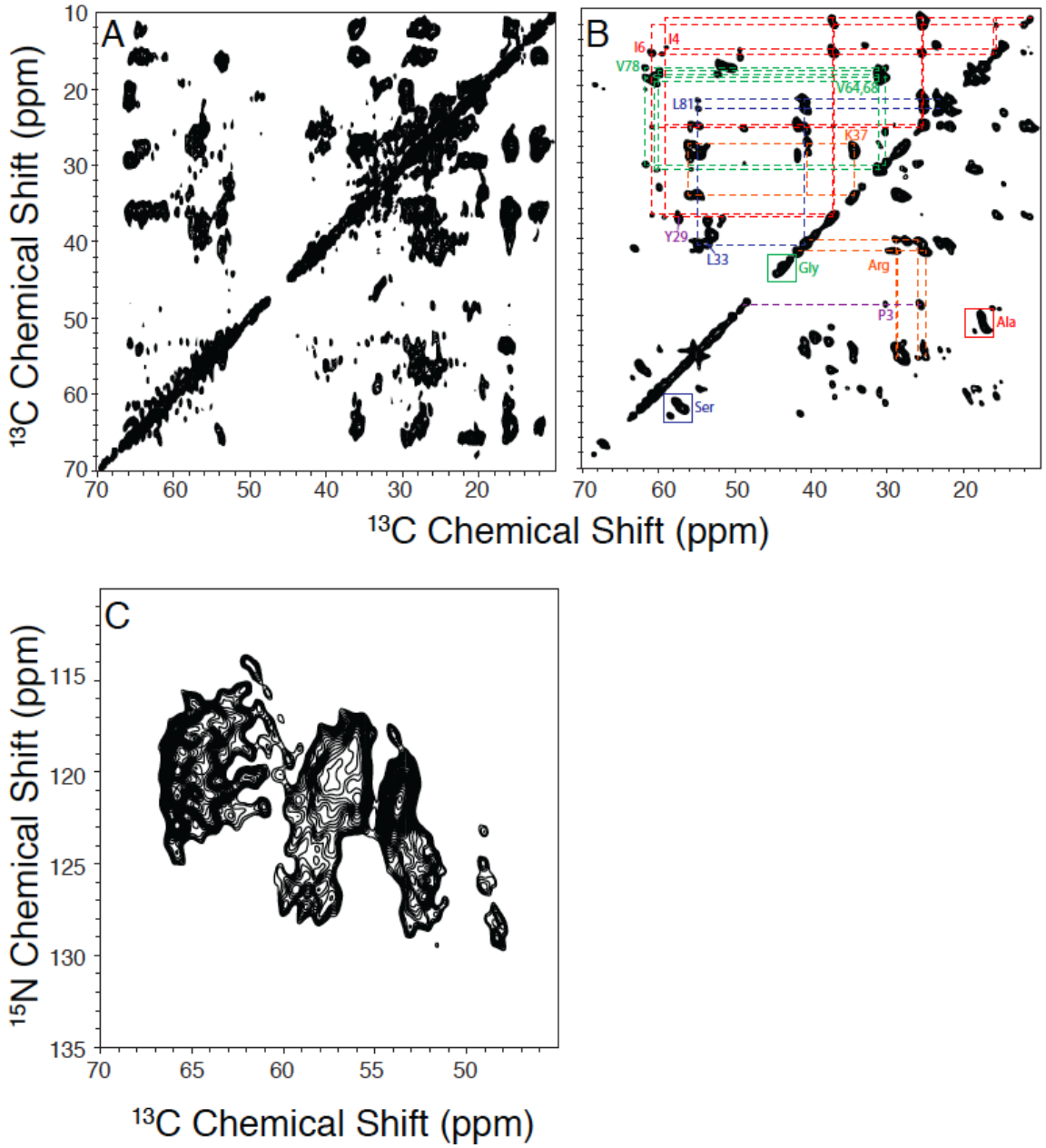

Figure 2.5 Correlation spectra of VpuFull in DMPC proteoliposomes.

A, $^{13}C/^{13}C$ correlation spectrum obtained with 50 ms PDSD mixing. B, $^{13}C/^{13}C$ TOBSY spectrum; the J-coupling based $^{13}C/^{13}C$ correlation spectrum indicates the mobile residues of VpuFull. C, $^{15}N/^{13}C$ HETCOR spectrum, where the $^{15}N/^{13}C$ transfer is obtained from SPECIFIC-CP. All of the experiments show that single-site resolution is achievable when VpuFull is incorporated in DMPC proteoliposomes at 25 °C.

Rotationally averaged dipolar coupling and chemical shift anisotropy powder patterns provide angular restraints and are essential for structure determination. However,

we would obtain degeneracies from structural calculations only relying on the angular restraints. For instance, the two helices in the cytoplasmic domain could be linear or form a U-shape based on the analysis of only dipolar couplings. Distance restraints help characterize the relationships between the secondary structure elements. In general, in solid-state NMR, the distance restraints could be extracted from homonuclear spin diffusion with long mixing times. However, since no significant correlations are found from $^{13}C/^{13}C$ correlation experiments with DARR mixing up to 200 ms for VpuFull, two PRE approaches were applied to obtain long-range restraints. (1) MTSL is labeled on L41C VpuFull to probe the distances of neighbor nuclei. (2) MnEDTA, a bulky paramagnetic reagent that is restricted to the aqueous environment, is utilized to distinguish if the residues are exposed to the solution or embedded in the lipids, which helps determine how the cytoplasmic domain of the full-length Vpu interacts with lipids. The intensities of the resonances from TOBSY spectra vary in the PRE experiments, and therefore we can assign the resonances for the mobile region more specifically. For instance, three alanines corresponding to A7, A49 and A74 are found in the TOBSY spectra (Figure 2.6B), yet they are ambiguous without assignment experiments. The intensities of both A49 and A74 are reduced by L41C-MTSL, suggesting the helix-2 and helix-3 form a U-shape conformation, and these resonances are assigned according to the ratios of the L41C-MTSL and its reduced form (Figure 2.6B). On the other hand, A74 disappears with the addition of MnEDTA (Figure 2.6D), which indicates A74 is exposed to the solvent. Similarly, we can assign serines according to the changes of intensities when the Cyto domain is a U-shape (Figure 2.6C). S61 is less affected by MnEDTA, suggesting that S61 in helix-3 may face the lipids or is slightly embedded into the lipids. S52 and S56 are more exposed in the

solution due to their presence in the loop; however, S56 is substantially more affected by MnEDTA than S52, suggesting that two serines adopt different orientation with S52 substantially more exposed to the aqueous solution. (Figure 2.6E).

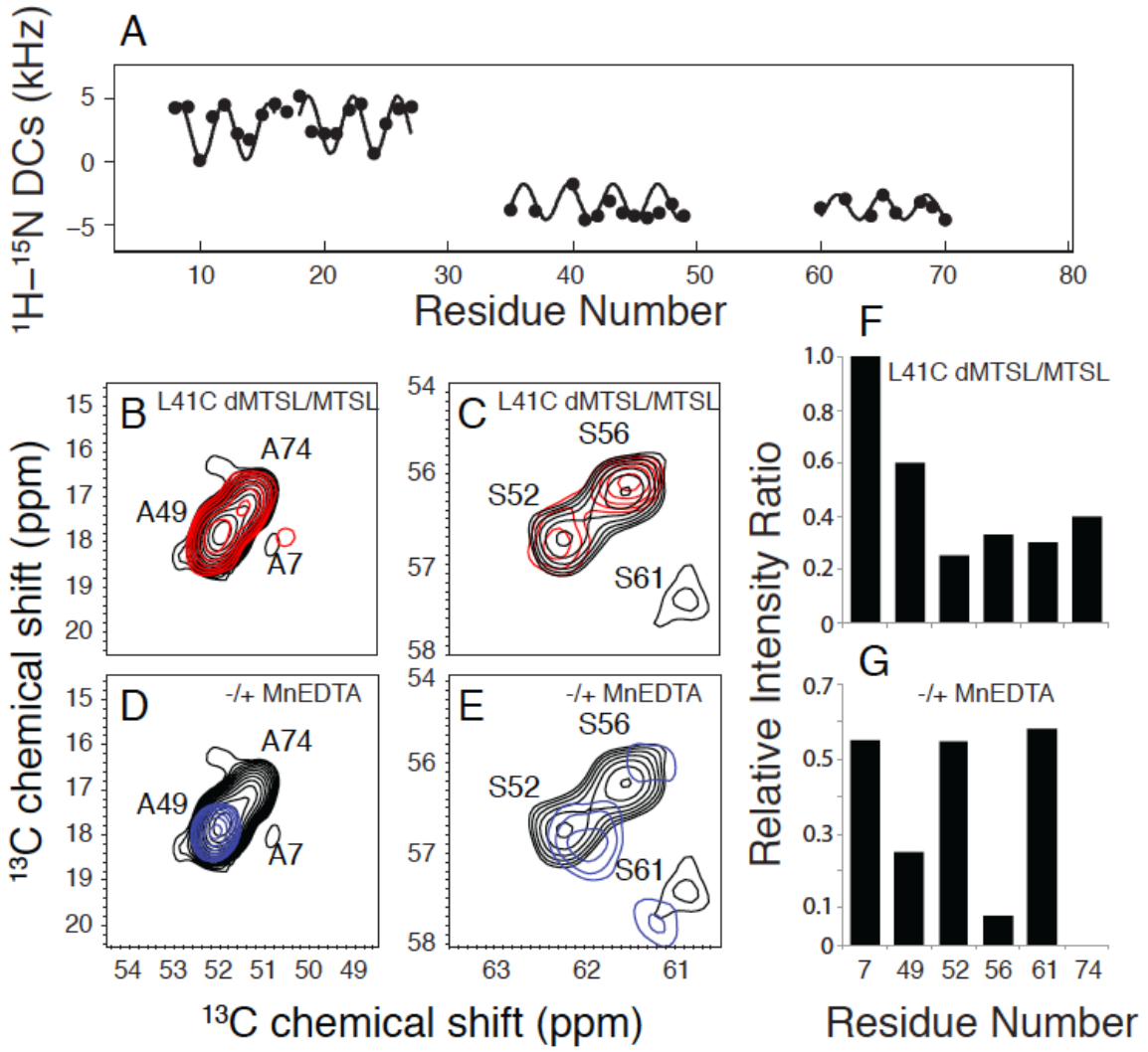

Figure 2.6. Solid-state NMR measurements for structure calculation of VpuFull in DMPC proteoliposomes.

A, Plot of ^{1}H-^{15}N dipolar couplings versus residue numbers, indicating the helical regions in VpuFull. B, Overlap of ^{13}C/^{13}C TOBSY spectrum of L41C-VpuFull with MTSL (red) and its reduced diamagnetic form (black) at the alanine region. C, Overlap of ^{13}C/^{13}C TOBSY spectrum of L41C-VpuFull with MTSL (red) and its reduced diamagnetic form (black) at the serine region. D, Overlap of ^{13}C/^{13}C TOBSY spectrum of VpuFull with (blue) and without (black) MnEDTA present at the alanine region. E, Overlap of ^{13}C/^{13}C TOBSY spectrum of VpuFull with (blue) and without (black) MnEDTA present at the serine region. F, Plot of residues intensity change caused by L41C-MTSL. G, Plot of residues intensity change caused upon addition of MnEDTA solution.

During calculation of VpuFull in DMPC liposomes, torsion angle restraints were obtained from the structure TALOS+ with chemical shift input of N, CA, CB and C'.

Orientational restraints were obtained from both ^{1}H-^{15}N and ^{1}H-^{13}C dipolar couplings. In addition, two types of distance restraints obtained from L41C-MTSL VpuFull and MnEDTA were incorporated to further refine the structure. Refined structures driven only by dipolar couplings give many possible conformations (Figure 2.11A), where the relative orientations between helix-2 and helix-3 are allowed to form either linear or U-shape. By considering the distant restraints obtain from L41C-MTSL VpuFull, the helix-3 is folded back, yet the relative orientation between cytoplasmic domain and membrane surface is still ambiguous (Figure 2.11B). Helix-3 is further confined to the lipid surface by introducing the plane distance restraint obtained from MnEDTA experiments (Figure 2.11C). The RMSD of ten lowest structures shows that all the helices are well defined, whose RMSD are 0.48 Å, 0.31 Å, and 0.23 Å for helix-1, helix-2, and helix-3, respectively. Most of the variations come from the loop regions (loop-1 is 1.92 Å and loop-2 is 2.74 Å), and the RMSD of the structural region (7-70) is significantly improved and converges at 5.18 Å.

The secondary structure of VpuCyto in both types of samples can also be confirmed by solution NMR experiments. VpuCyto in aqueous solution has a relatively short T_1 (from 690 ms to 1 s) and long T_2 (from 210 ms to 600 ms), indicating that the protein is undergoing rapid reorientation, and the backbone is highly mobile. Also the negative ^{1}H-^{15}N heteronuclear NOE value throughout the polypeptide suggests that the internal motions of VpuCyto in aqueous media are rapid. However, T_1, T_2 and NOE showed non-uniform distribution, where the terminal and inter-helical loop region (51-58) have longer T_1, longer T_2 and more negative ^{1}H-^{15}N heteronuclear NOE than the helical regions. The variation in T_1, T_2 and ^{1}H-^{15}N heteronuclear NOE agrees with CD data, suggesting that there is a

structural distinction between the helical regions and loop region in aqueous media, and that the structure is not fully disordered. In contrast, the Cα chemical shift index has values around +1 ppm, which cannot be categorized as helical. In addition, TALOS+ only predict residue 62-70 as helix, and failed to predict any secondary structure for the rest of the protein due to the low order parameters. VpuCyto in aqueous solution may be in an intermediate state between well structured and fully disordered, with the helix-3 somewhat more structured.

In DHPC micelles, plots of the relative intensities of resonances in the HSQC spectrum, and the Cα chemical shift index (Figure 2.7G and 7H) indicate two distinct helical religions connected by a mobile inter-helical loop. These helical regions are also consistent with the RDC data acquired in a 6% polyacrylamide stretched gel. When incorporated into DHPC micelles, the mobility is drastically reduced, as shown by the significant decrease of T_2 relaxation (70 ms to 170 ms). In addition, the same trends were observed for T_1, T_2 and ^{1}H-^{15}N heteronuclear NOE, suggesting a significant dynamic difference between the helical regions and the loop region. Overall, helix-3 and helix-2 exhibit similar restricted backbone dynamics, with similar values of ^{1}H-^{15}N heteronuclear NOEs, order parameters and ^{1}H-^{15}N HSQC peak intensities, in DHPC micelles. While residues at the N-, C-terminus and loop are significantly more flexible, with smaller values of the ^{1}H-^{15}N NOE and greater peak intensities.

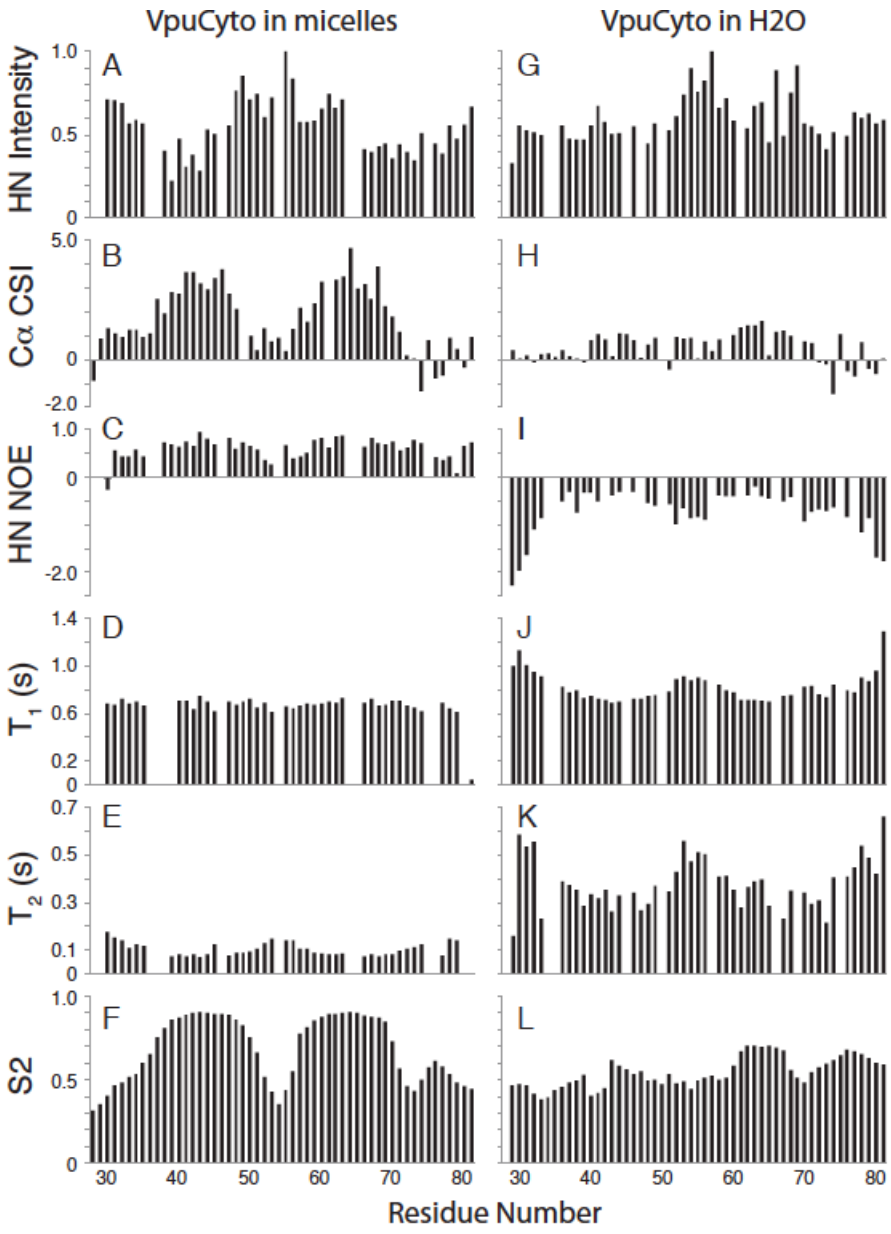

Figure 2.7 Secondary structure and dynamics of VpuCyto in aqueous solution and DHPC micelles.

A.-F. are obtained from VpuCyto in aqueous solution. G.-L. are obtained from VpuCyto in 100 mM DHPC micelles. A, $^{1}H/^{15}N$ HSQC resonance intensity plot. B, Cα chemical shift index. C, ^{1}H-^{15}N heteronuclear NOE. D, T1 relaxation. E, T_2 relaxation. F, Order parameters derived from TALOS+. G, ^{1}H-^{15}N HSQC resonance intensity plot. H, Cα chemical shift index. I, ^{1}H-^{1}N heteronuclear NOE. J, T_1 relaxation. K, T_2 relaxation. L, Order parameters derived from TALOS+.

Helical Residual dipolar coupling measurements not only provide reliable information on the secondary structure of the protein, but also yield relative orientations of the regions in the protein. Residues in both N- and C-terminal and the loop regions have close to 0 Hz RDCs (Figure 2.8A), which is an indication of the mobile properties of these regions. The RDC values of the helical region were fit by two separate dipolar waves with very different amplitude, indicating a considerable angle difference between the helices. These RDC values can be used as angular restraints in structure calculation (47,57,121). The PRE were measured as distance restraints. The secondary structure and motion information were considered before determining the optimal placement of the spin labels. Residues at three positions 41, 62 and 74, located at helix-2, helix-3 and the C-terminal region respectively, were mutated to cysteines independently for MTSL attachment. ^{1}H-^{15}N HSQC spectra were collected on the samples L41C-MTSL VpuCyto, S61C-MTSL VpuCyto and A74C-MTSL VpuCyto. In both of the L41C and A74C HSQC spectra, only residues near the mutation site showed small chemical shift changes compared to wild type spectra, which indicates that the mutation and the spin label did not change the protein structure dramatically. The S61C sample showed quite significant changes, so it was not used for PRE measurement. The ^{1}H-^{15}N HSQC spectra (Figure 2.8C) illustrate the overlapped spectra of the L41C-MTSL VpuCyto in red and its reduced form in black. Residues close to the mutation sites L41C were broadened beyond detection. Observable reductions in intensity due to PRE were also observed for residue 67, 70, even they are not close to L41C in the sequence; this indicates that they are close to L41 in the folded polypeptide. The normalized PRE intensity ratio versus residue number for L41C VpuCyto and A74C VpuCyto are plotted (Figure 2.8E and 8F), and it is obvious that when the spin

label is added to L41C, not only residues near 41, but also those at helix-3 and near C-terminus are broadened. Similarly, for MTSL-A74C, not only the residues in the C-terminal region are broadened, but also the intensities of residues at the helix-2 are also significantly reduced. To ensure that the PRE effect is not intermolecular instead of intramolecular, protein concentration were limited to 0.1mM during data acquisition; additionally, the intensity plot did not change significantly upon addition of unlabeled VpuCyto to the MTSL labeled sample, indicating that no internuclear PRE effect are observed.

The MTSL samples provide 72 PRE restraints that were particularly useful in defining distances and orientations between helix-2 and helix-3 in VpuCyto. Distance restraints were calculated base on the measured peak intensity ratios (I_{para}/I_{dia}) as described by Wagner (54) and Liang (56). The global correlation time of each residue (5 ns - 10 ns) was calculated based on T_1 and T_2 of the wild type VpuCyto in micelles (122,123). The calculated PRE distances were incorporated into the structure calculations with a lower bound of 4 Å and upper bound of 4 Å as compensation for inaccuracy in correlation time and other measurements.

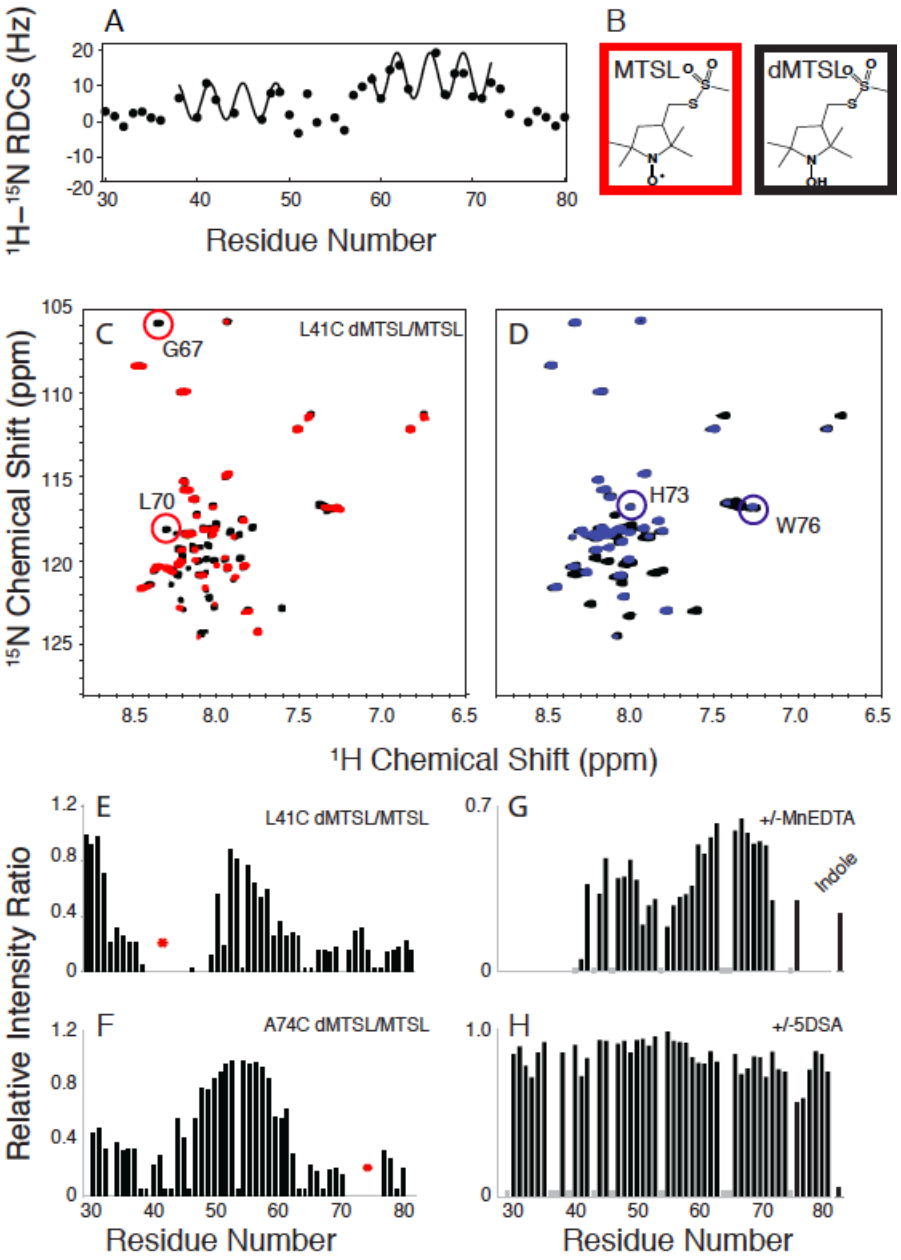

Figure 2.8 Solution NMR measurements for structure calculation of VpuCyto in DHPC micelles.

A. Plot of residual dipolar couplings as a factor of residue numbers obtained from weakly aligned sample in 6% polyacrylamide stretch gel. B. Chemical structure of MTSL (red box) and its reduced form (black box). C. Overlap of ^{1}H-^{15}N HSQC spectra of L41C VpuCyto with MTSL label (red) and its reduced diamagnetic label (black). D. Overlap ^{1}H-^{15}N HSQC spectra of VpuCyto with MnEDTA (blue) and without MnEDTA (black). E. Intensity plot shows PRE intensity ratio (Ipara/Idia) for L41C VpuCyto. F. Intensity plot shows PRE intensity ratio (Ipara/Idia) for A74C VpuCyto. G. Intensity change measured before and after addition of MnEDTA. H. Intensity change measured before and after addition of 5SDA to VpuCyto in DHPC micelles.

During the structure calculation of VpuCyto in DHPC micelles, torsion angle restraints were obtained from TALOS+ with chemical shift input of HN, N, CA, CB, C' and HA. Angular restraints were obtained from one RDC datasets with Da, Rh calculated by Xplor-NIH. Distance restraints were provided by ^{15}N NOESY-HSQC NOE mainly for short range, and by PRE mainly for long range. Although torsion angle, RDCs, and NOEs provide sufficient information to anneal the VpuCyto to two helices, they are not enough to converge a set of structures. The inclusion of long-range distance restraints from PRE data was essential to produce the three-dimenstional structures. Ensembles of 20 lowest energy structures calculated with only dihedrals and NOEs (Figure 2.12A), dihedral, NOEs and RDCs (Figure 2.12B), and dihedral, NOEs, RDCs and PREs (Figure 2.12C) with decreasing ensemble RMSDs, are observed. VpuCyto consists of two helices exhibiting a U-shape structure in DHPC micelles that are relatively well defined with an RMSD of 2.95 Å over all backbone atoms for a family of 20 VpuCyto structures.

The depth of micelle insertion of VpuCyto backbone amide sites is reflected by the distance-dependent broadening effects of MnEDTA and 5SDA (Figure 2.8G, 8H). When MnEDTA was added to VpuCyto incorporated in DHPC micelles, signals of residues that are accessible to MnEDTA in aqueous environment are broadened, and the corresponding intensities are lowered; residues associated with the hydrophobic region of the micelles are less affected. Signals of residues that are broadened by MnEDTA are colored red (Figure 2.13A). Addition of MnEDTA results in complete disappearance of signals from both N- and C-termini due to their exposure in the aqueous solvent and MnEDTA. In addition, signals of residue 34-40 in helix-2 completely disappeared, suggesting that the N terminal half of the helix-1 is located outside the micelles. Notably, in the completely exposed C-

terminal region, resonances signals of W76 amide, it's indole nitrogen and H73 amide are not completely elimination by MnEDTA, suggesting their partial insertion in the micelles. The aromatic side chains of tryptophan and histidine are frequently found inserted in membranes as a result of the dipole moment of their aromatic ring interacting with the phosphatidylcholine head group. Moreover, the loop region, believed to be highly mobile, is less broadened by MnEDTA than the terminal region. This suggests that the loop is more restricted in mobility as a result of partially micelle association, compared to the solvent exposed terminal region, and this finding agrees with what we observed in structure determination. The line broadening effects were not observed equally for both helices, and those in helix-2 are less affected, indicating that it is more structured and embedded in the center of the micelles. 5SDA is a fatty acid with an 18-carbon hydrophobic chain that has a nitroxide group labeled at the fifth carbon position, close to the headgroup. When incorporated into the DHPC micelles, the 5SDA partitions to the hydrophobic interior of the micelles, and the spin label is at the center of the micelles. Thus, it can be used to probe the portion of protein embedded in the micelles. Signals of residues that are broadened by 5SDA are colored yellow, and those less affected are colored blue (Figure 2.13 B). Opposite effects were observed compare to MnEDTA. The residues at helix-3 were slightly more affected than those of helix-2, and the C-terminal region seemed to be more affected than the N-terminal region, and W76 and especially its indole signals are the most broadened among all the residues. This is evidence that W76 is embedded in the micelles. Overall, line-broadening was invariant for VpuCyto in DHPC micelles with 5SDA compared to MnEDTA. The possible explanations are: (1) both DHPC and 5SDA are dynamic and undergoing rapid rearrangement, and it is possible that at the nitroxide group

is not always inserted the center of the micelles but sometimes located near the head group region; (2) due to the amphipathic nature of VpuCyto, it is highly mobile and is not firmly embedded in the micelle, but more likely loosely associated with the micelles.

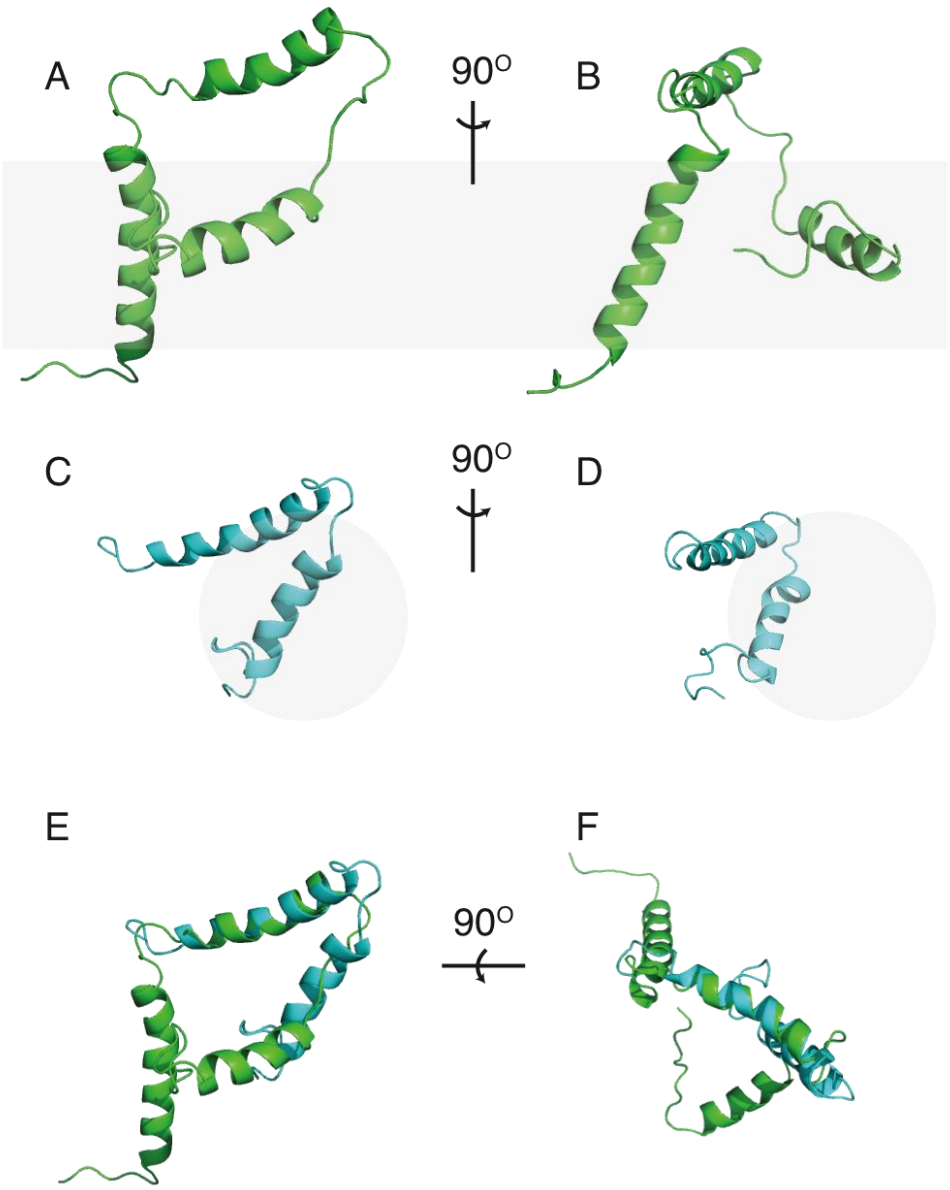

Figure 2.9 Structure comparison of VpuCyto and VpuFull.

A, Cartoon representation of VpuFull in DMPC proteoliposomes. B, 90º rotation of A about the x axis. C, Cartoon representation of VpuCyto in DHPC micelles. D, 90º rotation of C about the x axis. E, Alignment of VpuFull and VpuCyto structures (side view with respect to bilayer normal). F, Alignment of VpuFull and VpuCyto structures (top view with respect to bilayer normal).

2.4 Discussion

The structure ensemble of VpuCyto in DHPC micelles, disregarding the disordered terminal regions, has a well-defined helix-2-loop-helix-3 motif with 1.24 Å RMSD. The modest variations in the helices suggest that they are relatively rigid. The inter-helical loop itself appears to have RMSD of 0.7 Å. Along with a number of NOEs observed in residue 50-59 in the loop region, surprisingly it suggests that, the loop adopts as well defined structure. All the charged residues occur on either the end of the helices and the terminal region (R30, K31, D77, D79 and D80) or were restricted to the outer surface of the U-shape structure (R36, R40, R44, E65 and E69), presumably exposed to the aqueous media. The U-shape set of two helices also renders the more hydrophobic phase in the core of the structure.Both VpuFull and VpuCyto constructs have well-defined helix-2 and helix-3 (Figure 2.9). The lengths of both helices are slightly longer in VpuCyto in DHPC micelles than those in VpuFull in DMPC liposomes; however, the helical lengths in both constructs are longer than those in Vpu 39-81 obtained from DPC micelles. The tilt angles of the average structure of ten lowest structures of VpuFull are approximately 25°, 89°, and 79° from the bilayer normal for helix-1, -2, and -3, respectively, which are close to the estimations based on dipolar waves. This suggests that the helices in the Cyto domain are laying on the bilayer plane, parallel to the bilayer surface. The 25° tilt angle of the TM domain is quite similar to tilt angle of VpuTM construct obtained in DMPC liposomes which is 28°, and in DMPC bicelles which is 30°. The slightly difference may arise from the missing Cyto domain in the VpuTM construct. The angles between helix-2 and helix-3 of VpuFull and VpuCyto are approximately 42° and 36°, which shows that the orientations of Cyto domain are similar, but the spacing between helices is larger for

VpuFull, and it results from that VpuFull has longer and more flexible loop-2. And as a result, helix-3 in VpuFull was observed to have a high degree of flexibility, which may be attributed to fewer structural restraints imposed in the calculation or its intrinsic dynamic properties. Loop-2 of VpuCyto is shorter and partially structured, and this may be caused by the interactions with the short-chain lipids. Both the effects on loop-2 and the helical lengths suggest that micelles still affect the structures slightly from the bilayer environment.

It is challenging for solid-state NMR to quantify the dynamics of proteins, yet we still can investigate the dynamic properties with J-coupling based experiments, such as TOBSY. The signals raise from TOBSY require the motions of residues faster than μs range to average out the dipolar couplings, and this dynamics range is close to the lower-limit of measurements of T_1, T_2, and heteronuclear NOE in solution NMR. Based on the assignments from TOBSY spectrum, it suggests that both loops and C-terminus are mobile, and the results are similar with the dynamics studies in solution NMR.

The loop-2 region is the most highly conserved region in Vpu, which contains S52 and S56 as phosphorylation sites and are crucial to recruit ubiquitin ligase complex to lead CD4 and BST-2 to degradation. NMR studies performed by Willbold et al. (124) in DPC micelles suggests that phosphorylation cause no drastic structural change in Vpu except an elongation of helix-3, reduction in helicity at helix-2 and reduction in mobility of loop-2 region. While MD simulation done by Girault et al. (125-127) shows that helix-3 becomes unstructured upon phosphorylation. The lowest energy structure of VpuFull shows that S56 faces toward to the aqueous solution and S52 faces down to the lipid surface, and loop-2 roughly lies on the membrane, which might suggest that S56 is easier to be catalyzed by

CK2. Even though the conformation of loop-2 might be hindered for the phosphorylation by CK2, it could be compromised by the dynamics of loop-2, which provides more chance to expose itself into aqueous solution. Once S52 and S56 are phosphorylated, the recruiting of β-TrCP is more viable from the steric effect because it involves loop-2 and the loops in WD domain from β-TrCP, and both segments are relative flexible.

Biological studies have revealed several interaction partners of Vpu including CD4, BST-2, NTB-A and CCR7, etc., which are mostly membrane proteins. To downregulate BST-2, NTB-A, and CCR7, Vpu direct interacts with them through the TM domain and employs the A10, A14, A18 and W22 face in the interaction. In the lowest energy structure obtained for VpuFull in DMPC liposomes, it is shown that A10, A14, A18 and W22 are lined up, and face the opposite direction of where the Cyto domain sits. This open space appears to favor the approach of its interaction partners.

In the case of interaction with CD4, helix-2 and 3 and the C-terminal were in Vpu were shown to be involved as well as the membrane proximal region in CD4. Based on the CD4 structure obtained in DPC micelles, the Vpu binding residues 402-420 are laying on the surface of micelles. The structures of both constructs we got here also shown that cytoplasmic is closely associated with the membrane surface, which provides a feasibility of interaction to CD4 in space.

When Vpu antagonizes BST-2, the W76 at the C terminal region is found critical for counteraction of the restricted virion release, and the phenotype is attributed to the ability of W76 to displace BST-2 from site of plasma membrane where virion assembly is taking place. NMR experiments done on VpuCyto in both DHPC and aqueous media suggested that this might due to anchoring property of W76 to the plasma membrane. Here,

the VpuFull structure in DMPC liposomes show that helix-3 is closer to the membrane surface than helix-2, and in most structures in the ensemble, W76 and the indole side chain is facing the lipid head group, which supports the previous membrane anchoring model. In addition, no signals were found on TOBSY spectra from W76, although it is in the very mobile C-terminal region. This may indicates that W76 is immobilized due to interaction with the lipid head group.

2.5 Materials and methods

Vpu expression plasmids for NL4-3 VpuFull and VpuCyto constructs were prepared similarly to those previously described (128). Synthesized DNA corresponding to VpuCyto (Integrated DNA Technologies) was ligated into phLV vector for expression as a Trp-leader fusion. Synthesized DNA for the VpuFull sequence was inserted into pET31b(+) vector (Agilent Technologies) for expression as a KSI fusion. For both constructs, the methionines were mutated to leucine to assist protein purification, and were shown to have no effect on the properties of Vpu. Expression plasmids encoding mutant VpuCyto-L41C, VpuCyto-A74C and VpuFull-L41C were constructed using the QuikChange Lightning Site-Directed Mutagenesis Kit (Agilent Technologies), and the primers were synthesized by Integrated DNA Technologies. BL21-CodonPlus competent cells were obtained from Agilent, and Overexpress C41(DE3) competent cells were obtained from Lucigen. The chelated manganese was prepared by adding manganese sulfate (MnSO4) to ethylenediaminetetraacetic acid (EDTA) (0.5 M) as a 2:1 molar ratio in 20mM HEPES pH 7.3 buffer, and a MnEDTA precipitate was formed overnight. The precipitated complex was centrifuged, washed with water and methanol, and dried by

lyophilization. The lipids 1,2-dihexanoyl-sn-glycero-3-phosphocholine (DHPC) and 1,2-dimyristoyl-sn-glycero-3-phosphocholine (DMPC) were purchased from Avanti Polar Lipids, Inc. MTSL, 5-DOXYL-stearic acid, free radical (5DSA), ascorbic acid and deuterium oxide (D2O) were obtained from Sigma. ^{13}C-glucose and $(^{15}NH_4)_2SO_4$ were obtained from Cambridge Isotope Laboratories. TrisHCl buffer were obtained from Teknova, Inc. Dithiothreitol (DTT) and HEPES buffer were purchased from Invitrogen Corporation.

The expression and purification of VpuFull, VpuCyto and mutants were performed similarly to the methods described previously (128,129). Briefly, the proteins were overexpressed in BL21-CodonPlus competent cells and Overexpress C41 (DE3) competent cells, respectively for VpuCyto and VpuFull in LB or minimal M9 growth media with $(^{15}NH_4)_2SO_4$ and/or ^{13}C-glucose for preparation of unlabeled or isotopically labeled samples. The proteins were isolated using nickel affinity chromatography, and then separated from the fusion partner by cyanogen bromide cleavage, followed by reverse phase high performance liquid chromatography (HPLC) for final purification. The molecular weight of the purified protein was confirmed to be correct using SDS-PAGE and Matrix-assisted laser desorption/ionization *(*MALDI) mass spectrometry. Milligram amounts of the isotopically labeled protein were obtained for the NMR experiments.

Protein samples for solution NMR were prepared by dissolving purified and lyophilized VpuCyto protein powder in either aqueous solution with 10%(V/V) D_2O with the pH adjusted to 3.0, or aqueous solution containing 100 mM DHPC with 10% (v/v) D_2O with the pH adjusted to 4.0. For RDC measurements, DHPC containing VpuCyto was weakly aligned in vertically stretched 6% polyacrylamide gels, as previously described

(130). Proteoliposome samples for solid-state MAS experiments were prepared by first mixing purified lyophilized Vpu powder with DMPC powder (1:3.5 mass ratio) and dissolving in 10% SDS buffer to obtain a clear solution with 10mg/mL DMPC concentration. Then the sample was diluted 20-fold, and incubated at room temperature for 4 hours. Subsequently, SDS was removed from the solution by first dialysis against 20mM HEPES, pH 7.3 buffer overnight, and then 5 days dialysis against 20 mM KCl in 20 mM HEPES, pH 7.3. After dialysis, the proteoliposomes were collected by ultracentrifugation at 235,000 ×g overnight at 15 °C. The concentrated proteoliposome sample was packed into a 3.2 mm MAS rotor for solid-state NMR experiments.

To measure PREs, the cysteines in each of the mutants were covalently linked to (1-oxyl-2,2,5,5-tetramethyl-3-pyrroline-3-methyl) methanesulfonate (MTSL) using the following protocol (54). Purified, lyophilized mutant protein powder was dissolved in 8 M urea in 20 mM TrisHCl, pH 8.0 with 20-fold molar excess of dithiothreitol (DTT) and incubated for 2 hours. Then the protein solution was run over a G10 desalting column pre-equilibrated with urea buffer to remove DTT. A 10-fold excess of MTSL dissolved in acetonitrile was added to the reduced protein, and the mixture was incubated in the dark at room temperature overnight. Free MTSL was separated from MTSL-labeled protein by passing the sample through a G10 desalting column followed by dialyzed against water for a day. The protein precipitated during dialysis, and the MTSL-labeled protein was obtained by lyophilization. For solution NMR measurements, MTSL-labeled protein was refolded in 100 mM DHPC micelles with a final protein concentration of ~0.1 mM. For MAS experiments, MTSL-labeled protein was reconstituted into proteoliposomes with DMPC, as previously described. MTSL-labeled protein was reduced by addition a 10-fold excess

of ascorbic acid in either micelles or liposomes. 5SDA and/or MnEDTA were incorporated into either VpuCyto in 100 mM DHPC or VpuFull in DMPC proteolipsomes to a final concentration of 0.5 mM for 5SDA and 1 mM for MnEDTA respectively.

The secondary structures of VpuFull in DHPC micelles, VpuCyto in aqueous media and DHPC micelles were analyzed by CD spectroscopy in the far UV (176 - 260 nm) region. Lyophilized protein was dissolved in either H_2O or 100mM DHPC to a final concentration of 1 mg/mL to obtain the spectra. Samples were transferred to a 0.1 mm path-length cell for data collection. (NSG Precision Cells, Inc., Farmingdale, NY) Data were collected on an AVIV model 2.98 at 25 °C, in 1.0 nm wavelength interval. Data was analyzed using an online server DichroWeb (131,132).

For MAS solid-state experiments, ^{13}C-detected cross polarization (CP) spectra were acquired with MAS spinning speed of 5K Hz from 5 °C to 30 °C to determine the minimum temperature that allows VpuFull to undergo fast rotational diffusion about the bilayer normal. Two- and three-dimensional experiments were acquired with MAS spinning speed of 10K Hz, at 25 °C. $^{13}C/^{13}C$ correlations were obtained with 50 ms mixing of proton-driven spin diffusion (PDSD) (133) and 200 ms mixing of dipolar-assisted rotational resonance (DARR) (134,135), and magnetization transform from ^{15}N to $^{13}C\alpha$ were obtained with SPECIFIC-CP (136). The ^{15}N and $^{13}C\alpha$ chemical shifts were assigned with 3D NCACX and NCOCX experiments. The ^{1}H-^{13}C and ^{1}H-^{15}N dipolar couplings were assigned based on a combination of assigned chemical shifts and 3D separated local field (SLF) experiments including ^{1}H-$^{13}C/N/C\alpha$ and ^{1}H-$^{15}N/N/C\alpha$, where $R18^{7}_{1}$ pulse sequences (137) with 100 kHz ^{1}H B_1 fields, were implemented to acquire heteronuclear dipolar couplings. Details of all the experiments can be found in Table 2.2. All the experiments

were performed at 700 MHz using a home-built triple-resonance MAS probe and a Bruker Avance II console. All of the NMR data were processed using NMRPipe (138) and analyzed with Sparky. All of the figures were prepared using Sparky (T. D. Goddard and D. G. Kneller, SPARKY 3, University of California, San Francisco). The resonance intensities and chemical shifts were extracted using Sparky.

Solution NMR experiments were performed on Bruker Avance 600 MHz and Varian 800 MHz spectrometers equipped with 5 mm z-axis pulse-field gradient, $^{1}H/^{15}N/^{13}C$ triple resonance cryoprobes. All of the experiments were performed at 50 °C. Triple-resonance HNCA, HNCACB, HN(CO)CA and HNCO experiments were performed on uniformly ^{13}C and ^{15}N labeled protein for the backbone amide resonance assignments. The side-chain assignments were completed using HCC(CO)NH, CC(CO)NH and TOCSY-HSQC experiments. ^{1}H chemical shifts were referenced to the H_2O resonance frequency at 50 °C, ^{13}C chemical shifts were referenced to TPS, and ^{15}N chemical shifts were referenced to AMS. ^{15}N-edited NOESY-HSQC (mixing time, 120 ms) and ^{13}C-edited NOESY-HSQC (mixing time, 120 ms) experiments were performed to measure distance restraints. ^{15}N T_1 measurements were recorded with relaxation delays of 20, 220, 420, 620, 820, 1020, 1320, and 1520 ms.^{15}N T_2 measurements were recorded with relaxation delays of 10, 30, 50, 70, 90, 130, and 170 ms. Both T_1 and T_2 relaxation time were fitted and calculated using SPARKY. Heteronuclear ^{1}H-^{15}N NOEs were obtained using a gradient sensitivity enhanced ^{1}H-^{15}N NOE experiment, recorded with and without ^{1}H saturation after a relaxation delay of 4 s. The heteronuclear NOE values for each residue were calculated by comparing the peak intensities of cross-peaks in the presence and absence of ^{1}H saturation. RDCs were measured with HSQC in-phase and anti-phase (IPAP) experiments.

Structure calculations for VpuFull were carried out with Xplor-NIH[16]. A total of 100 structures were generated in the refinement step, and the 20 structures with lowest-energy were used for analysis. For structure calculation of VpuFull in proteoliposome, a three-step process was employed, and the lowest structures were chose as the initial structure for refinement in the following step. Dipolar couplings and torsion angle were used in the initial determination, and distance restraints between the residues and the plane distance restraints (139) were added into the second and third steps, sequentially, where kdih = 400 kcal mol^{-1} rad^{-2}, ^{1}H-^{15}N krdc was ramped from 0.01 to 2 kacal mol^{-1} rad^{-2}, and ^{1}H-^{13}C krdc was ramped from 0.01 to 1 kacal mol^{-1} rad^{-2}, know was rampped from 2 to 40 kcal mol^{-1} $Å^{-2}$, kplane was rampped from 0.01 to 5 kcal mol^{-1} $Å^{-2}$.

Structure calculations for VpuCyto were carried out with Xplor-NIH (51,52) *ab initio* simulated annealing protocol with two steps: (1) high temperature simulated annealing, and (2) refinement. The initial structures were generated from a extended random coil base on dihedral angle restraints derived from TALOS+ (50) and distance restraints derived from the NOE cross-peaks in the simulated annealing. Residual dipolar couplings as angular restraints and paramagnetic relaxation data as distance restraints were incorporated during the refinement step. Simulated annealing was performed with a starting temperature of 3500 K and cooling to 25 K in steps of 12.5 K. kdih = 400 kcal mol^{-1} rad^{-2}. Knoe was rampped from 2 to 50 kcal mol^{-1} $Å^{-2}$. The refinement was performed with Xplor-NIH torsion angle molecular dynamics and experimental restraints included. The temperature was cooled to 50 K from an initial value of 2000 K in steps of 12.5 K. kdih = 400 kcal mol^{-1} rad^{-2}, knoe = 40 kcal mol^{-1} A^{-2}, krdc was ramped from 0.2 to 2 kacal mol^{-1} rad^{-2}.

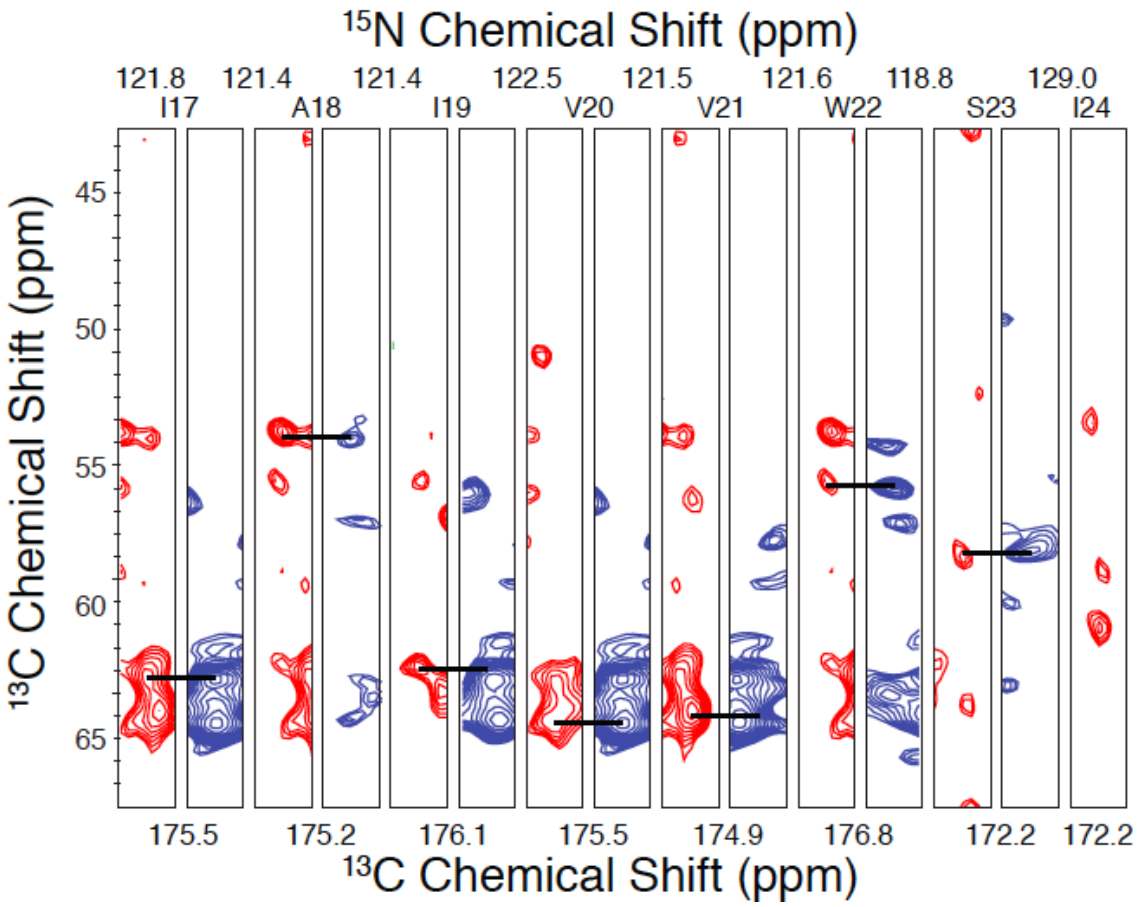

Figure 2.10 Backbone assignment of VpuFull in DMPC proteoliposomes.

Strip plots from NCACX (red) and NCOCX (blue) demonstrate the backbone walk on VpuFull.

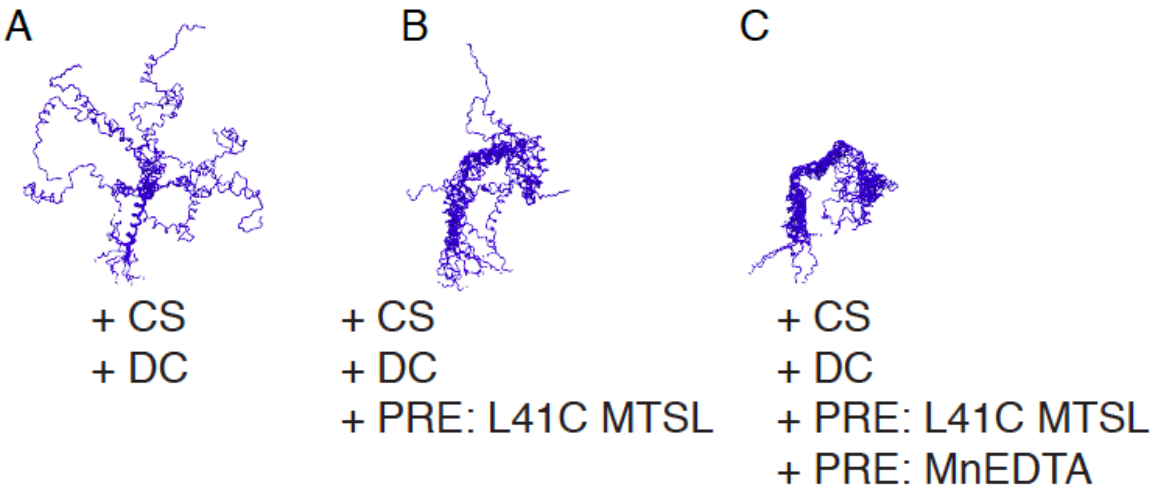

Figure 2.11 Structure refinement of VpuFull in DMPC proteoliposomes.

Ten lowest structures obtained in each step, and the structure with the lowest energy was used as the initial structure for the refinement in the next step. The restraints used in each step: A, ^{1}H-^{15}N and ^{1}H-^{13}C dipolar couplings and dihedral angles. B, Distance restraints derived from L41C-MTSL VpuFull plus the restraints used in (A.). C, Plane distance restraints derived from MnEDTA experiment plus the restraints used in (B.).

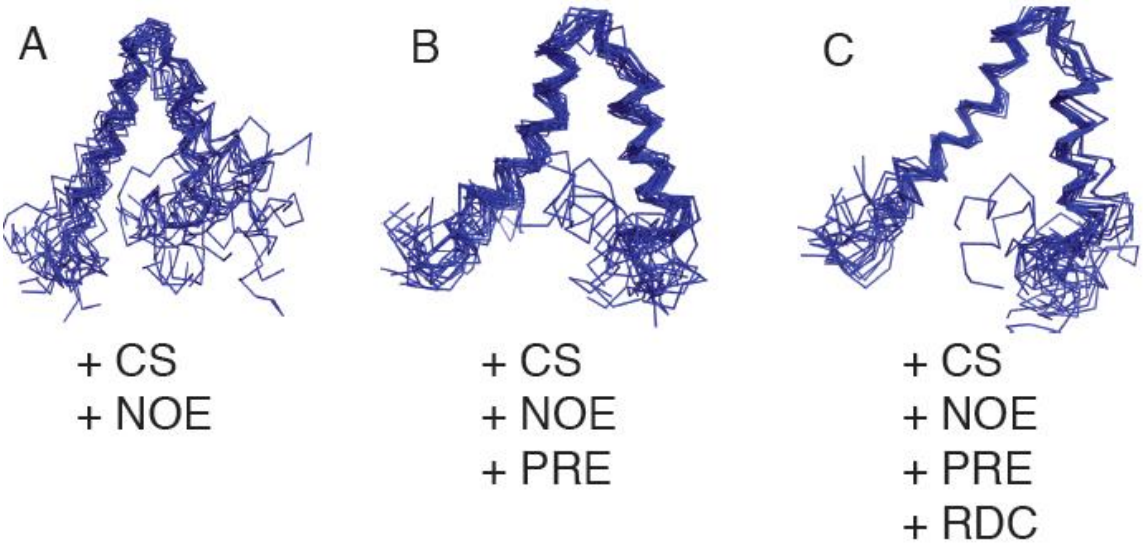

Figure 2.12 Structure refinement of VpuCyto in DHPC micelles.

Ensembles with 20 lowest energy structures obtained from A, Refinement with only chemical shift. B, Refinement with chemical shift and PRE. C, Refinement with both PRE and RDC.

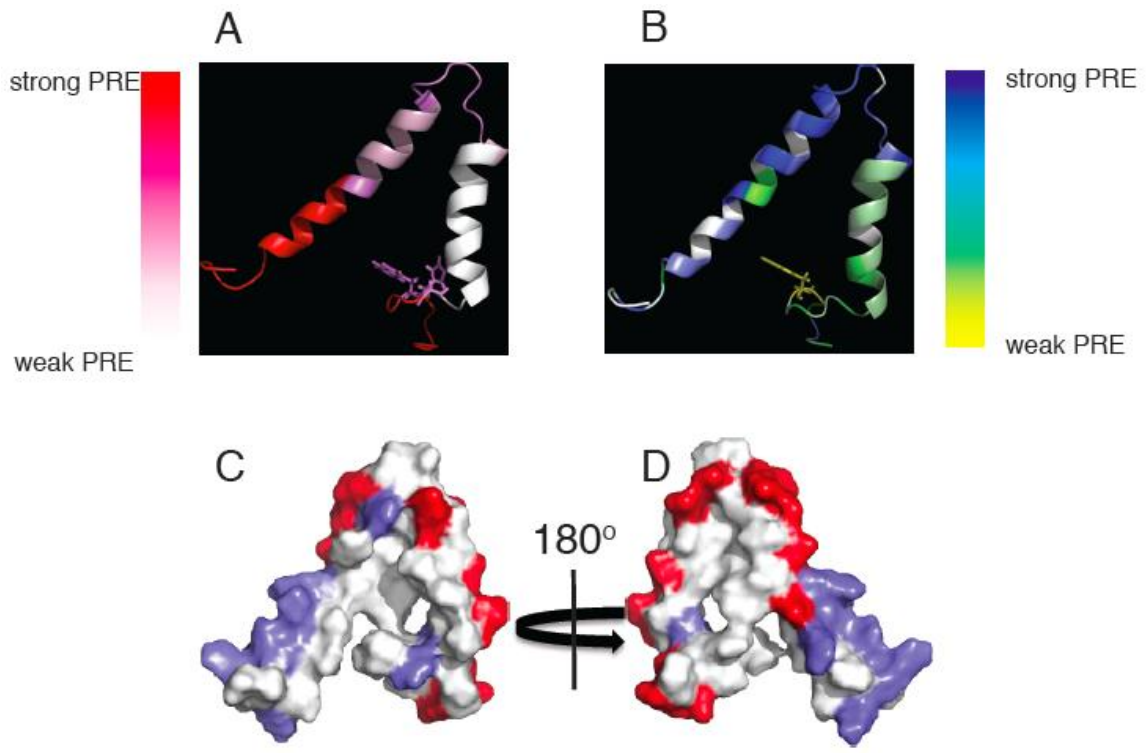

Figure 2.13. Micelles association of VpuCyto.

A, Residues colored according to the PRE effect observed upon addition of MnEDTA. B, Residues colored according to the PRE effect observed upon addition of 5SDA. C, The surface view of the lowest energy structure with acidic residues labeled red and basic residues labeled blue. D, 180° rotate through y axis of C.

All the experiments were acquired with 10,000 Hz of spinning rate, at 25 °C. Abbreviations used in the table: CP, cross-polarization; PDSD, proton driven spin diffusion; DARR, dipolar assisted rotational resonance; sw-TPPM, frequency-swift two-pulse phased-modulated; SPECIFIC-CP, spectrally induced filtering in combination with CP; TOBSY, through-bond correlation spectroscopy.

Table 2.2 Details of solid-state NMR experiments.

Two-dimensional $^{13}C/^{13}C$ correlation	
PDSD / DARR Mixing time [ms]	50 / 200
Acquisition time (t1 / t2) [ms]	2.6 / 12.9
Carrier frequency (t1 / t2) [ppm]	40 / 100
$\pi/2$ pulse (^{1}H / ^{13}C) [μs]	5 / 2.7
CP contact time [μs]	400
CP pulse shape (^{1}H)	Linear (100-50%)
CP rf field strength (^{1}H / ^{13}C) [kHz]	70 / 100
^{1}H decoupling field strength (sw-TPPM) [kHz]	100
Recycle delay (s) / number of acquisitions	2 / 1280, 3840 (PRE)
Spectral width (F1 / F2) [kHz]	12.32 / 39.68

Two-dimensional $^{15}N/^{13}C\alpha$ correlation	
Acquisition time (t1 / t2) [ms]	8.5 / 10.2
Carrier frequency (t1 / t2) [ppm]	120 / 100
$\pi/2$ pulse (^{1}H / ^{13}C) [μs]	5 / 2.7
CP contact time ($^{1}H/^{15}N$) [μs]	1000
CP pulse shape (^{1}H)	Linear (100-50%)
CP rf field strength (^{1}H / ^{15}N) [kHz]	75 / 43
SPECIFIC-CP contact time (^{15}N / ^{13}C) [μs]	4000
SPECIFIC-CP pulse shape (^{13}C)	Linear (100-90%)
SPECIFIC-CP rf field strength (^{15}N / ^{13}C) [kHz]	43 / 33
^{1}H decoupling field strength (sw-TPPM) [kHz]	100
Recycle delay (s) / number of acquisitions	2 / 2624
Spectral width (F1 / F2) [kHz]	2.84 / 50

Two-dimensional ^{1}H-$^{13}C/^{13}C\alpha$ SLF	
Acquisition time (t1 / t2) [ms]	5.28 / 10.24
Carrier frequency (^{1}H / ^{13}C) [ppm]	8 / 100
$\pi/2$ pulse (^{1}H / ^{13}C) [μs]	2.7 / 5
CP contact time [μs]	400
CP pulse shape (^{1}H)	Linear (100-50%)
CP rf field strength (^{1}H / ^{13}C) [kHz]	70 / 100
$R18^{7}_{1}$ pulse length [μs]	5
^{1}H decoupling field strength (sw-TPPM) [kHz]	100
Recycle delay (s) / number of acquisitions	2 / 512
Spectral width (F1 / F2) [kHz]	30.03 / 100

Table 2.2 Details of solid-state NMR experiments, continued.

Two-dimensional ^{1}H-$^{15}N/^{13}C\alpha$ SLF	
Acquisition time (t1 / t2) [ms]	1.2 / 10.24
Carrier frequency (^{1}H / ^{13}C / ^{15}N) [ppm]	8 / 100 / 120
$\pi/2$ pulse (^{1}H / ^{13}C / ^{15}N) [μs]	2.7 / 5 / 5.8
CP contact time ($^{1}H/^{15}N$) [μs]	1000
CP pulse shape (^{1}H)	Linear (100-50%)
CP rf field strength (^{1}H / ^{15}N) [kHz]	75 / 43
SPECIFIC-CP contact time ($^{15}N/^{13}C$) [μs]	4000
SPECIFIC-CP pulse shape (^{13}C)	Linear (100-90%)
SPECIFIC-CP rf field strength (^{15}N / ^{13}C) [kHz]	43 / 33
$R18^{7}_{1}$ pulse length [μs]	5
^{1}H decoupling field strength (sw-TPPM) [kHz]	100
Recycle delay (s) / number of acquisitions	2 / 1216
Spectral width (F1 / F2 / F3) [kHz]	10 / 50

Two-dimensional TOBSY $^{13}C/^{13}C$ correlation	
Acquisition time (t1 / t2) [ms]	9.5 / 20.48
Carrier frequency (t1 / t2) [ppm]	80 / 80
$\pi/2$ pulse (^{1}H / ^{13}C) [μs]	2.7 / 5
J-evolution period for $^{1}H/^{13}C$ transfer and refocusing [ms]	1
Adiabatic pulse shape / pulse length	tanh tan / 90
TOBSY mixing period [ms]	11.34
^{1}H decoupling field strength (sw-TPPM) [kHz]	50
Recycle delay (s) / number of acquisitions	2 / 64
Spectral width (F1 / F2) [kHz]	26.32 / 50

Three-dimensional assignments	$^{15}N/^{13}C\alpha/^{13}C$
Acquisition time (t1 / t2 / t3) [ms]	1.51 / 2.82 / 10.2
Carrier frequency (t1 / t2 / t3) [ppm]	120 / 55 / 100
$\pi/2$ pulse (^{1}H / ^{13}C / ^{15}N) [μs]	2.7 / 5 / 5.8
CP contact time ($^{1}H/^{15}N$) [μs]	1000
CP pulse shape (^{1}H)	Linear (100-50%)
CP rf field strength (^{1}H / ^{15}N) [kHz]	75 / 43
SPECIFIC-CP contact time ($^{15}N/^{13}C$) [μs]	4000
SPECIFIC-CP pulse shape (^{13}C)	Linear (100-90%)
SPECIFIC-CP rf field strength (^{15}N / ^{13}C) [kHz]	43 / 33
^{1}H decoupling field strength (sw-TPPM) [kHz]	100
DARR mixing time [ms]	20
Recycle delay (s) / number of acquisitions	2 / 240
Spectral width (F1 / F2 / F3) [kHz]	5.67 / 10.56 / 50

Table 2.2 Details of solid-state NMR experiments, continued.

Three-dimensional assignments	$^{15}N/^{13}C'/^{13}C$
Acquisition time (t1 / t2 / t3) [ms]	1.11 / 8.5 / 10.2
Carrier frequency (t1 / t2 / t3) [ppm]	120 / 175 / 100
π/2 pulse (^{1}H / ^{13}C / ^{15}N) [μs]	2.7 / 5 / 5.8
CP contact time ($^{1}H/^{15}N$) [μs]	1000
CP pulse shape (^{1}H)	Linear (100-50%)
CP rf field strength (^{1}H / ^{15}N) [kHz]	75 / 43
SPECIFIC-CP contact time ($^{15}N/^{13}C$) [μs]	4000
SPECIFIC-CP pulse shape (^{13}C)	Linear (100-90%)
SPECIFIC-CP rf field strength (^{15}N / ^{13}C) [kHz]	43 / 33
^{1}H decoupling field strength (sw-TPPM) [kHz]	100
DARR mixing time [ms]	20
Recycle delay (s) / number of acquisitions	2 / 480
Spectral width (F1 / F2 / F3) [kHz]	5.67 / 10.56 / 50

Three-dimensional SLF	^{1}H-$^{15}N/^{15}N/^{13}C\alpha$
Acquisition time (t1 / t2 / t3) [ms]	2.21 / 8.5 / 10.2
Carrier frequency (^{1}H / ^{13}C / ^{15}N) [ppm]	8 / 100 / 120
π/2 pulse (^{1}H / ^{13}C / ^{15}N) [μs]	2.7 / 5 / 5.8
CP contact time ($^{1}H/^{15}N$) [μs]	1000
CP pulse shape (^{1}H)	Linear (100-50%)
CP rf field strength (^{1}H / ^{15}N) [kHz]	75 / 43
SPECIFIC-CP contact time ($^{15}N/^{13}C$) [μs]	4000
SPECIFIC-CP pulse shape (^{13}C)	Linear (100-90%)
SPECIFIC-CP rf field strength (^{15}N / ^{13}C) [kHz]	43 / 33
$R18^{7}_{1}$ pulse length [μs]	5
^{1}H decoupling field strength (sw-TPPM) [kHz]	100
Recycle delay (s) / number of acquisitions	2 / 576
Spectral width (F1 / F2 / F3) [kHz]	10.01 / 2.5 / 39.68

Table 2.2 Details of solid-state NMR experiments, continued.

Three-dimensional SLF	^{1}H-^{13}C/^{15}N/^{13}Cα
Acquisition time (t1 / t2 / t3) [ms]	1.11 / 8.5 / 10.2
Carrier frequency (^{1}H / ^{13}C / ^{15}N) [ppm]	8 / 100 / 120
π/2 pulse (^{1}H / ^{13}C / ^{15}N) [μs]	2.7 / 5 / 5.8
CP contact time (^{1}H/^{15}N) [μs]	1000
CP pulse shape (^{1}H)	Linear (100-50%)
CP rf field strength (^{1}H / ^{15}N) [kHz]	75 / 43
SPECIFIC-CP contact time (^{15}N/^{13}C) [μs]	4000
SPECIFIC-CP pulse shape (^{13}C)	Linear (100-90%)
SPECIFIC-CP rf field strength (^{15}N / ^{13}C) [kHz]	43 / 33
$R18^{7}_{1}$ pulse length [μs]	5
^{1}H decoupling field strength (sw-TPPM) [kHz]	100
Recycle delay (s) / number of acquisitions	2 / 512
Spectral width (F1 / F2 / F3) [kHz]	30.03 / 2.5 / 39.68

Chapter 2, in full, is currently being prepared for submission for publication of the material. Zhang, H., Lin, E. C., Tian, Y., Das, B. B., and Opella, S. J. The dissertation author was the primary investigator and author of this material.

Chapter 3 Membrane Anchoring by a C-terminal Tryptophan Enables HIV-1 Vpu to Displace BST2 from Sites of Viral Assembly

3.1 Abstract

The restriction factor BST2 (tetherin) prevents the release of enveloped viruses from the host cell and is counteracted by HIV-1 Vpu. Vpu and BST2 interact directly via their transmembrane domains. This interaction enables Vpu to induce the surface-downregulation and the degradation of BST2, but neither of these activities fully accounts for Vpu's ability to enhance virion release. During a study of naturally occurring Vpu proteins, we found that a tryptophan residue near the Vpu C-terminus is particularly important for enhancing virion release. Vpu proteins with a W76G polymorphism degraded and downregulated BST2 from the cell surface, yet they inefficiently stimulated virion release. Here we explore the mechanism of this anomaly. We find that W76 is critical for the ability of Vpu to displace BST2 from sites of viral assembly in the plane of the plasma membrane. This effect does not appear to involve a general reorganization of the membrane microdomains associated with virion assembly, but rather is a specific effect of Vpu on BST2. Using NMR spectroscopy, we find that the cytoplasmic domain of Vpu and W76 specifically interact with lipids. Moreover, paramagnetic relaxation enhancement studies show that W76 inserts into the lipid. These data are consistent with a model whereby W76 anchors the C-terminus of Vpu's cytoplasmic tail to the plasma membrane, enabling the movement of Vpu-bound BST2 away from viral assembly sites.

3.2 Introduction

HIV-1 counteracts the interferon-inducible restriction factor BST2[4]/tetherin with its accessory protein Vpu (140,141). BST2 entraps lipid enveloped virions as they bud from the plasma membrane, preventing their release. Vpu, a single-pass type I transmembrane protein (142), binds directly to BST2, a single-pass type II transmembrane protein with a GPI-anchor (143), via an anti-parallel interaction between the proteins' transmembrane domains (144-148). This interaction enables Vpu to decrease the concentration of BST2 on the plasma membrane and to induce the degradation of BST2 by an endo-lysosomal mechanism (146,147,149-152).

However, the analysis of certain Vpu mutants reveals that neither the surface-downregulation nor the degradation of BST2 strictly correlates with the ability of Vpu to enhance virion release. For example, site-directed mutation of the β-TrCP-binding-site, through which Vpu links its cellular targets to an E3 ubiquitin ligase complex, renders Vpu unable to degrade or downregulate BST2 (141,147,149,150,153), yet such a Vpu mutant (Vpu-S52,56N) can partially enhance virion release (147,150,154,155) compared to no Vpu (ΔVpu). The source of this residual activity has been attributed to the ability of Vpu to displace BST2 from virion-assembly sites in the plane of the membrane, an activity that has been roughly mapped to the C-terminal portion of Vpu's cytoplasmic domain (155). During an analysis of naturally occurring Vpu proteins, we found the converse phenotype: preserved ability to degrade and downregulate BST2 yet impaired enhancement of virion release (156). This phenotype mapped to a W76G polymorphism, a mutation that presumably arises in infected hosts to provide escape from cytotoxic T lymphocytes. Site-directed mutagenesis confirmed that optimal enhancement of virion release depends upon

W76, which is near the C-terminus of Vpu and is well conserved in certain HIV-1 clades (156). Substitution of a glycine for W76 impairs virion release without affecting the ability of Vpu to co-localize with BST2, to downregulate BST2 from the cell surface, or to reduce the steady-state amount of cellular BST2. Notably, the defect in virion release caused by the W76G-substitution is additive with that caused by mutation of the β-TrCP-binding site (S52,56N), indicating that the effects of these mutations are mechanistically distinct.

How W76 contributes to maximal virion release without affecting BST2 downregulation or degradation is investigated here. Our central hypothesis was that W76 is instrumental in the ability of Vpu to displace BST2 from sites of viral assembly along the plasma membrane (155). In support of this, we show using immunofluorescence microscopy that W76 is required for the displacement of BST2 from viral assembly sites by Vpu. Since BST2 has been proposed to link lipid rafts to each other (143,157) and to the actin cytoskeleton (158), we considered that Vpu might distort the membrane topology of viral assembly sites through its influence on BST2. Instead, we observed that cellular markers of lipid rafts and of tetraspanin-enriched membrane domains (TEMs), proteins that define the assembly sites of HIV-1 virions (159-161), remained associated with Gag, the viral structural protein that drives viral assembly, despite the Vpu-induced redistribution of BST2. To elaborate the mechanism of the displacement effect, we show using NMR spectroscopy that the Vpu cytoplasmic domain interacts with lipids, and we support a model in which W76 anchors the C-terminal region of the protein to the lipid bilayer. While this interaction was enhanced in the presence of lipid head groups of net positive charge, phenylalanine did not substitute functionally for tryptophan at this position; this result suggests that tryptophan's ability to bind lipid cannot be explained fully by a cation-π

interaction but likely depends on the residue's hydrophobic nature. Based on these data, we propose a refined topological model for the counteraction of BST2 by Vpu: tryptophan-mediated anchoring of the Vpu C-terminus to the lipid bilayer enables Vpu to displace BST2 from virion-assembly sites.

3.3 Experimental procedures

Plasmids, Cells, and Reagents—Proviral plasmids pNL4-3, pNL4-3ΔVpu (pNL4-3/Udel (162)), pNL4-3-Vpu-S52,56N (163), pNL4-3-Vpu-W76G (156), pNL4-3-S52,56N+W76G (156) and pNL4-3-Vpu-A10,14,18F (164) have been described previously. Rev-dependent FLAG-tagged Vpu expression constructs for NL4-3 Vpu, Vpu-S52,56N, Vpu-W76G, Vpu-S52,56N, and Vpu-S52,56N+W76G were described previously (156). Expression plasmids encoding Vpu-W76F and Vpu-S52,56N+W76F with a C-terminal FLAG tag were constructed by site-directed mutagenesis of expression constructs for NL4-3 Vpu and Vpu-S52,56N, respectively, using a QuikChange II site-directed mutagenesis kit (Agilent Technologies). For NMR studies, DNA encoding the Vpu NL4-3 strain cytoplasimic domain (VpuCyto) sequence was inserted into pHLV Trp-leader (TrpΔLE) vector for expression as a TrpΔLE fusion. The methionine in VpuCyto was substituted with leucine to facilitate protein purification. Mutant W76G VpuCyto and W76F VpuCyto were prepared using the QuikChange Lightning Site-Directed Mutagenesis Kit (Agilent Technologies) and primers synthesized by Integrated DNA Technologies. HeLa P4-R5 cells (165-167) were acquired from the NIH AIDS Research & Reference Reagent program from Nathaniel Landau and maintained in Dulbecco's modified Eagle's medium (DMEM) supplemented with 10% fetal bovine serum, penicillin-

streptomycin, and 1 μg/ml puromycin. The chelated manganese was prepared by adding excess manganese sulfate ($MnSO_4$) to EDTA (0.5M) in 20mM HEPES pH 7.3 buffer, and MnEDTA was precipitated overnight. The precipitated complex was collected by centrifugation, washed with methanol to remove excess amounts of $MnSO_4$ and EDTA, and dried by lyophilization. The lipids 1,2-dimyristoyl-sn-glycero-3-phosphocholine (DMPC), 1,2-dimyristoyl-sn-glycero-3-ethylphosphocholine (DMEPC), 1,2-dimyristoyl-3-trimethylammonium-propane (DMTAP), 3ß-[N-(N',N'-dimethylaminoethane) carbamoyl] cholesterol hydrochloride (DC-Cholesterol) and 1,2-dihexanoyl-sn-glycero-3-phosphocholine (DHPC) were purchased from Avanti Polar Lipids, Inc. 5-DOXYL-stearic acid, free radical (5DSA) and Deuterium oxide (D_2O) were obtained from Sigma.

Transfections—HeLa P4-R5 cells in 12-well plates were transfected with 600 ng proviral plasmid or 600 ng proviral mutant pNL4-3ΔVpu plus 500 ng Rev-dependent Vpu-FLAG expression plasmid in triplicate using Lipofectamine 2000 (Life Technologies). Interferon-treated cells were cultured in 30 ng/ml human interferon-α1 (Cell Signaling, 8927LC). Supernates and cells were harvested the next day for p24 ELISA, immunoblot analysis and staining for flow cytometry.

Virion Release Assays—Supernates from provirus-transfected HeLa P4-R5 cells were collected, pelleted through a 20% sucrose cushion, then measured for Gag by p24 ELISA (Advanced Bioscience Laboratories) as previously described (141,156).

Immunoblots—Immunoblot analysis for actin, BST2 and the FLAG epitope were performed as previously described (151,168), developed using enhanced chemiluminescence and imaged using the ChemiDoc MP System (Bio-Rad). For PNGase F treatment, lysates in 1X SDS-PAGE buffer were diluted two-fold with water, G7

Reaction Buffer (NEB) and NP40, then treated with PNGase F (Glycerol Free, NEB, P0705S) for 2 hours at 37°C according to the manufacturer's instructions before immunoblotting.

Flow Cytometry—Transfected HeLa P4-R5 cells were stained with Alexa Fluor 647 anti-human CD317 (BST2, tetherin; RS38E [Biolegend]), or Alexa Fluor 647 mouse IgG1, κ isotype control, according to manufacturer's instructions, fixed and permeabilized using a BD Cytofix/Cytoperm kit according to the manufacturer's instructions, followed by staining with fluorescein isothiocyanate (FITC)-conjugated anti-HIV-1 p24 antibody (KC57; Beckman Coulter) as previously described (156). Surface expression of BST2 was analyzed using a BD Accuri C6 flow cytometer after gating on live p24-positive cells.

Immunofluorescence Microscopy—HeLa P4-R5 cells were plated at 120,000 per well on glass coverslips in a 24-well plate. The following day, they were transfected with 800 ng of proviral plasmid using Lipofectamine 2000 (Life Technologies). Four to six hours after transfection, the cell culture medium was changed to DMEM supplemented with 10% fetal bovine serum and penicillin-streptomycin. For studies of BST2 localization, 1000 U/ml human interferon-α A/D (Sigma) was also added to the culture medium. For studies of Gag/BST2 and Gag/BST2/Vpu colocalization, 24 hours post-transfection, the cells were fixed with 3% paraformaldehyde in PBS for 15 minutes at 4°C, washed twice with PBS, then permeabilized with 0.2% NP-40 for 7 minutes at 4°C. Fixed and permeabilized cells were washed twice with PBS, then blocked with 5% normal donkey serum and 3% BSA for 30 minutes at 4°C. Cells were stained with rabbit anti-Vpu antiserum (from the NIH AIDS Research and Reference Reagent Program, contributed by Klaus Strebel) diluted 1:800 and/or mouse anti-BST2/HM1.24/CD317 antibody (Chugai

Pharmaceutical Co., Kanagawa, Japan) diluted 1:250 for 30 min at 4°C. Cells were washed three times with PBS, then incubated with Alexa Fluor 647-conjugated donkey-anti-rabbit antibody and/or Rhodamine Red-X-conjugated donkey-anti-mouse antibody (Jackson ImmunoResearch) diluted 1:150 for 30 minutes at 4°C, then washed four times with PBS. Cells were blocked with 5% mouse antiserum for 30 minutes at 4°C, washed four times with PBS, then stained with FITC-mouse-anti-p24 (KC57) antibody (Beckman Coulter) diluted 1:150 for 30 minutes at 4°C. The cells were washed 5 times with PBS, mounted, and imaged using a fluorescence microscope (Olympus) and SlideBook version 4.1 software (Intelligent Imaging Innovations, Denver, CO). For each field, a series of images along the Z axis was collected, the images were deconvolved using the nearest-neighbor method, and a representative single image plane was chosen. Images were assembled using Adobe Photoshop software. For studies of Env and BST2 colocalization, cells were plated and transfected as above, then after 24 hours blocked with 3% BSA, 5% donkey and 5% human serum in PBS for 30 minutes at 4°C. Cells were stained with mouse anti-BST2/HM1.24/CD317 antibody (Chugai) diluted 1:250 and human anti-Env (2G12, from the NIH AIDS Research and Reference Reagent Program) diluted 1:150 for 30 minutes at 4°C. Cells were washed three times with PBS, then stained with FITC-conjugated donkey-anti-human antibody and Rhodamine Red-X-conjugated donkey-anti-mouse antibody (Jackson Immuno Research) diluted 1:150 for 30 minutes at 4°C, then washed six times with PBS and fixed, mounted and imaged as above. For studies of Env and membrane microdomain markers CD55, CD59, and CD81, after blocking with 3% BSA, 5% donkey and 5% human serum in PBS for 30 minutes at 4°C, cells were stained with human anti-Env (2G12) diluted 1:150 and either mouse anti-CD55 (Biolegend) diluted 1:200, mouse

anti-CD59 (Biolegend) diluted 1:200 or mouse anti-CD81 (Biolegend) diluted 1:30 for 30 minutes at 4°C. Cells were washed three times with PBS, then stained with FITC-conjugated donkey-anti-human antibody and Rhodamine Red-X-conjugated donkey-anti-mouse antibody (Jackson ImmunoResearch) diluted 1:150 for 30 minutes at 4°C, then washed six times with PBS and fixed, mounted and imaged as above. For studies of Gag and membrane microdomain markers CD55, CD59, and CD81, after blocking with 3% BSA and 5% donkey serum in PBS for 30 minutes at 4°C, cells were stained with either mouse anti-CD55 (Biolegend) diluted 1:200, mouse anti-CD59 (Biolegend) diluted 1:200 or mouse anti-CD81 (Biolegend) diluted 1:30 for 30 minutes at 4°C. Cells were washed three times with PBS, then stained with Rhodamine Red-X-conjugated donkey-anti-mouse antibody (Jackson Immuno Research) diluted 1:150 for 30 minutes at 4°C, then washed four times with PBS. Cells were fixed with 3% paraformaldehyde for 15 minutes at 4°C, washed twice with PBS, then permeabilized with 0.2% NP-40 for 7 minutes at 4°C. Cells were washed twice with PBS, blocked with 5% mouse antiserum for 30 minutes at 4°C, washed four times with PBS, then stained with FITC-mouse-anti-p24 (KC57) antibody (Beckman Coulter) diluted 1:150 for 30 minutes at 4°C. Cells were washed six times with PBS before imaging as above.

Protein Expression—The expression and purification of VpuCyto and mutants were performed essentially as previously described (169). The protein was overexpressed in BL21-CodonPlus competent cells (Agilent) in M9 medium for isotopically labeled samples. Purification was performed using nickel affinity chromatography, cyanogen bromide cleavage from the fusion protein, a second nickel affinity chromatography, and

reverse phase HPLC. Milligram amounts of isotopically labeled protein were obtained for the NMR experiments.

Sample Preparation for NMR—Samples in micelles were prepared by dissolving purified and lyophilized protein powder of VpuCyto in an aqueous solution containing 100 mM DHPC with 10% (v/v) D_2O with pH adjusted to 4.0. Samples for paramagnetic relaxation enhancement (PRE) measurements were prepared by adding either MnEDTA powder or 5DSA powder to Vpu-containing DHPC in aqueous solution to a final concentration of 1mM for MnEDTA and 0.5mM for 5SDA.

Samples with liposomes were prepared by mixing the trifluoroethanol (TFE) dissolved protein with chloroform dissolved phospholipids, lipids and/or cholesterol and were vaporated under a stream of nitrogen followed by lyophilization to generate proteoliposome films. These films were hydrated at 42 °C with aqueous buffer and vortexed to a final concentration of 0.1mM protein and 1.8mM lipid, and the pH of the samples was adjusted to 3.0.

Solution NMR Spectroscopy and Data Processing—The NMR experiments were performed on a 600 MHz Bruker AVANCE spectrometer equipped with a 5-mm triple resonance cryoprobe (^{1}H, ^{13}C, and ^{15}N) and z axis pulsed gradient. All of the experiments were performed at 50°C. ^{1}H-^{15}N heteronuclear single quantum correlation (HSQC) experiments were acquired with 2048 and 256 points in the direct and indirect dimensions, respectively. Triple resonance HNCA, HNCACB, HN(CO)CA experiments were performed on uniformly ^{13}C and ^{15}N labeled protein samples to obtain the backbone amide resonance assignments. The NMR data were processed using NMRPipe (170) and the figures were displayed using Sparky (T. D. Goddard and D. G. Kneller, SPARKY 3,

University of California, San Francisco). The resonance intensities and chemical shifts were extracted using Sparky. Chemical shift perturbations were calculated using the following equation.

$$\Delta d = \frac{\sqrt{d_H^2 + (d_N / 5)^2}}{2}$$

3.4 Results

Mutation of Vpu W76 to Glycine Specifically Impairs Virion Release in Interferon-Treated Cells—We recently showed that mutation of W76 near the C-terminus of Vpu to glycine impairs the ability of Vpu to enhance virion release without affecting the surface-downregulation of BST2 (156). As BST2 is induced by interferon in response to HIV infection *in vivo* (171), we first evaluated the phenotypes of the Vpu-W76G mutant in the setting of the high levels of BST2 expression induced by α-interferon *in vitro*. HeLa P4-R5 cells were transfected in triplicate with NL4-3 proviral plasmids encoding no Vpu (NL4-3ΔVpu), wild-type Vpu, the β-TrCP-binding mutant Vpu-S52,56N, Vpu-W76G, and the combined mutant Vpu-S52,56N+W76G, and then treated (or not) with human interferon-α1 overnight. Viral supernates were harvested and pelleted through a 20% sucrose cushion to isolate virion-associated Gag/p24 before analysis by p24 ELISA. Cells were collected and lysed for immunoblot as well as stained for surface BST2 and intracellular p24 before analysis by flow cytometry (FACS). Figure 3.1A shows the results of ELISA for p24 released into the supernates. Vpu-W76G was as impaired for virion release enhancement as Vpu-S52,56N, which cannot degrade BST2. The combined mutant Vpu-S52,56N+W76G was as impaired for enhancement of virion release as the no Vpu

mutant (ΔVpu), indicating that the S52,56N and W76G mutations have additive effects and that these regions of Vpu likely contribute to its function by distinct mechanisms. These relationships recapitulated our previous findings, but here they hold in the setting of the increased levels of BST2 induced by interferon. An immunoblot of the cell lysates is shown in Figure 3.1B; the smears in the top panels are consistent with the reported heterogeneous glycosylation of BST2 in HeLa cells (151,172,173). In the bottom panels, the same lysates were treated with PNGase F, which cleaves N-linked glycans from BST2 and yielded discrete lower molecular weight bands. These immunoblots confirmed that BST2 expression was substantially increased with interferon treatment. They also show that Vpu-W76G induced nearly wild-type levels of BST2 degradation both in the presence or absence of interferon-treatment [compare lane 3 to 7 (no IFN) and 4 to 8 (with IFN)]. As expected, Vpu-S52,56N and Vpu-S52,56N+W76G did not degrade BST2 [compare lane 3 to 5 and 9 (no IFN); also lane 4 to 6 and 10 (+IFN)]. The surface-downregulation of BST2 was likewise similar for wild-type and W76G mutant Vpu. Figure 3.1C shows two-color FACS plots for BST2 surface staining (y-axis) versus intracellular p24 expression (x-axis) for these cells; the data indicate that the wild-type and the W76G mutant each downregulate BST2, whereas the Vpu-S52,56N and Vpu-S52,56N+W76G mutants fail to downregulate and cause a paradoxical increase in cell-surface BST2. Figure 3.1D shows the average MFI for surface BST2 in p24-positive (infected) cells measured in triplicate. In summary, in the presence or absence of interferon treatment, Vpu-W76G effectively downregulated BST2, while Vpu-S52,56N and Vpu-S52,56N+W76G did not. Yet, Vpu-W76G was impaired for virion release.

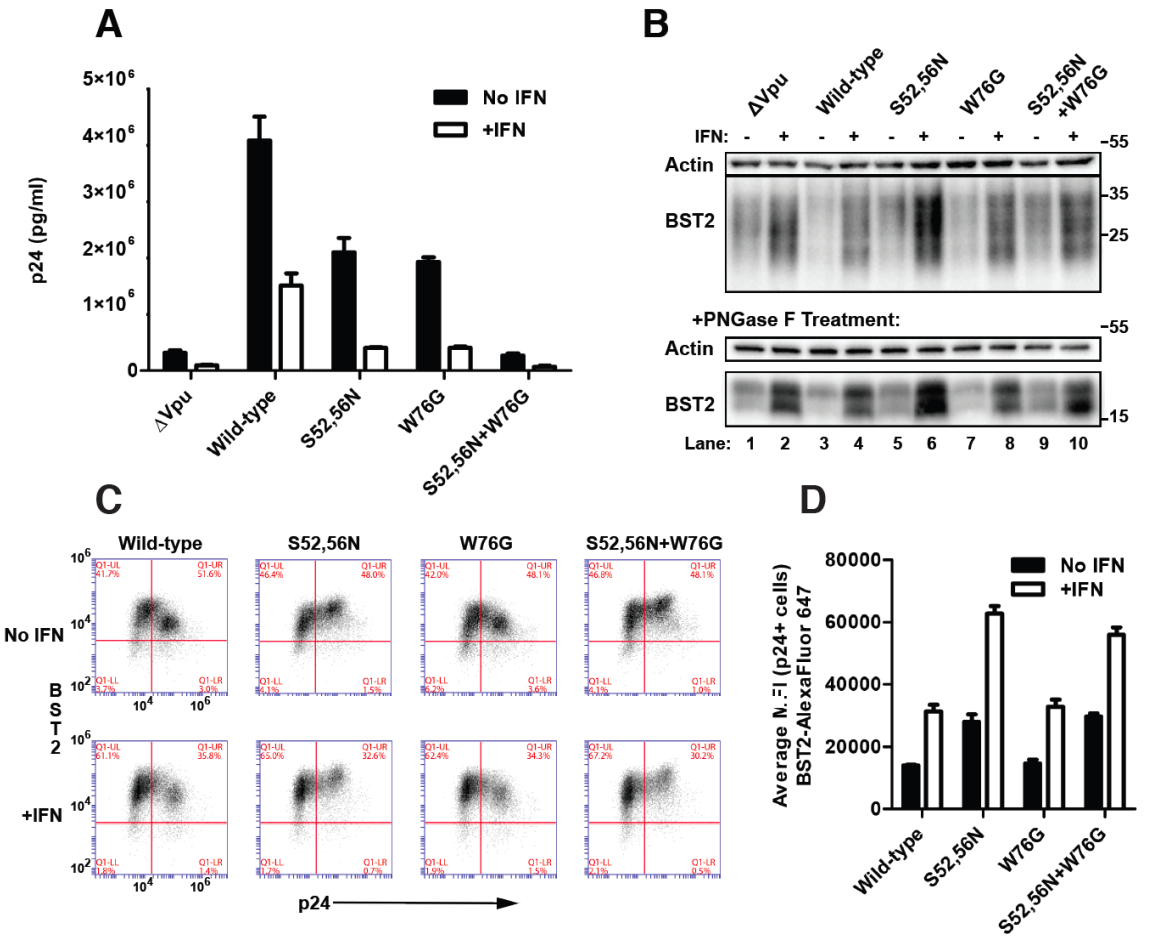

Figure 3.1 Characterization of W76G mutation in interferon-treated cells expressing high levels of BST2.

A, Enhancement of HIV-1 virion release by "wild-type" Vpu and site-directed mutants (ΔVpu, S52,56N, W76G and S52,56N+W76G). The concentration of pelletable p24 antigen in the culture supernates in triplicate was measured by ELISA. Error bars represent the standard deviation. B, Immunoblot analysis of cell lysates showing the induction of BST2 expression in HeLa-P4-R5 cells following treatment with interferon and degradation of BST2 by wild-type and W76G mutant Vpu. The top panels show untreated lysates, whereas the bottom panels show lysates that were treated with PNGase F. Actin is shown as a loading control. C, Downregulation of surface BST2 in cells transfected with proviral DNA harboring the indicated Vpu mutations in the absence (top panels) or presence (bottom) of interferon-α. Wild-type and W76G Vpu are able to downregulate surface BST2 while the S52,56N and S52,56N+W76G mutants are not, regardless of interferon treatment. The two-color plots show BST2 expression (y axis) versus intracellular p24 expression (x axis). Results are representative of triplicates. D, Bar graph of average MFI for surface BST2 in p24-positive cells. Error bars are the standard deviations of triplicates.

W76 is Required for the Displacement of BST2 from Sites of Viral Assembly—

Since the W76G substitution did not markedly affect either the surface-downregulation or

the degradation of BST2 by Vpu, but did impair the enhancement of virion release, we reasoned that this residue might play a role in the ability of Vpu to displace BST2 from sites of viral assembly within the plane of the plasma membrane (155). To test this, we transfected HeLa P4-R5 cells with HIV-1 (NL4-3) proviral plasmids encoding no Vpu (ΔVpu), wild-type, Vpu-S52,56N, Vpu-W76G, and Vpu-S52,56N+W76G and then treated the cells with human interferon-α overnight. Cells were fixed, permeabilized and stained for BST2 and HIV Gag/p24, then analyzed by immunofluorescence microscopy as described in the Experimental Procedures. Figure 3.2A shows BST2 (in red), Gag (in green) and their overlap (in yellow) for cells transfected with the indicated Vpu-mutant proviral plasmids; the single image planes shown depict optical sections along the cover glass. In the absence of Vpu (ΔVpu), BST2 and Gag colocalized extensively as indicated by the substantial (yellow) overlap seen in the rightmost image. As reported previously (155), both wild-type Vpu and the β-TrCP-binding site mutant Vpu-S52,56N induced the displacement of BST2 from Gag at the plasma membrane. This is shown by the decrease in yellow color in the merged image for wild-type ("WT") and Vpu-S52,56N ("S52,56N") compared to ΔVpu in Figure 3.2A as well as the lower Pearson's correlation coefficients for the colocalization of BST2 and Gag in Figure 3.2B. The effect of wild-type Vpu on the colocalization of BST2 and Gag is likely due both to surface-downregulation as well as the displacement of BST2 from Gag in the plane of the plasma membrane. In contrast, Vpu-S52,56N was unable to downregulate BST2 (see Figure 3.1B, C and D), so that its ability to decrease the colocalization of BST2 and Gag in the plane of the plasma membrane is presumably due solely to the displacement effect. In the case of Vpu proteins with the W76G mutation, BST2 and Gag colocalized to a relatively greater extent; this was the case

both when Vpu-W76G was compared to wild-type Vpu (p-value 5.52×10^{-8}, unpaired t test) and when the combination mutant Vpu-S52,56N+W76G was compared to Vpu-S52,56N (p-value 2.22×10^{-14}, unpaired t test). Moreover, when the Vpu-S52,56N+W76G mutations were combined, the coefficient of correlation between Gag and BST2 was the same as when no Vpu was expressed (p-value 0.3407, unpaired t test). These data indicate that the colocalization of BST2 and Gag along the plasma membrane is inversely related to virion-release (compare Figure 3.1A with 3.2B). They also indicate that W76 is critical to the ability of Vpu to displace BST2 from Gag within the plane of the membrane.

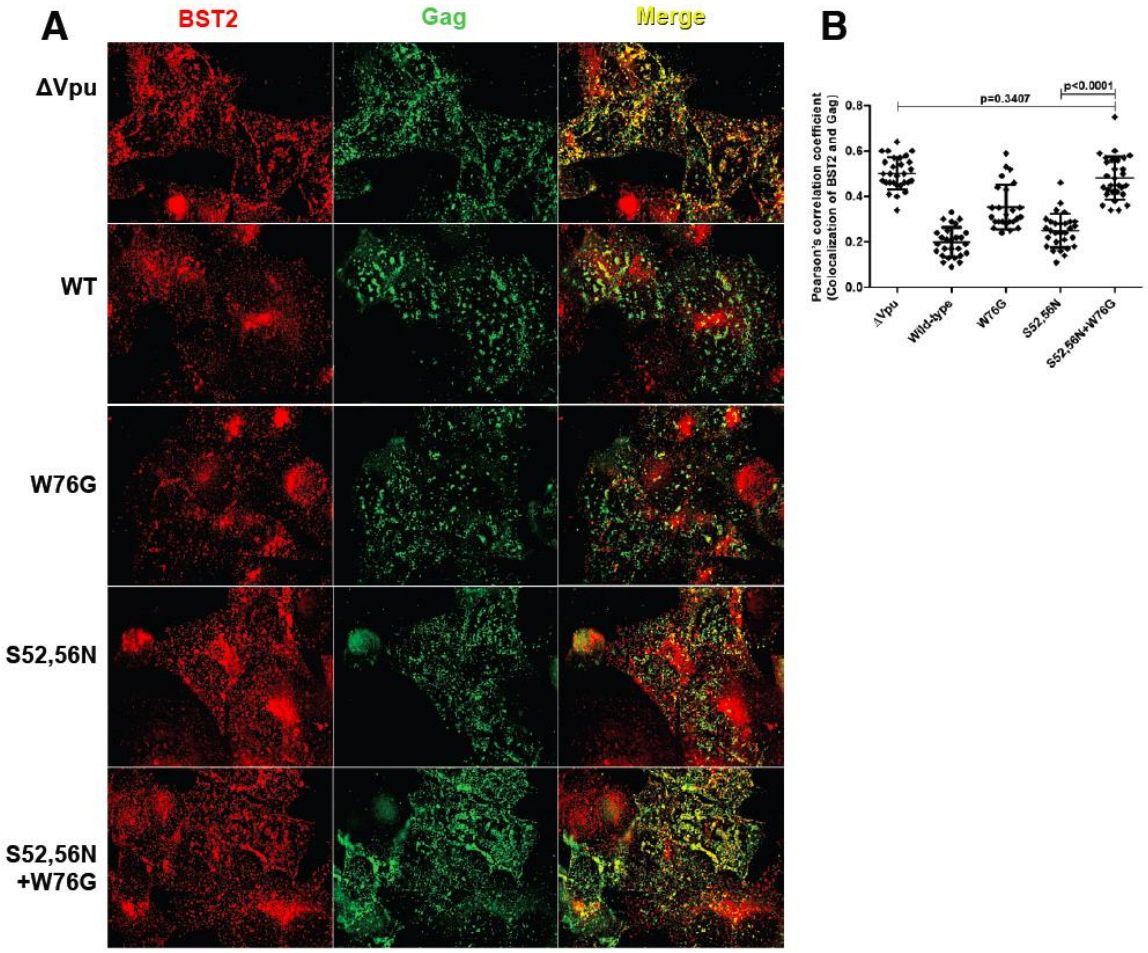

Figure 3.2 Vpu displaces BST2 from Gag in a W76-dependent manner.

A, HeLa P4-R5 cells were transfected with proviral plasmids, either pNL4-3 ("WT") or the indicated Vpu-mutants. The following day, the cells were fixed, permeabilized, and stained for p24 and BST2. Wide field images were acquired as a Z-series, and the plane along the cover-glass that captures the cell surface is shown after deconvolution of the image using a "nearest neighbors" algorithm. The left column shows anti-BST2 staining; the middle column shows anti-Gag/p24; and the right column shows a merged image in which the overlapping Gag and BST2 appears yellow. Wild-type ("WT") Vpu and the S52,56N mutant are each able to displace BST2 from Gag (compared to ΔVpu), and this activity is lost when W76 is mutated to G. B, Pearson's correlation coefficients for the colocalization of BST2 and Gag along the plasma membrane in the presence of Vpu or mutants from the experiment shown in A. At least 25 cells were assessed for each condition, using the image plane adjacent to the cover glass. Error bars are the standard deviations. P-values for unpaired two-tailed t tests were as noted on the graph and for ΔVpu vs. WT, W76G and S52,56N were <0.0001; for WT vs. S52,56N P=0.0094; for WT vs. W76G and S52,56N+W76G P<0.0001; and for W76G vs. S52,56N and S52,56N+W76G P<0.0001.

To confirm that our staining for Gag was consistent with virion assembly sites and not nonspecific aggregates of Gag, we stained the surface of virus-producing cells for the HIV-1 envelope glycoprotein (Env). When the relationship between BST2 and sites of viral assembly stained for Env was analyzed, a pattern similar to that seen with Gag emerged (Figure 3.3). For these experiments, HeLa P4-R5 cells were transfected with Vpu-mutant provirus as above, then the staining for Env and BST2 was performed to allow "copatching" of the proteins as described in the Experimental Procedures. In this technique, cells are labeled before chemical fixation at 4°C with primary and fluorophore-labeled secondary antibodies to detect the proteins of interest. This allows antibody-mediated crosslinking and aggregation ("co-patching") of the proteins, provided that they both initially reside in the same membrane microdomains. This approach yielded robust colocalization of BST2 and Env in the absence of Vpu. As shown in Figure 3.3A, BST2 is in red, Env is in green and regions of the plasma membrane where they overlap are shown in yellow in the merge column on the right. [Note that the single image planes shown here depict optical sections 1-3 μ above the cover glass, since the cell surface along the cover glass stained poorly without prior chemical fixation (data not shown).] Compared to provirus lacking *vpu* (ΔVpu), the colocalization of BST2 and Env was decreased by wild-type Vpu ("WT") and Vpu-S52,56N (Figure 3.3A), a conclusion supported by the lower Pearson's correlation coefficients for the colocalization of Env and BST2 (p-value for ΔVpu vs. WT: 3.79×10^{-13}, for ΔVpu vs. S52,56N: 5.93×10^{-8}, unpaired t test) in Figure 3.3B. Vpu-mutants W76G, S52,56N+W76G and the transmembrane domain mutant A10,14,18F (which does not bind BST2) permitted co-patching of Env and BST2 to levels near that of ΔVpu (p-values of 0.0810, 0.2486 and 0.7940, respectively, by unpaired t test),

indicating that these mutants are impaired in their ability to displace BST2 from sites of viral assembly. For Vpu-A10,14,18F, this impairment presumably relates to its inability to bind BST2(145).

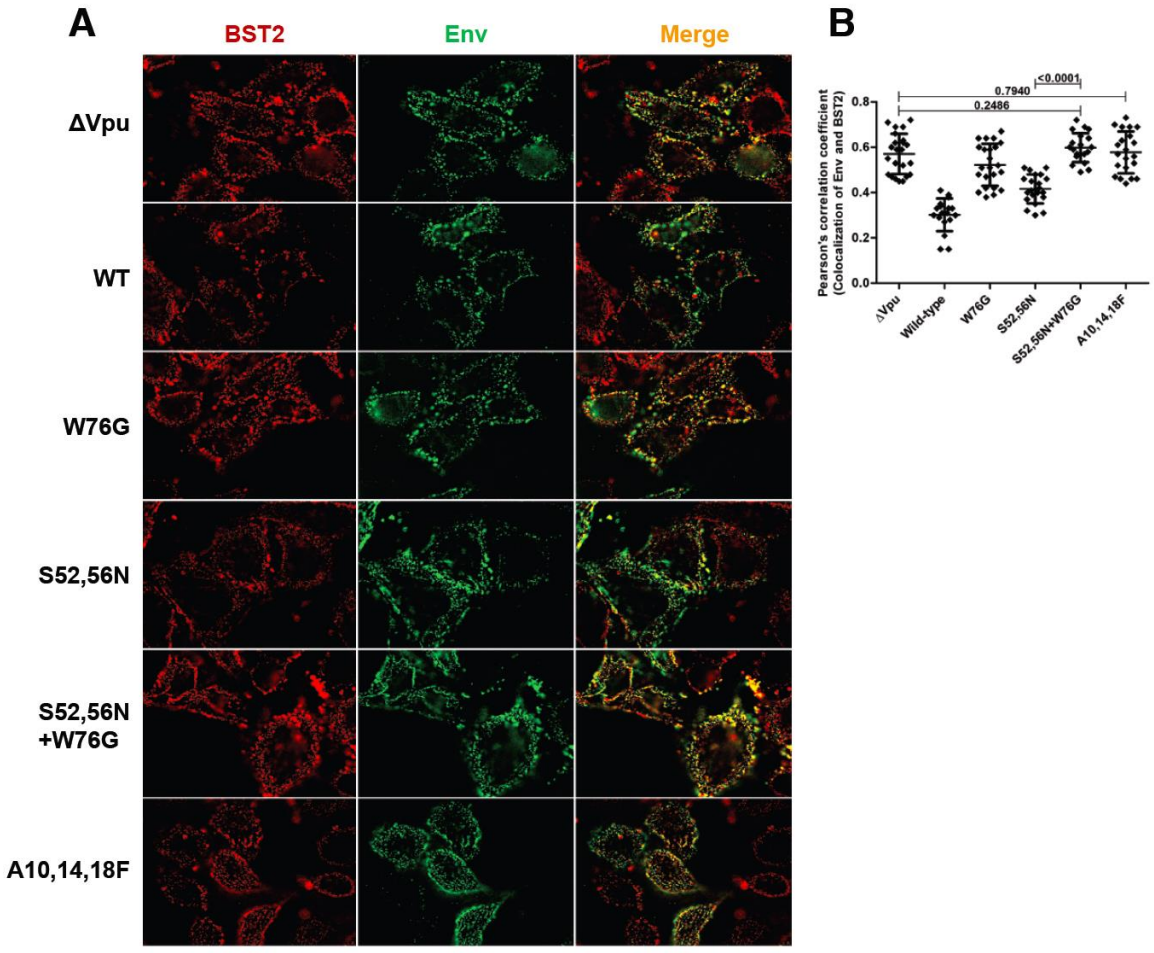

Figure 3.3 Staining for surface Env and BST2 in the presence of Vpu-mutants also reveals the displacement effect.

A, HeLa P4-R5 cells were transfected with the indicated proviral Vpu-mutant plasmids and the next day were stained for BST2 (in red) and Env (in green), then fixed and imaged. The merged image is shown on the right with BST2-Env overlap in yellow. Wild-type ("WT") Vpu and the S52,56N mutant are each able to displace BST2 from Env (compared to ΔVpu), and this activity is lost for W76G and for the Vpu transmembrane-domain mutant A10,14,18F, which is unable to interact with BST2. B, Pearson's correlation coefficients for the colocalization of BST2 and Env along the plasma membrane in the presence of Vpu or mutants from the experiment shown in A. At least 25 cells were assessed for each condition, using the image plane adjacent to the cover glass. Error bars are the standard deviations. P-values for unpaired two-tailed t tests were as noted on the graph and for ΔVpu vs. WT and S52,56N were <0.0001; for ΔVpu vs. W76G P=0.0810; for WT vs. W76G, S52,56N, S52,56N+W76G, and A10,14,18F P<0.0001; for W76G vs. S52,56N P<0.0001; for W76G vs. S52,56N+W76G P=0.0037; for W76G vs. A10,14,18F P=0.0554; for S52,56N vs. A10,14,18F P<0.0001; and for S52,56N+W76G vs. A10,14,18F P=0.4075.

The most straightforward model for the W76-dependent ability of Vpu to displace BST2 from sites of viral assembly involves a direct interaction between Vpu and BST2 at the plasma membrane. However, whether Vpu acts at the plasma membrane is somewhat controversial, with some data suggesting that the Vpu-BST2 interaction occurs within endosomes (149,174) and/or the *trans*-Golgi network (146,175-177) while other findings support a role for Vpu at the plasma membrane (147,178). To investigate whether Vpu is positioned on or near the plasma membrane and to confirm that the displacement effect requires the interaction between the two proteins, we transfected HeLa P4-R5 cells with provirus harboring *vpu* mutants ΔVpu, Vpu-S52,56N or the transmembrane domain mutant Vpu-A10,14,18F; stained the cells for BST2, Gag and Vpu; and then imaged as described in the Experimental Procedures. Figure 3.4A shows expression of BST2 in red, Gag in green, and Vpu in blue with overlap shown in the merge column on the right. As in Figure 3.2, the single image planes shown depict optical sections along the cover glass. Colocalization of BST2 and Vpu is shown in magenta, and as expected was less for the Vpu-A10,14,18F, as these mutations disrupt the interaction between Vpu and BST2 (see Pearson's correlation coefficients for the colocalization of Vpu and BST2 in Figure 3.4B). Consistent with the data of Figure 3.2, the colocalization of BST2 and Gag (yellow in the merged image) was less for Vpu-S52,56N than for ΔVpu (Figure 3.4A and C), supporting the displacement effect. In contrast, Vpu-A10,14,18 F was inactive; in its presence, BST2 and Gag colocalized to levels similar to those seen in the case of ΔVpu (see Pearson's correlation coefficients for the colocalization of Gag and BST2 in Figure 3.4C). These imaging data are consistent with a location of Vpu on or near the plasma membrane, such that it can directly mediate the displacement effect. The data also confirm that the

interaction between the transmembrane domains of the proteins is required for Vpu to displace BST2 from viral assembly sites.

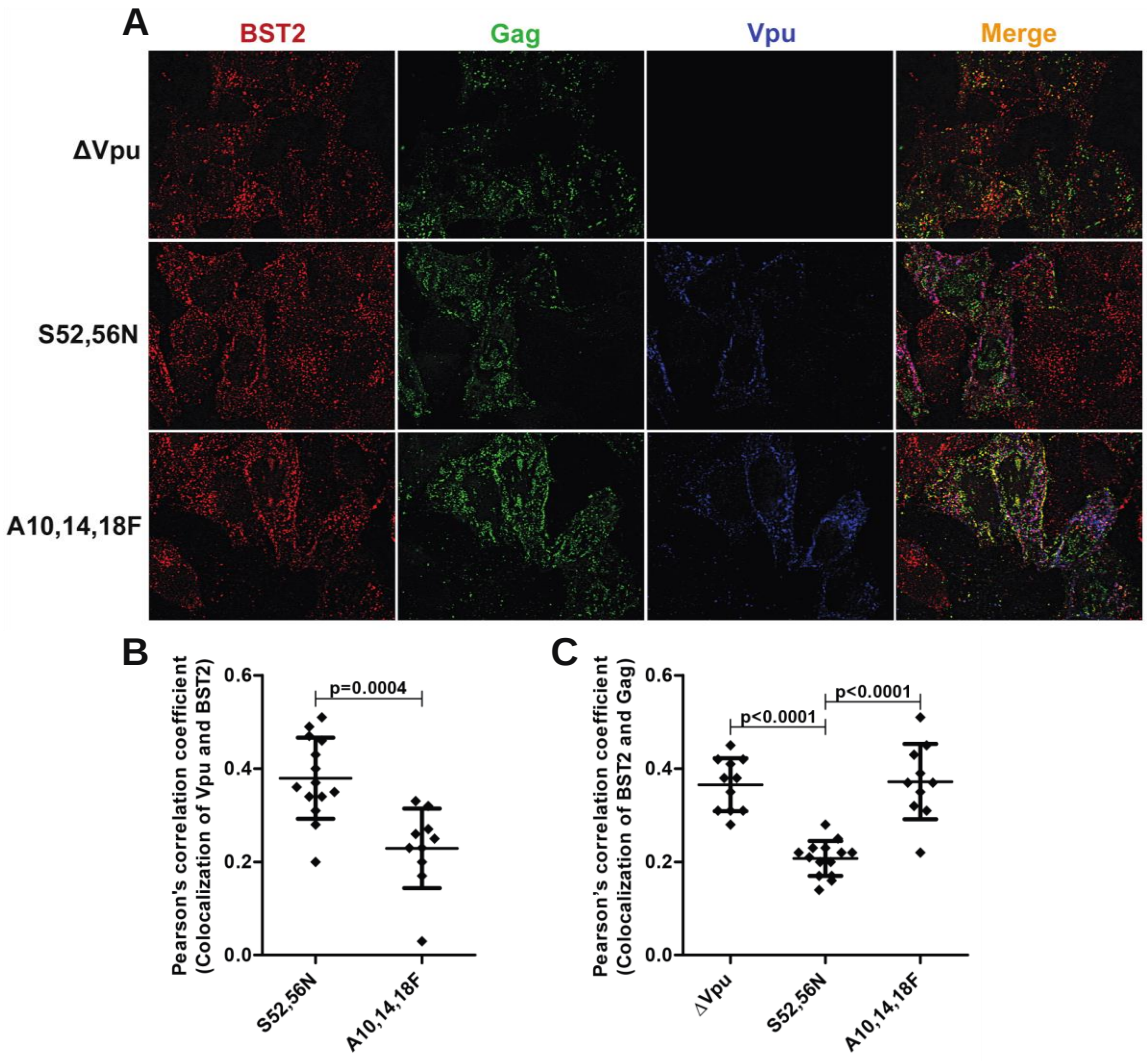

Figure 3.4 The location of Vpu relative to BST2 and Gag reveals that Vpu is positioned to mediate the displacement effect.

A, HeLa P4-R5 cells were transfected with HIV-1 (NL4-3) proviral plasmids encoding the indicated Vpu mutants, fixed, permeabilized, and stained for BST2 (first column, in red), Gag (second column, green), and Vpu (third column, blue). The merged image is shown on the right with BST2-Gag overlap in yellow, BST2-Vpu overlap in magenta and overlap of all three in white. B, Pearson's correlation coefficients for the colocalization of Vpu mutants and BST2 from the experiment shown in A. At least 25 cells were assessed for each condition, using the image plane adjacent to the cover glass. Error bars are the standard deviations. The P-value was calculated by unpaired two-tailed t test. C, Pearson's correlation coefficients for the colocalization of BST2 and Gag along the plasma membrane in the presence of Vpu or mutants from the experiment shown in A. At least 25 cells were assessed for each condition, using the image plane adjacent to the cover glass. Error bars are the standard deviations. The P-values were calculated by unpaired two-tailed t test. The P-value for ΔVpu vs. A10,14,18F was 0.8311.

Vpu does not Reorganize Membrane Microdomains during the Displacement of BST2 from Sites of Viral Assembly—BST2 has been proposed to link lipid rafts to each other and to the actin cytoskeleton (158,179), while HIV assembly sites are known to include both lipid-rafts and TEMs (159-161). In light of this, we wondered whether the displacement of BST2 from viral assembly sites by Vpu might disrupt the organization of membrane microdomains at assembly sites. To test this hypothesis, HeLa P4-R5 cells were transfected with proviral plasmids lacking *vpu* (ΔVpu) or encoding the Vpu-S52,56N mutant, then stained for either Gag or Env and a lipid raft marker (CD55 or CD59) or the tetraspanin CD81 in a co-patching experiment as described in the Experimental Procedures. Figure 3.5A shows the merged images for Gag staining in green on the left and Env staining in green on the right as well as the indicated membrane microdomain markers in red. Colocalization is shown in yellow. The images on the left in Figure 3.5A and the Pearson's correlation coefficients for the colocalization of Gag and the domain markers in Figure 3.5B show that the Vpu-S52,56N mutant displaced neither CD55 nor CD81 from Gag. Instead, we observed a small but statistically significant increase in the colocalization between Gag and CD55 ($p=0.0442$, unpaired t test), and Gag and CD81 ($p=0.0217$, unpaired t test), the cause of which is currently obscure. Results for another lipid raft marker, CD59, were similar to CD55 (data not shown). The right column of Figure 3.5A and the Pearson's correlation coefficients for the colocalization of Env and the domain markers in Figure 3.5C show that the expression of Vpu-S52,56N had no effect on the colocalization of Env and CD55 ($p=0.4653$, unpaired t test) or CD81 ($p=0.7983$, unpaired t test). Overall, Vpu does not appear to substantially affect the organization of markers of membrane microdomains, either lipid raft or TEM, with respect to Gag and Env. Therefore,

the displacement of BST2 from sites of viral assembly likely involves the direct and specific action of Vpu on BST2, and this does not induce a general reorganization of membrane microdomains.

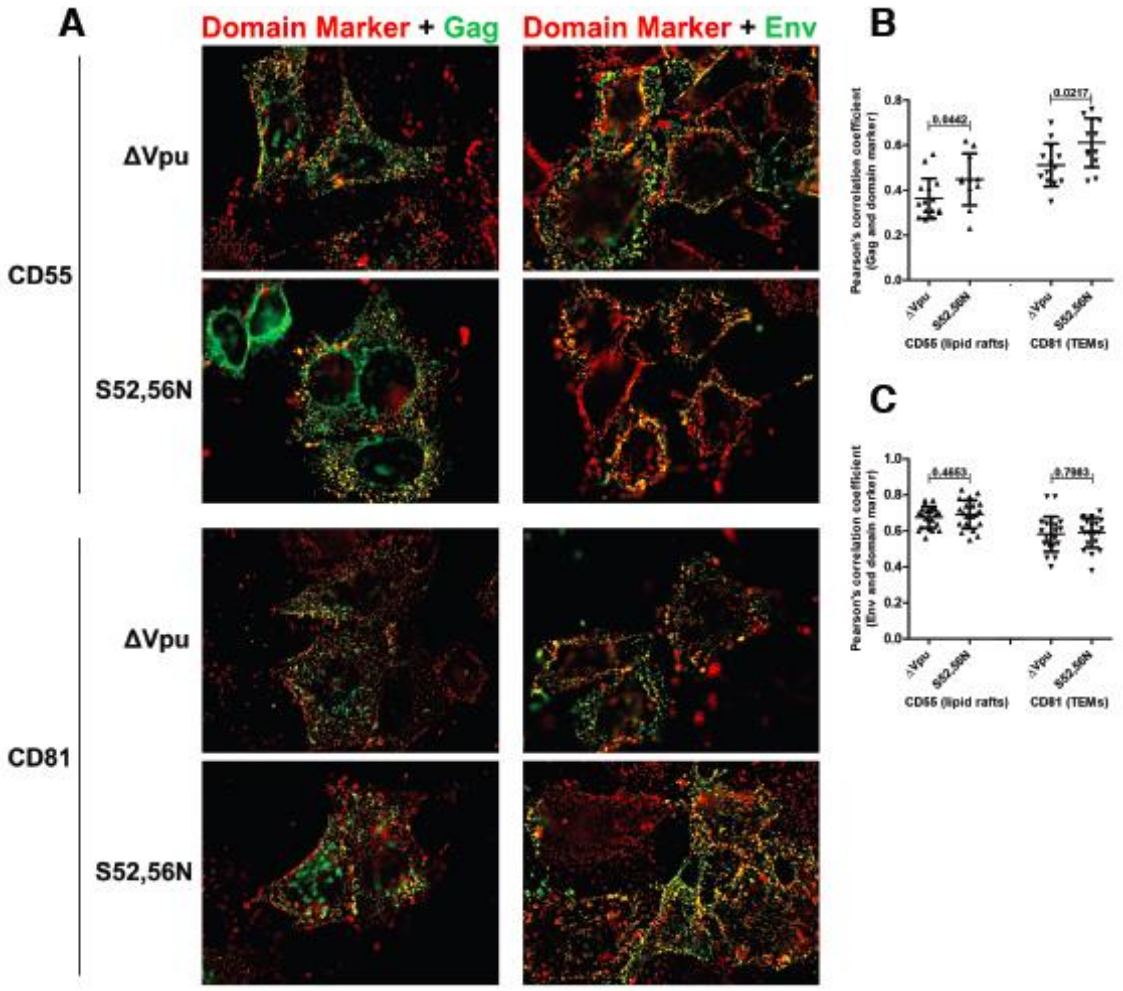

Figure 3.5 Vpu does not change the relationship of HIV assembly sites to markers of lipid rafts or tetraspanin-enriched microdomains.

A, HeLa P4-R5 cells were transfected with either pNL4-3ΔVpu or pNL4-3-Vpu-S52,56N mutant proviral plasmids and stained for the indicated membrane microdomain marker: CD55 (top two rows) as a marker of lipid rafts and CD81 (bottom two rows) as a marker of tetraspanin-enriched microdomains (TEMs). In addition, cells were either then fixed, permeabilized, and stained for p24 (left column) or co-patched for Env (right column). For all panels, the domain marker (CD55 or CD81) is in red, Gag (left) or Env (right) is in green and the overlap is in yellow. B, Pearson's correlation coefficients for the colocalization of the indicated membrane microdomain markers and Gag along the plasma membrane in the presence or absence of Vpu-S52,56N. C, Pearson's correlation coefficients for the colocalization of the indicated membrane microdomain markers and co-patched Env in the presence or absence of Vpu-S52,56N. For the analysis in B and C at least 25 cells were assessed for each condition, using the image plane adjacent to the cover glass. Error bars are the standard deviations. P-values were calculated by unpaired two-tailed t test.

W76 but not G76 Interacts with Lipids—Tryptophans are known to anchor the transmembrane domains of proteins in membranes and typically occur at or near the non-polar/polar interface where the hydrophobic acyl chain meets the hydrophilic lipid head group. For example, Vpu contains such a conserved tryptophan near the C-terminal end of its TMD. Although membrane anchoring of cytoplasmic domains by tryptophan is apparently rare, we considered that such an anchoring activity of W76 might explain its role in the BST2 displacement phenotype. To test this, we studied the interaction of the cytoplasmic domain of Vpu with lipids by NMR spectroscopy. For these studies, we expressed and purified uniformly ^{15}N-labeled polypeptides corresponding to the wild-type Vpu cytoplasmic domain sequence (VpuCyto) and the tryptophan 76 to glycine mutant (W76G VpuCyto). A well-resolved, fully assigned ^{1}H-^{15}N HSQC NMR spectrum for VpuCyto in aqueous solution was obtained (Figure 3.6A, black contours). When DMPC liposomes were added to the aqueous solution, VpuCyto resonances linewidths were broadened, resulting in reduced intensities. The reduced intensities indicate a change of reorientation rate due to the interaction of VpuCyto with the liposomes (Figure 3.6B). In addition, chemical shift changes were observed for a number of resonances from VpuCyto residues; among them, W76 was the most affected, suggesting that W76 undergoes a significant environmental or conformational change upon addition of liposomes (Figure 3.6C). When uniformly ^{15}N-labeled W76G VpuCyto was dissolved in aqueous solution, the frequencies of most resonances were very similar to those of VpuCyto, suggesting a minimal perturbation in the structure upon mutation (Figure 3.6D). When the DMPC liposomes were added to the aqueous solution containing W76G VpuCyto, smaller intensity changes were observed for resonances from W76G VpuCyto compared to wild-

type VpuCyto (Figure 3.6E). Moreover, no significant chemical shift changes were observed for G76 (Figure 3.6F). These data indicate that the cytoplasmic domain of Vpu interacts with lipids. The data also suggest that W76 is an important determinant of that interaction and its molecular environment is altered upon lipid-binding.

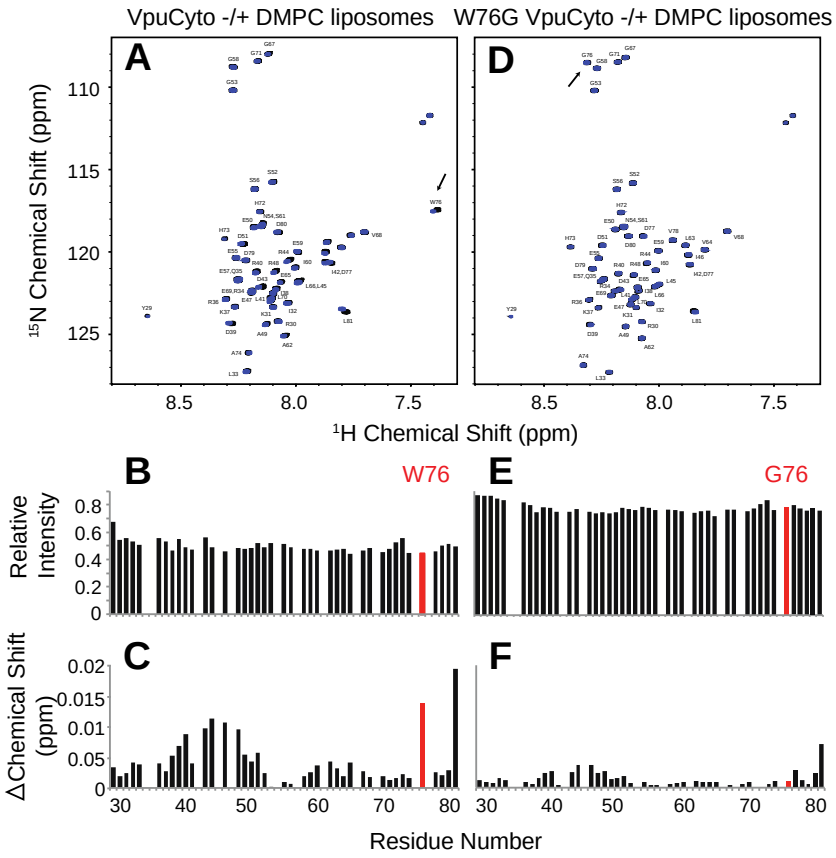

Figure 3.6 NMR chemical perturvation shows that W76 but not G76 interacts with lipids.

A, Assigned ^{1}H-^{15}N HSQC NMR spectrum of uniformly labeled ^{15}N labeled VpuCyto peptide in H_2O either with (blue) or without (black) DMPC liposomes. B, VpuCyto resonances relative intensity measured before and after addition of DMPC liposomes. C, Chemical shift change induced in VpuCyto residues by addition of DMPC liposomes. D, Assigned ^{1}H-^{15}N HSQC NMR spectrum of uniformly labeled ^{15}N labeled W76G VpuCyto peptide in H_2O either with (blue) or without (black) DMPC liposomes. E, W76G VpuCyto resonances relative intensity measured before and after addition of DMPC liposomes. F, Chemical shift change induced in W76G VpuCyto residues by addition of DMPC liposomes is shown to be much smaller than for W76 (C).

W76 is inserted in the Lipid Bilayer—Next we tested whether W76 inserts into the lipid bilayer using PRE distance measurements. The PRE effects were measured by comparing the signal intensities with and without addition of either of two paramagnetic probes, MnEDTA and 5DSA. MnEDTA is a bulky paramagnetic reagent restricted to the aqueous environment, whereas 5SDA is restricted to the hydrophobic region of the lipid micelle as described in detail below. When MnEDTA was added to VpuCyto incorporated in DHPC micelles, signals from residues that are accessible to MnEDTA in solution are broadened and the corresponding intensities are lowered. In Figure 3.7A, the largest intensity changes were observed among signals from residues in both the N- and C terminal as well as the loop regions of VpuCyto, indicating that these regions are exposed to aqueous solvent and MnEDTA. However, resonance signals of W76 amide and its indole in the C terminus were relatively unaffected, suggesting that W76 was protected by insertion into the micelles (Figure 3.7A). 5SDA is a fatty acid that has a nitroxide functional group labeled at the fifth carbon position in the hydrophobic chain. When incorporated into the DHPC micelles, 5SDA partitions to the hydrophobic region of the micelles, and the spin label is at the center of the micelle, as shown in the schematic in Figure 3.7C. Consequently, 5SDA can be used to detect the portion of the protein embedded in the micelles. For VpuCyto in DHPC micelles with 5SDA, we observed that the residues in the membrane-proximal cytoplasmic domain helix were slightly more affected than the C-terminal region, but W76 and especially its indole signals were the most broadened (Figure 3.7B). Together, these PRE experiments using different lipid partitioned paramagnetic probes suggest that W76 embeds in the lipid micelles.

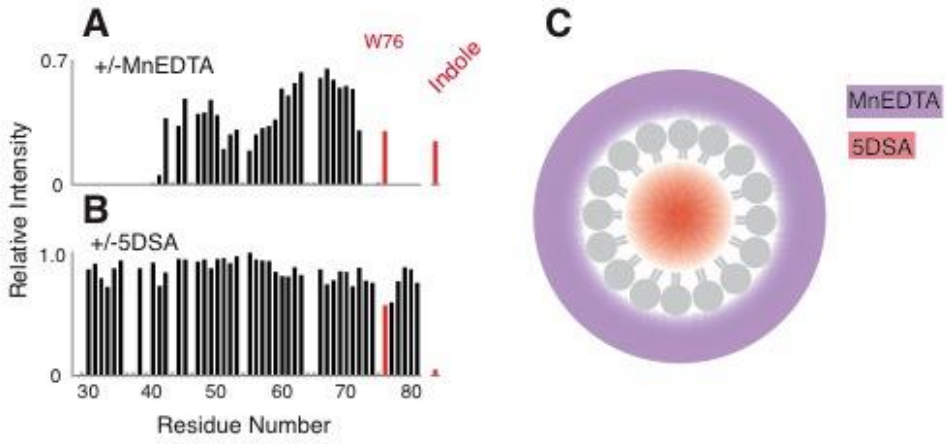

Figure 3.7 W76 is inserted into micelles.

Paramagnetic relaxation effect of MnEDTA and 5SDA on VpuCyto in DHPC micelles characterized using differential signal intensities measured from ^{1}H-^{15}N HSQC spectra. A, Relative intensity measured before and after addition of MnEDTA reveals that the W76 amide and its indole are relatively unaffected compared to VpuCyto N-terminal, C-terminal and loop regions, which are comparatively more exposed to aqueous solvent. B, Relative intensity measured before and after addition of 5SDA, demonstrating the largest effects on W76 and its indole, which supports a structure where W76 is embedded in the micelles. C, A schematic demonstrating the accessibility of MnEDTA (purple) and 5SDA (red) in the DHPC micelles.

W76 can interact with Positively Charged Lipids—The interaction of tryptophan with lipids can involve hydrophobic interactions as well as cation-π interactions between the aromatic ring and positively charged lipid head groups. To determine whether Vpu-W76 interacts with positively charged lipids, we compared the effects of positively charged and neutral lipids on VpuCyto resonances. When positively charged DMEPC liposomes (structure shown in Figure 3.8C) were added to VpuCyto in aqueous media, resonance intensities were further reduced as compared to the effect of adding neutral DMPC liposomes, especially for the second helix and the C-terminus of the cytoplasmic domain. Moreover, the intensity for W76 was drastically reduced upon addition of DMEPC liposomes (Figure 3.8A). The same trend was observed for the chemical shift perturbation

(Figure 3.8B); W76 was even more affected by positively charged lipids (DMEPC liposomes) than by neutral lipids (DMPC liposomes). Other positively charged lipids, specifically DMTAP and DMPC mixed with DC-Cholesterol, were tested, and similar patterns of intensity changes and chemical shift perturbations were observed (Figure 3.8C-F). The structures of DMPC, DMEPC, DMTAP and DC-Cholesterol are shown in Figure 3.8G. These data indicate an enhanced interaction of VpuCyto and W76 with positively charged lipids relative to neutral lipids, and supports the notion that cation-π interactions might contribute to this interaction.

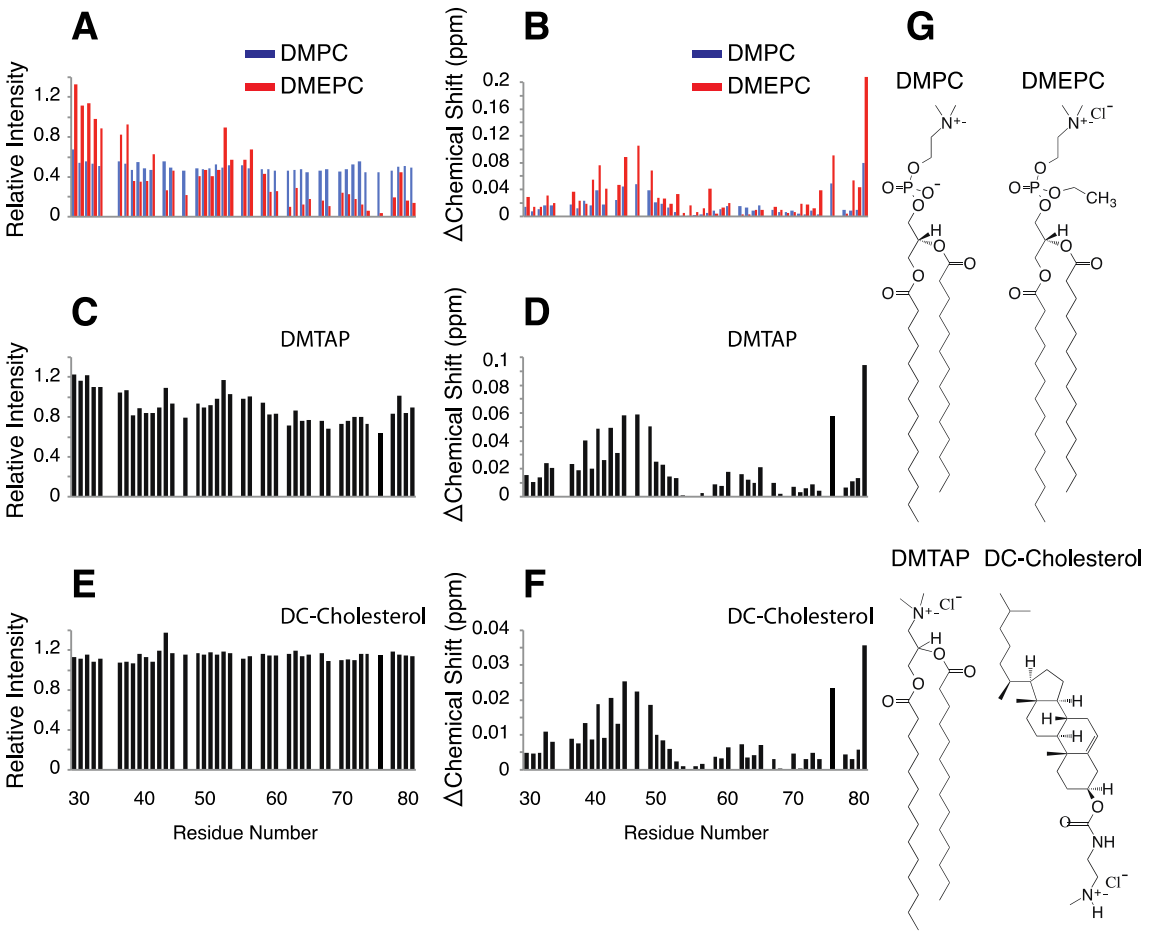

Figure 3.8 Enhanced interaction of the Vpu cytoplasmic domain and W76 with positively charged lipids.

A, VpuCyto resonances relative intensity measured before and after addition of either DMPC liposomes (blue) or DMEPC liposomes (red). B, Chemical shift change induced in VpuCyto residues by addition of either DMPC liposomes (blue) or DMEPC liposomes (red). C, Relative intensity of VpuCyto resonances measured before and after addition of DMTAP liposomes. D, Chemical shift change induced in VpuCyto residues by the addition of DMTAP liposomes. E, Relative intensity of VpuCyto resonances measured before and after the addition of DMPC liposomes mixed with DC-Cholesterol. F, Chemical shift change induced in VpuCyto residues by the addition of DMPC liposomes mixed with DC-Cholesterol. G, Structures of DMPC, DMEPC, DMTAP and DC-Cholesterol.

Phenylalanine cannot Substitute for the Activity of W76—Since our NMR studies supported a possible role for cation-π interactions between the aromatic ring and positively charged lipid head groups during the interaction of the Vpu cytoplasmic domain with

membranes, we tested whether another aromatic amino acid, phenylalanine, could substitute functionally for W76. To test whether Vpu-W76F could downregulate BST2 from the cell surface, we transfected HeLa P4-R5 cells with proviral plasmids lacking *vpu* plus expression constructs encoding FLAG-epitope tagged wild-type NL4-3 Vpu, mutant Vpu-W76G or Vpu-W76F alone or in combination with the S52,56N mutations. As shown in the two-color FACS plots in Figure 3.9A and the graph of average MFI for surface BST2 in p24-positive cells in Figure 3.9B, Vpu-W76F was functional for surface-downregulation of BST2; its activity was indistinguishable from wild-type (W76 Vpu) and W76G Vpu. The addition of the S52,56N mutations abrogated this activity. These results are shown quantitatively in Figure 3.9C, where the BST2 downregulation by each Vpu mutant is shown relative to that of wild-type Vpu. In contrast, the Vpu-W76F mutant did not support wild-type levels of virion release enhancement, as shown in Figure 3.9D. Supernatant p24 released by provirus encoding Vpu-W76F was similar to that encoding Vpu-S52,56N, just under half that of wild-type NL4-3. Notably, Vpu-W76F was slightly more active for virion release-enhancement than was Vpu-W76G. Immunoblot for the FLAG epitope tag in Figure 3.9E revealed no significant difference in the expression of the mutant Vpu proteins to account for their ability to enhance virion release.

Similar to W76G (see Figure 3.6B and C), W76F VpuCyto showed no significant changes in its HSQC spectrum compared to wild type VpuCyto. Also like W76G VpuCyto, both the intensity change (Figure 3.9F) and the chemical shift perturbation data (Figure 3.9G) indicate that F76 and W76F VpuCyto do not interact with DMPC liposomes as strongly as wild-type VpuCyto. These results suggest that both the W76G and W76F mutations impair the protein-lipid interaction. The results also suggest that the interaction

of W76 with lipids is unlikely to solely depend on an aromatic side chain. Importantly, the functional data with regard to virion-release are consistent with the NMR data: a phenylalanine (like a glycine) cannot support the function of W76 with regard to enhancing virion release or interacting with the lipid bilayer.

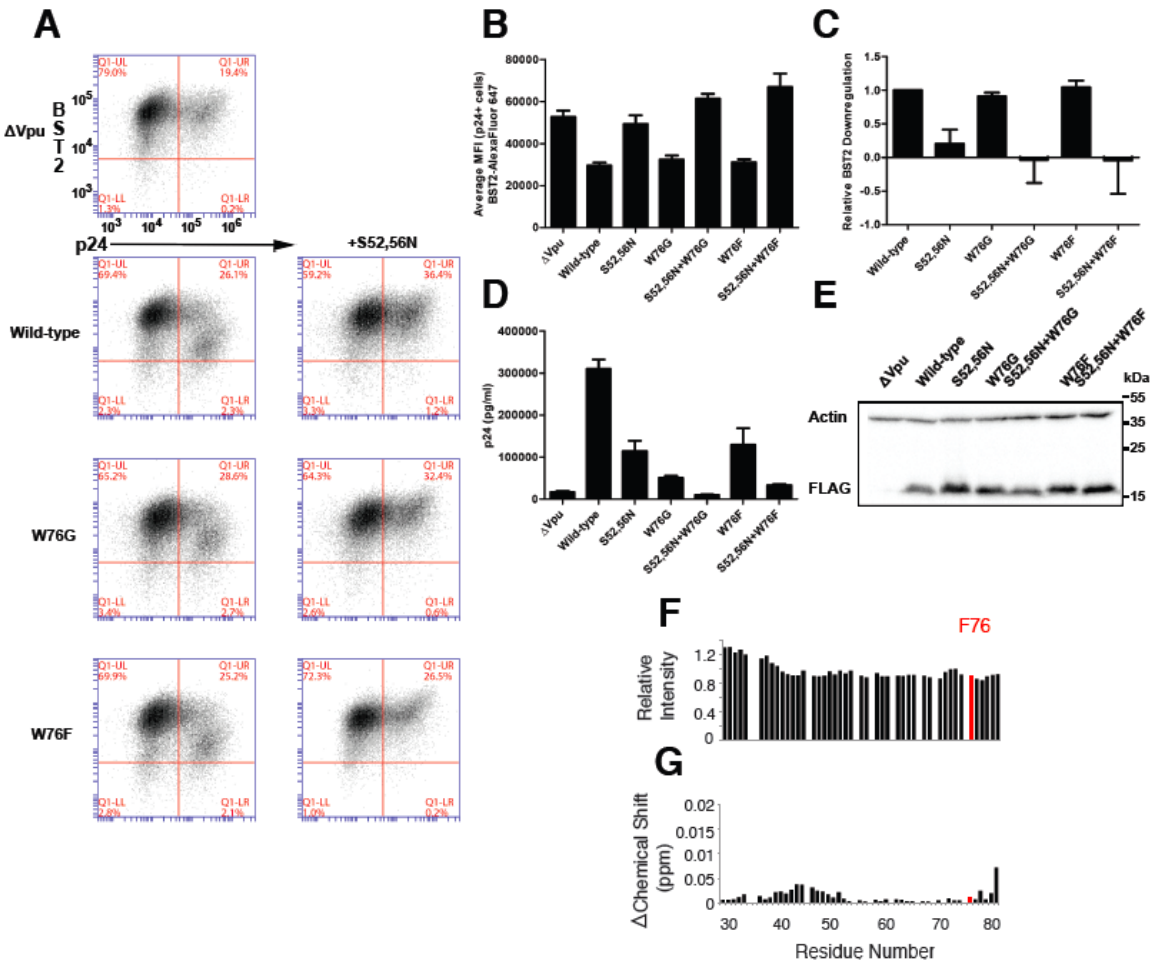

Figure 3.9 F76 supports neither optimal virion release nor the binding of Vpu's C-terminus to lipids.

A, Two-color plots showing BST2 downregulation (y-axis) and p24 expression (x-axis) in HeLa P4-R5 cells co-transfected with a proviral plasmid lacking Vpu (pNL4-3ΔVpu) and a Rev-dependent expression plasmid encoding the indicated Vpu mutants with a C-terminal FLAG epitope tag. Plots are representative of four experiments done in triplicate. B, Bar graph of average MFI for surface BST2 in p24-positive cells. Error bars are the standard deviations of triplicates. C, Quantification of relative levels of BST2 downregulation by the Vpu mutants in A shows that Vpu-W76F is as functional for surface-downregulation of BST2 as WT and Vpu-W76G. Samples were gated on live p24-positive cells. The MFI of BST2 staining for each Vpu mutant was subtracted from that of the no-Vpu (ΔVpu) control, and this value was divided by the same calculation made for NL4-3 Vpu to derive the relative activity. Error bars are the standard deviations of triplicates. D, The concentration of pelletable p24 antigen in the culture supernates from the cells shown in A was measured by ELISA. Vpu-W76F is impaired in its ability to enhance virion release compared to wild-type Vpu although not to the same extent as Vpu-W76G. Error bars represent the standard deviation of triplicates. E, Immunoblot analysis of cell lysates for the FLAG epitope tag showing expression levels of the Vpu mutants from the cells in A. Actin is shown as a loading control. F, W76F VpuCyto resonances relative intensity measured before and after addition of DMPC liposomes. G, Chemical shift change induced in W76F VpuCyto residues by addition of DMPC liposomes.

3.5 Discussion

The ability of Vpu to displace BST2 from sites of viral assembly in the plane of the plasma membrane appears to be an important aspect of the mechanism by which Vpu enhances virion release, distinct from both surface-downregulation and degradation of BST2. This activity is shown here to be a direct and specific effect of Vpu on BST2 localization relative to viral assembly sites (as defined by Gag and Env proteins), and is neither a consequence of a reorganization of the membrane microdomains (lipid rafts, TEMs) associated with viral assembly sites nor does it induce changes in those domains. This BST2-displacement activity of Vpu depends in large part on the C-terminal residue W76, at least for clade B Vpu. This activity now explains the anomalous phenotype of the W76G polymorphism described in recent studies of naturally occurring Vpu proteins (156).

How does W76 contribute to this displacement-activity? Our NMR data obtained using recombinant protein associated with either DHPC micelles or with liposomes containing neutral or positively charged lipids support a direct interaction of W76 with membrane phospholipids. Similar conclusions with regard to W76 have been suggested previously based on chemical shift perturbation and PRE measurements on VpuCyto in DPC micelles (180). Based on these biochemical properties, we propose a modified model of Vpu structure in which the extreme C-terminus attaches to the membrane via the insertion of W76 into the lipid phase. This C-terminal attachment of Vpu to the membrane appears to be critical for activity, as neither the naturally occurring variant glycine nor our site-directed substitution of phenylalanine supported membrane-interaction or optimal virion-release. Exactly how C-terminal membrane attachment supports Vpu's ability to displace BST2 from viral assembly sites remains to be elucidated. One possibility is that

Vpu's C-terminus inserts into specific lipid domains that are distinct from viral assembly sites. Vpu's preference for such sites and its direct interaction with BST2 would enable it to "drag" BST2 away from the sites of viral assembly. Another possibility is that the C-terminal membrane attachment correctly orients Vpu's cytoplasmic domain such that it can interact with a cellular peripheral membrane or cytoskeletal protein, and this connection ultimately provides the movement of BST2 relative to viral assembly sites. Such a co-factor might, for example, be a clathrin adaptor, an hypothesis consistent with the role reported for the $ExxxLV_{64}$ adaptor protein binding sequence in the displacement effect (155,181). In either case, Vpu would presumably need to interact with BST2 at assembly sites initially, and then move together with BST2 away from those sites. In this regard, we speculate that Vpu might sample C-terminal attached and unattached conformations, providing alternate binding (or not) to the membrane microdomains or cellular co-factors that support the displacement effect. This would allow Vpu to first bind BST2, and then direct it from the sites of viral assembly. A prior NMR study of the Vpu cytoplasmic domain supports this notion insofar as the C-terminal end of Vpu seems able to participate in more than one conformation: one in which W76 is exposed to the aqueous phase and another in which it is embedded in the lipid phase (180).

Tryptophan residues in trans-membrane helices are commonly located at the boundary of the hydrocarbon core of the bilayer and the polar lipid head groups. Indeed, Vpu has such a tryptophan at the C terminal end of its transmembrane domain, and this residue is strictly conserved among HIV-1 isolates (182,183). In contrast, evidence for the involvement of membrane attachment via tryptophan such as we propose here is rare. We are aware of only two similar examples, vinculin and annexin V, neither of which are

transmembrane proteins (184,185). In the case of vinculin, like Vpu, the tryptophan occurs very near the protein's C-terminus and in an unfolded, flexible region. The membrane attachment sequence of vinculin, TPWYQ, is notable for a proline that precedes the W; this is also seen in the consensus sequence of clade B Vpu proteins, APWDV, but not in the case of annexin V, in which the key tryptophan is not located near the C-terminus.

The mechanism by which tryptophan residues interact with biological membranes at the hydrophobic/hydrophilic interface seems to be multi-faceted, potentially involving hydrophobic interactions with the hydrocarbon chain, cation-π interactions between the aromatic ring and positively charged lipid head groups, and hydrogen bonding between indole and lipid head groups. Here, our NMR data indicate that the cytoplasmic domain of Vpu interacted even more strongly with positively charged lipid than it did with neutral lipid. However, phenylalanine at position 76 supported neither the interaction with lipid nor the enhancement of virion-release by Vpu. These results suggest that cation-π interactions, although they might contribute to the interaction, are apparently not sufficient for membrane insertion of the Vpu C-terminus, and consequently, they are not sufficient to support enhancement of virion-release. The interaction may be reinforced by hydrogen bonding between the tryptophan indole nitrogen and a lipid head group, which is not possible with phenylalanine. At least in the context of clade B Vpu proteins, tryptophan seems uniquely suited to this function. In this regard, however, we note that W76, although conserved in clades B, D and G, does not occur in Vpu proteins of other clades such as C, which is the most prevalent in the HIV-1 pandemic. The corresponding region of clade C Vpu typically contains the sequence RLLDV, and whether or not this sequence provides

membrane-insertion and/or the ability to displace BST2 from viral assembly sites remains to be determined.

Finally, we note that virion-assembly sites are not random; in the case of HIV-1, they are enriched in markers of cholesterol-enriched lipid rafts and in tetraspanins. HIV-1 Gag specifically binds the acidic lipid phosphatidyl inositol 4,5-bisphosphate (PIP2), and its assembly appears to drive the coalescence of lipid rafts and TEMs (159-161). BST2 appears to associate both with lipid-rafts and TEMs (179). Moreover, due to its unusual topology, an N-terminal transmembrane domain and a C-terminal GPI-anchor, BST2 has been proposed to cross-link lipid rafts. Consequently, the displacement effect might well have disrupted the associations between membrane microdomains that accompany virion-assembly. Surprisingly, we found no morphological evidence for this; Vpu displaced BST2 from both Gag and Env (viral assembly sites), while displacing neither raft nor TEM markers from these sites. Our data suggest that the movement of BST2 relative to these sites by Vpu is specific, and it does not in turn cause a more general disruption of membrane topology.

In summary, the anomalous phenotype of the Vpu-W76G polymorphism, a defect in enhancing virion release despite preserved activity in downregulating BST2 from the cell surface, can be explained by the key role of W76 in the Vpu-mediated displacement of BST2 from virion assembly sites within the plane of the plasma membrane. This activity correlates with the ability of W76 to mediate the attachment of the Vpu C-terminus to the lipid bilayer *in vitro*, and it supports a modified view of Vpu's topology with respect to the membrane. We speculate that membrane-anchoring of the C-terminus either drives a specific association of Vpu with lipid microdomains distinct from those where viral

assembly occurs, or it orients the cytoplasmic domain of Vpu such that it can interact with an as yet unidentified cellular protein cofactor to mediate the displacement effect.

Chapter 3, in full, is a reprint of the material as it appears in the Journal of Biological Chemistry 2015. Lewinski, M. K., Jafari, M., Zhang, H., Opella, S. J., and Guatelli, J. The dissertation author was the co-first author of this paper.

Chapter 4 Revealing of Protein-Protein Interaction between Transmembrane domains of Vpu and NTB-A

4.1 Introduction

Natural killer (NK) cells are innate lymphocytes, which are able to lyse virus-infected cells by secretion of lytic granules; therefore, NK cells are a crucial part of the innate immune system that fights viruses(186). A broad range of receptors, expressed on NK cells is able to regulate NK cells (187-189). One of the activation receptors is NKG2D, which is recognized by ligands such as ULBP-1 and -2; on the other hand, there are inhibitory receptors, such as HLA-A and –B. For NK cells to release lytic granules, apart from NKG2D, it requires triggering of a co-activation receptor, NK-cell and B cell antigen (NTB-A) (189,190).

NTB-A is expressed on a variety of immune cells including NK-cells, T-cells, B-cells, and eosinophils. NTB-A belongs to the signaling lymphocytic activation molecule (SLAM) family (191), which includes a wide range of receptors that regulate innate and adaptive immune responses. NTB-A is a homophilic receptor and a self-ligand. It is a type 1 membrane protein, which consists of a cytoplasmic tail with tyrosine phosphorylation site to recruit SLAM associated protein, a transmembrane domain, and an ectodomain composed of a C-terminal membrane proximal IgC2 domain in a β-sheet, and an N-terminal IgV domain (192,193). The structure of the ectodomain of NTB-A has been solved by X-ray crystallography. It is in a dimeric form composed of two rod-like monomers arranged in a nearly orthogonal fashion, with an end-to-end distance of 100 Å (194). The main function of NTB-A on NK cells is to enhance cytotoxicity and cytokine secretion.

HIV-1 accessory protein Vpr induces ligands ULBP-1 and -2 to activate NKG2D (195), while another HIV-1 accessory protein Nef downmodulates ligands for ULBP-1 and -2. The collective effect of these two factors should make HIV-1 infected cells ideal targets for NK cells to degranulate. However, NK cells fail to effectively degranulate HIV-1 infected cells. This is due to the ability of HIV-1 accessory protein Vpu to downmodulate NTB-A from the surface of virus infected cells, and as a result prevent HIV-1 infected cell from being lysed by NK cells (99,105). And the serine phosphorylation sites in the loop of Vpu cytoplasmic domain have been shown to be dispensable for downmodulation of NTB-A; instead, the phenotype has been mapped to the transmembrane domains of both proteins (99,105).

Even though research in Prof. Edward Barker's group have shown the key residues involved in the downmodulation, in order to understand how does Vpu downmodulate NTB-A on molecular level, we need to determine whether and how the transmembrane domain of Vpu (VpuTM) directly interacts with the transmembrane domain of NTB-A (NTB-A TM). The knowledge of mechanism of downmodulation is essential for development of novel therapeutics methods to regain NK cell's ability to counteract HIV-1.

We investigated the interaction by a combination of biological and spectroscopic approaches. All of the biological experiments involving cell lines and expression levels were performed by members of Barker group, and the experiments used mutagenesis approach to reveal important residues involved in the downmodulation at the cellular level.

For spectroscopic study, solution NMR and chemical shift perturbation techniques are used to reveal residues involved in protein-protein interaction in a DHPC micelle

environment. For this approach, a construct of the NTB-A TM domain was made corresponding to residues 223 to 250 of the human NTB-A sequence with two extra glycines and five extra lysines added at the C-terminus to increase the solubility of the polypeptide. Cysteine 235 is mutated to serine to prevent aggregation in protein purification; in addition, methionine is mutated to leucine to facilitate purification. The mutated residues do not have any biological significance for NTB-A function. The full sequence of the NTB-A TM construct is shown below, and the TM domain is underscored.

DTKLILFLVSGISIVFGFIILLLLVLRKGGKKKKKM

4.2 Experimental

Expression plasmids for NTB-A TM and VpuTM were constructed similarly to those previously described (115,116). DNA encoding the NTB-A TM (Integrated DNA Technologies) was inserted into phLV vector with TrpΔLE as fusion partner and expresses as inclusion bodies to avaoid cytotoxicity. VpuTM has been expressed in pET31b(+)vector (Agilent Technologies) with KSI fusion partner. Expression plasmids encoding mutant VpuTM A10, A14 and A18 to F10, F14 and F18 (VpuFFF) and VpuTM A10, A14, A18 and W22 to F10, F14, F18 and A22 (VpuFFFA) were prepared using QuikChange Lightning Site-Directed Mutagenesis Kit (Agilent Technologies), and the primers were synthesized by Integrated DNA Technologies. Plasmid for NTB-A TM was transformed into BL21(Agilent Technologies) and OverExpress C41(DE3) competent cells (Lucigen) for expression. Plasmids for VpuTM were transformed into OverExpress C41 (DE3) competent cells (Lucigen) for protein expression. All constructs were expressed in either LB medium for unlabeled protein or M9 minimum medium for isotopically labeled protein

production. For labeled growth, ^{13}C-glucose and $(^{15}NH_4)_2SO_4$ were obtained from Cambridge Isotope Laboratories. Isopropyl □-D-1-thiogalactopyranoside (IPTG) was purchased from Genesse Scientific, Inc**.** 1,2-dihexanoyl-sn-glycero-3-phosphocholine (DHPC) was obtained from Avanti Polar Lipids, Inc. Deuterium oxide (D_2O) and Guanidine Hydrochloride (GdnHCl) were obtained from Sigma.

The expression and purification of NTB-A TM, VpuTM and mutants were similar to that previously described (115,116). Briefly, the cells were collected by centrifugation and lysed by sonication. The fusion protein in the inclusion bodies were denatured by 6M GdnHCl and isolated with nickel affinity chromatography. The proteins were separated from fusion partners by cyanogen bromide cleavage. After cleavage, NTB-A was separated from TrpΔLE by reverse phase high performance liquid chromatography (HPLC) for final purification. VpuTM and mutants were separated from KSI by organic precipitation method. The purity of the proteins were checked by SDS-PAGE, and the molecular weight of the proteins were confirmed by matrix-assisted laser desorption/ionization (MALDI) mass spectrometry. The plasmids, purification protocol and SDS-PAGE gels for NTB-A expression and purification were shown (Figure 4.1), along with MALDI spectrum of purified NTB-A TM with correct molecular weight at 3900Da.

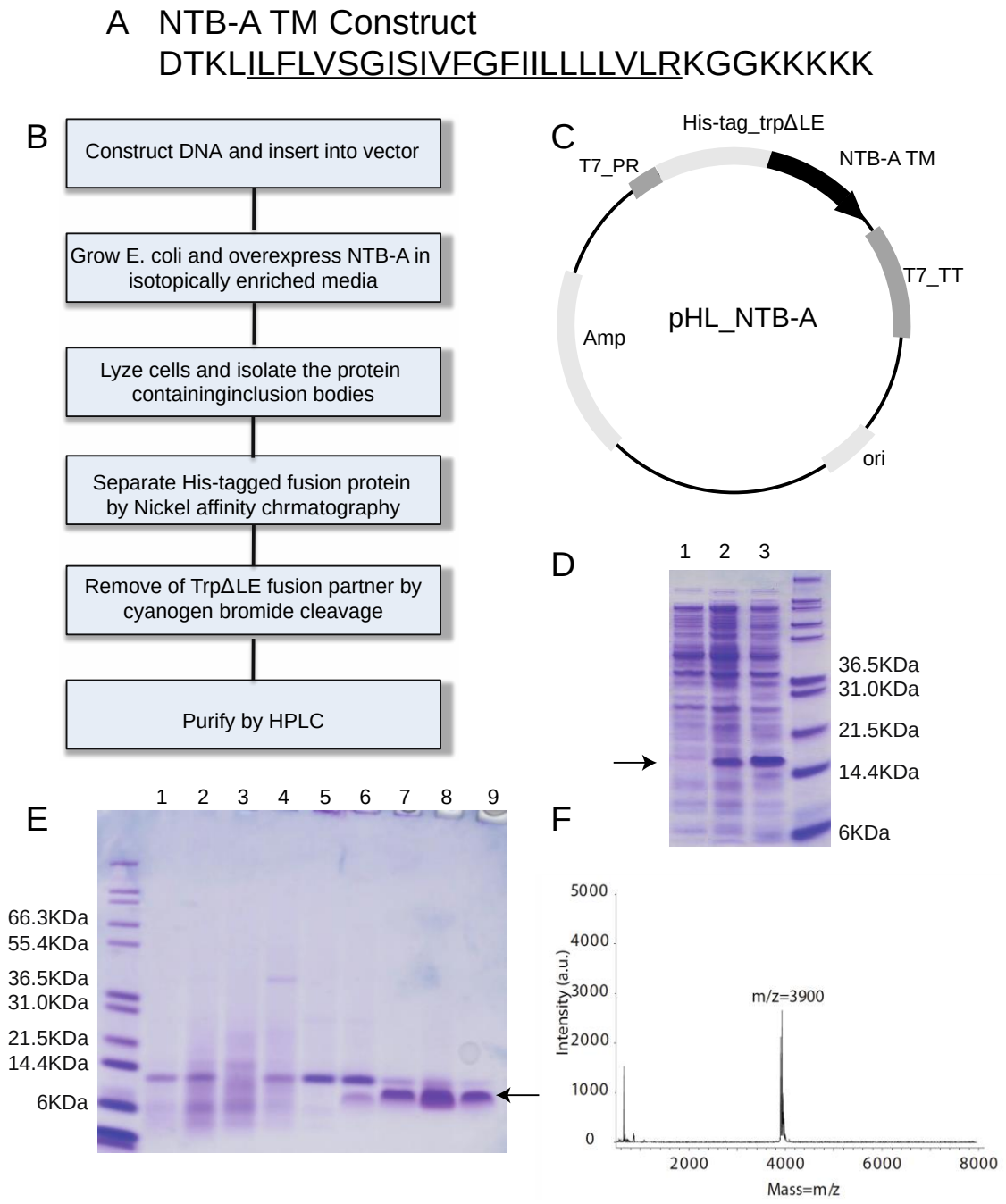

Figure 4.1 Expression and purification of NTB-A TM.

A, NTB-A TM construct peptide sequence. B, Purification protocol. C, Plasmid vector for NTB-A purification. D, SDS-PAGE showing overexpressed NTB-A TM after induction. E, SDS-PAGE showing HPLC fractions. F, MALDI spectrum of NTB-A.

Samples of protein in micelles for solution NMR experiments were prepared by dissolving purified and lyophilized protein in 100mM DHPC with 10% (V/V) (D_2O), and the pH was adjusted to 4.0. Solution NMR experiments were performed on a Bruker 600 MHz spectrometer equipped with a 5 mm z-axis pulse-field gradient, and triple-resonance $^{1}H/^{15}N/^{13}C$ cryoprobe. Chemical shift changes were calculated base on ^{1}H-^{15}N HSQC experiments, with equation 3.1. Triple-resonance HNCA experiments were performed for assignment of backbone amide resonances of NTB-A TM. All of the experiments were performed at 50^{o}C. Data were process using NMRPipe, and displayed by either Sparky (T. D. Goddard and D. G. Kneller, SPARKY 3, University of California, San Francisco).

4.3 Solution NMR study of Vpu and NTB-A interaction

After uniformly ^{15}N-labeled NTB-A TM was purified, a range of detergents were tested for micelle sample preparation including SDS, DPC and DHPC. The ^{1}H-^{15}N HSQC NMR spectra indicate that NTB-A behaves best in DHPC micelles, with well resolved peaks with homogeneous intensity (Figure 4.2).

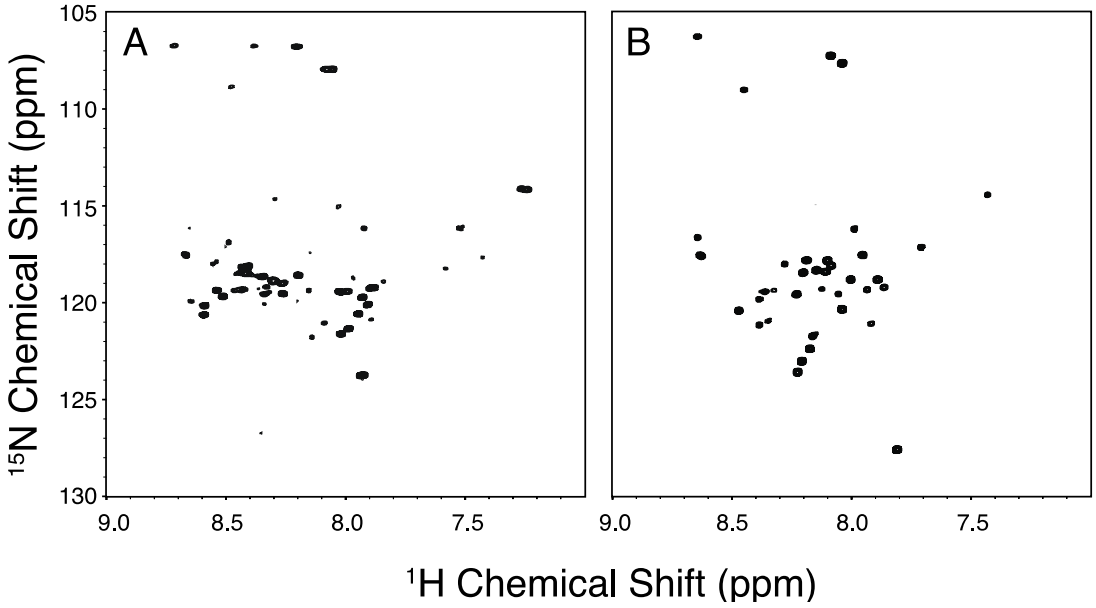

Figure 4.2 HSQC spectra of NTB-A TM in micelles.

A, HSQC spectrum of ^{15}N-labeled NTB-A in 450mM SDS. B, HSQC spectrum of ^{15}N-labeled NTB-A in 100mM DHPC.

When increasing amount of ^{14}N VpuTM were titrated into ^{15}N NTB-A in DHPC micelles, for certain residues, chemical shift changed following a trend, while other residues remains unperturbed (Figure 4.3). This suggests that specific interactions are taking place between Vpu TM and NTB-A TM.

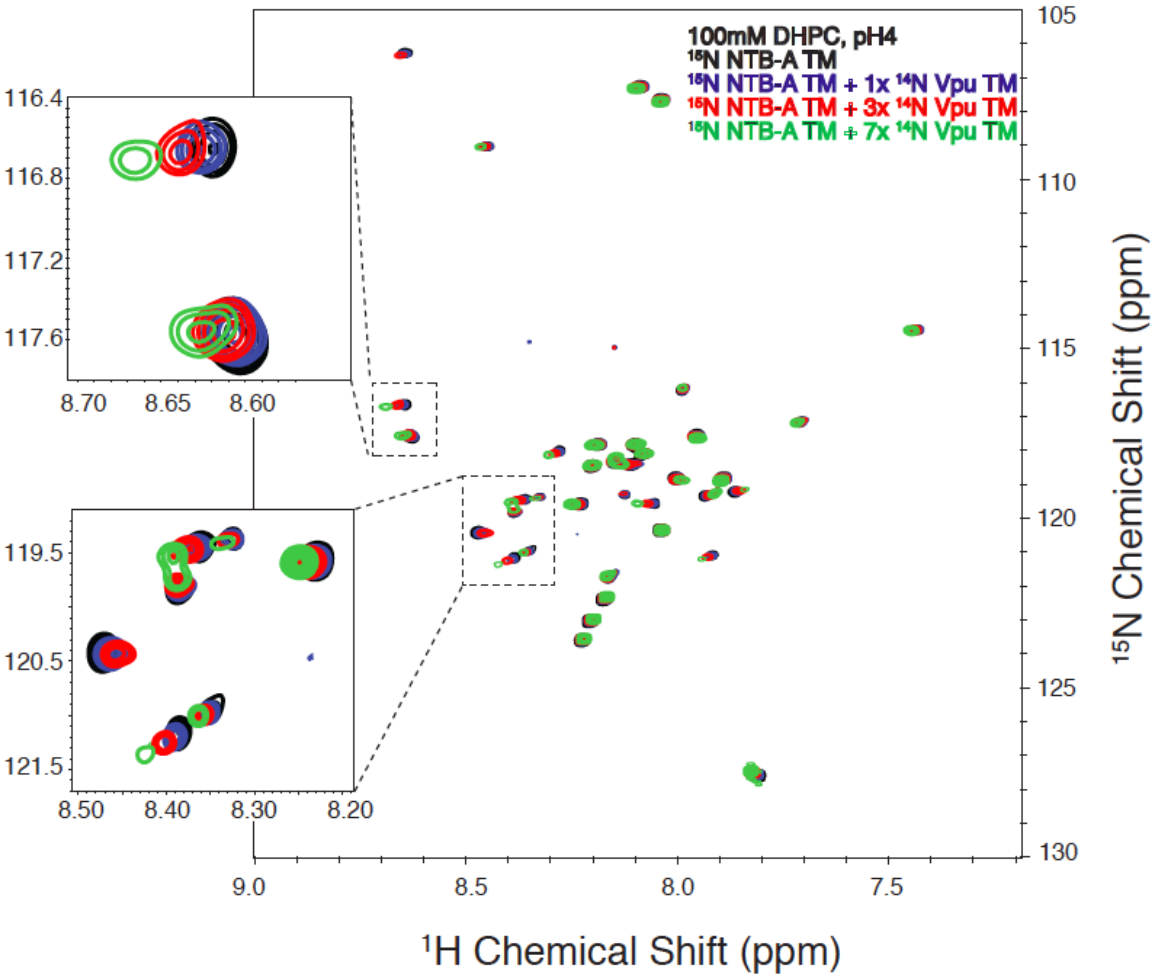

Figure 4.3 Titration of unlabeled VpuTM to ^{15}N labeled NTB-A TM.

A fully assigned ^{1}H-^{15}N HSQC NMR spectrum of NTB-A TM in DHPC micelles are shown in Figure 4.4. When ^{14}N Vpu TM peptide was added to ^{15}N-labeled NTB-A TM in micelles, chemical shift changes were observed in several NTB-A residues including Phe229, Ser232, Ile236, and Gly239, and signal intensity was reduced significantly for Phe240, indicating that these residues were directly involved in the helix-helix interaction between the TMs of the two proteins (Figure 4.4).

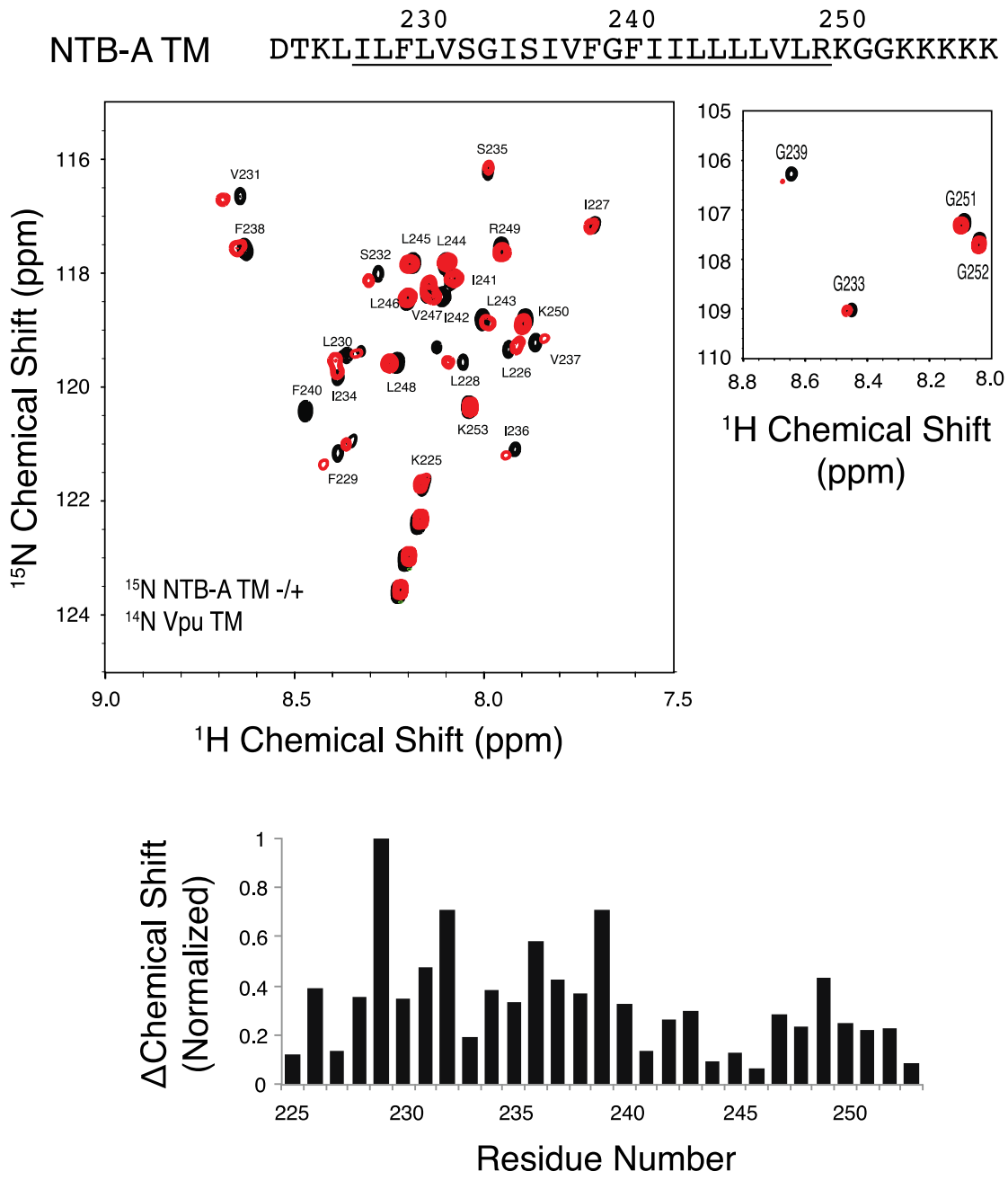

Figure 4.4 NTB-A TM Chemical shift change induced by addition of Vpu TM.

Assigned ^{1}H-^{15}N HSQC NMR spectrum of ^{15}N-NTB-A TM peptide in DHPC lipid micelles either without (black) or with (red) added unlabeled Vpu TM peptide, and chemical shift change induced in NTB-A residues by Vpu.

On the other side, when^{14}N NTB-A TM was added to ^{15}N Vpu TM in DHPC lipid micelles, perturbation in chemical shifts was observed for Ile11, Ile15 and Trp22 in Vpu

TM (Figure 4.5). The chemical shift perturbation in Vpu TM induced by NTB-A TM matches with changes in Vpu TM induced by BST-2 TM (94). This suggests that Vpu employs same AXXXAXXXAXXXW face to interact with both BST-2 and NTB-A.

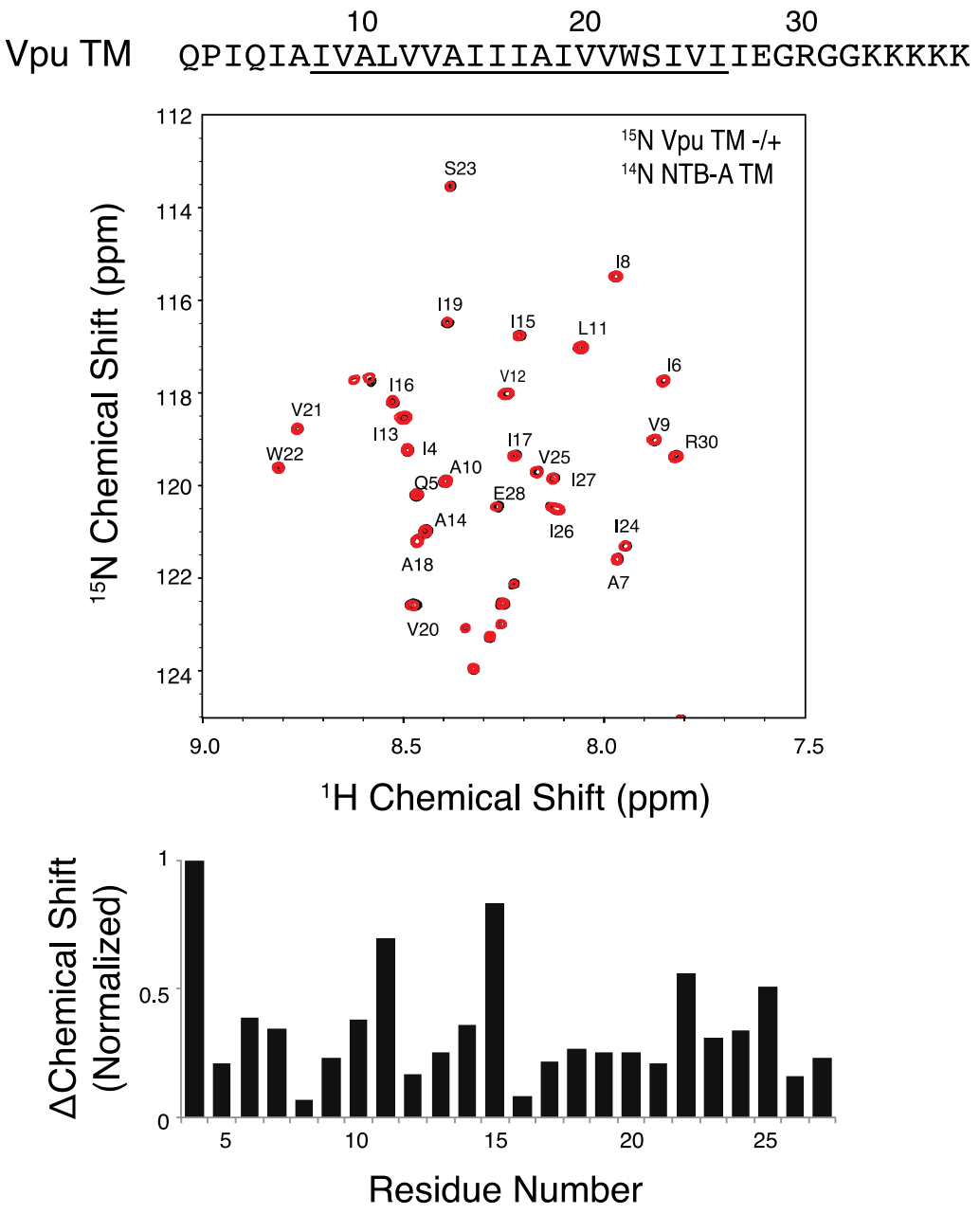

Figure 4.5 Vpu TM Chemical shift change induced by addition of NTB-A TM.

Assigned ^{1}H-^{15}N HSQC NMR spectrum of ^{15}N Vpu TM peptide in DHPC lipid micelles either without (black) or with (red) added unlabeled NTB-A TM peptide, and chemical shift change induced in Vpu residues by NTB-A.

NMR spectroscopy has shown that mutant Vpu TM FFF was not able to induce significant chemical shift change on BST2, indicating that this mutant impairs the

interaction between TMs of BST2 and Vpu. Hense, we want to test if same mutant will impair the interaction between Vpu and NTB-A. When unlabeled Vpu FFF and/or VpuFFFA are added to ^{15}N labeled NTB-A TM, the resulting HSQC spectrum shows very similar pattern in chemical shift change in comparison to changes induced by wild type mutant (Figure 4.6) Phe229, Ser232, Ile236, Gly239 and Phe 240 in NTB-A involved in interaction with wild type Vpu were shown to change most significantly upon addition of mutant Vpu. This is a clear indication that the two constructs still have binding interaction. And the result disapproves the interaction mechanism as insertion of bulky side-chain into alanine pocket proposed for Vpu-BST2, and leans toward the mechanism of hydrophobic interaction.

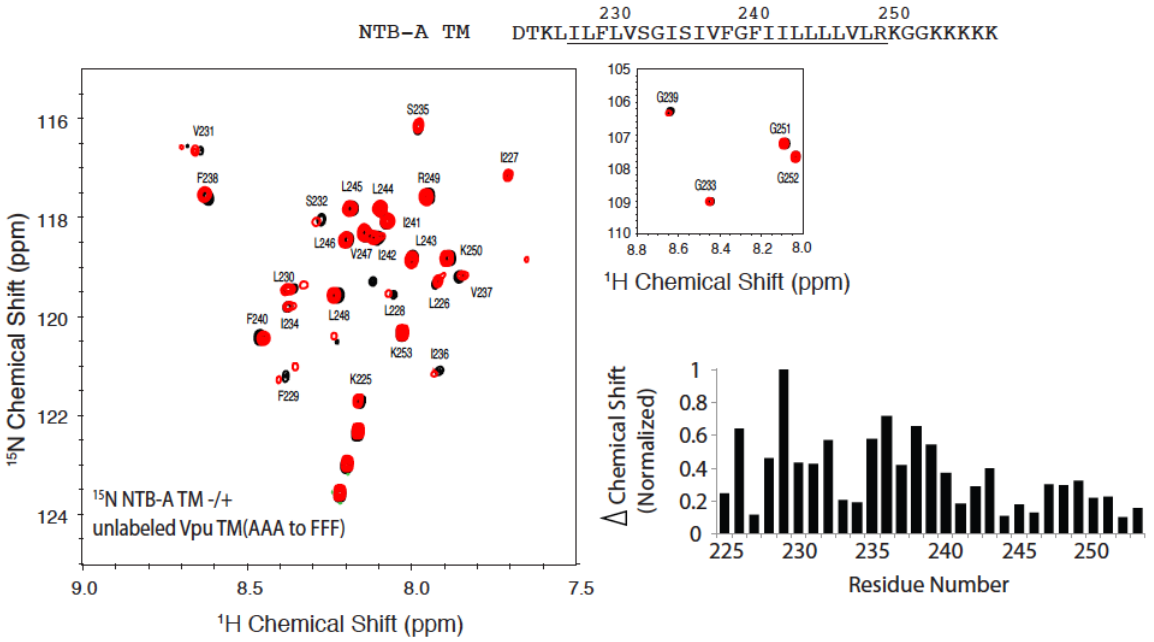

Figure 4.6 NTB-A TM Chemical shift change induced by addition of Vpu TM FFF.

Assigned ^{1}H-^{15}N HSQC NMR spectrum of ^{15}N NTB-A TM peptide in DHPC lipid micelles either without (black) or with (red) added unlabeled Vpu TM FFF peptide, and chemical shift change induced in NTB-A residues by VpuTM FFF.

4.4 Biological study of Vpu and NTB-A Interaction

Dr. Bharatwaj Sowrirajan in Prof. Edward Barker's group performed all of the cellular and molecular biology experiments, and the results will be briefly described here. The cell surface downmodulation of the wild type and mutant forms of NTB-A by Vpu is evaluated by analyzed via flow cytometry. The results suggest that Vpu fails to downmodulate mutant of NTB-A I,F,L,V to A,A,A,A. Note that I236, F240 are also indicated by NMR results as residues involved in the interaction, and L234 and V247 are on the same interaction face. The results are further confirmed by immunoprecipitation, showing that wild type NTB-A and Vpu co-precipitated while mutant NTB-A and Vpu don't. On the other hand, mutant Vpu A 14F, A18F, W22A, and AAW to FFA were shown to lose the ability to downmodulate NTB-A.

4.5 Computational simulation of Vpu and NTB-A Interaction

Ideal helices of NTB-A TM, wild type and mutant of Vpu TM were generated in Chimera (UCSF) and energy minimized. All models are further relaxed and embedded into the implicit membrane in Xplor-NIH IMMx package, using 500 steps of minimization followed by 100 ps dynamics in Cartesian space. The implicit membrane thickness was set to 25.4 Å. The relaxed models are docked together with the interacting phases facing each other. Two complexes, Vpu/NTB-A and VpuFFFA/NTB-A are made. Both complexes are inserted into the membrane region of the implicit membrane potential, 1 ns molecular dynamics simulations are applied to both complexes for comparison, with Vpu/ NTB-A serving as a positive control. The model of Vpu/ NTB-A complex adopts a parallel helix-helix interaction. In which the AXXXAXXXAXXXW motif on Vpu serves as a pocket to receive the bulky motif FXXSXXXIXXXF. The interaction face of NTB-A is lined by residues 229, 232, 236 and 240, while the interaction face of Vpu is lined by residues 10, 14, 18 and 22. Surfaces in the interaction interface are colored white in Figure 4.7B, and are apparently in the core of the complex. When the same docking simulation was performed with a back-to-back face as the starting point, the helix-helix complex could not be formed. The docking simulation also suggests the hydrogen bond formed between N-term Lysine in NTB-A and Glutamine in Vpu, or C-term lysine 31 in NTB-A and glutamic acid in Vpu favor the helix-helix interaction between the two proteins.

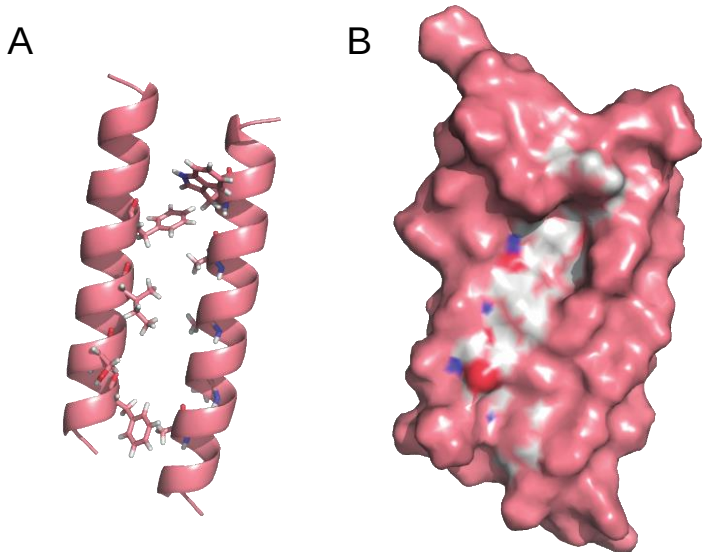

Figure 4.7 Docking simulation of the Vpu/ NTB-A interaction.

A, Both proteins are shown in cartoon form, with residues in the interaction phases shown with sidechain. B, Complex is shown in surface mode, with interaction phases shown in white.

In agreement with the NMR results, Vpu FFFA and NTB-A also forms the complex in simulation, and the model is shown in Figure 4.8 The complex also adopts parallel fashion with slight tilt. NTB-A employs same face to interact with Vpu mutant FXXXFXXXFXXXA face. Due to the bulky residues lined up on interaction faces, the distance between two proteins in the complex are slightly longer than wild type complex, especially for the C terminal end. The successful generation of the complex suggests that the interaction between TM domain of Vpu and NTB-A are driven by strong hydrophobic/ Van der Walls interaction, since all residues involved interaction in both wild type and mutant complex are non-polar hydrophobic residues.

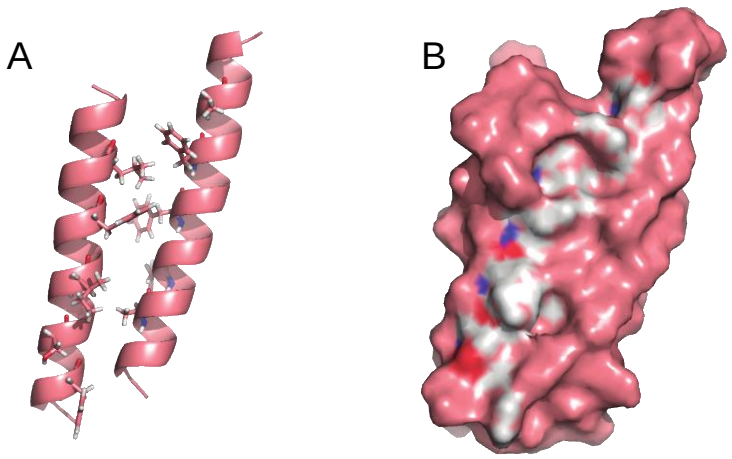

Figure 4.8 Docking simulation of the VpuFFFA/ NTB-A interaction.

A, Both proteins are shown in cartoon form, with residues in the interaction phases shown with sidechain. B, Complex is shown in surface mode, with interaction phases shown in white.

4.6 Summary

A combination of biological, spectroscopic and computational methods was applied to study the interaction of NTB-A and Vpu. All approaches define the same faces in TM domains of both interaction partners, in which Vpu employs the AXXXAXXXAXXXW motif and NTB-A employs the FXXSXXXIXXXFXXXIXXXL motif. In addition, biological studies show that the ability of Vpu to downmodulate NTB-A from the cell surface was lost upon mutation of A14, A18 and W22 to F14, F18 and A22; however, both NMR and computational results imply that mutant Vpu and NTB-A still form interaction complex, with same interaction faces. Notify that docking simulation also suggests that there is a shift and tilt angle change in the complex upon mutation of VpuTM, which might be an explanation for the failure of mutant Vpu to control NTB-A.

Chapter 5 Conclusion

30% of open reading frames encode membrane proteins (1), which play numerous vital cellular functions. Despite the importance of MPs, the structure characterization of MPs is still quite challenging. MPs stay in the lipid bilayer environment, in where they interact with lipids, other MPs and soluble proteins as ligands. Understand the structure and dynamics of MPs in the physiological lipid bilayer environment is a key to understand cellular functions and interactions of MPs. MPs can be expressed with a fusion protein partner as inclusion body to avoid cytotoxicity. After purification, it requires reconstitution of MPs into lipid environment for proper folding and activities. Various membrane-mimicking environments have been applied, such as detergent micelles, nanodiscs, bicelles, bilayers, etc. NMR spectroscopy is a viable tool to study MPs in a variety of membrane-mimicking environments, and provides both structural and dynamics information of MPs. In addition, it can be applied to study protein-protein interactions in lipid environment.

Vpu is a small viral membrane protein encoded in HIV-1 genome with multiple biological functions to counteract human immune system. To study the structure and functions of Vpu in membrane environments, three constructs were made as the Vpu transmembrane domain (VpuTM), Vpu cytoplasmic domain (VpuCyto) and Vpu full-length protein (VpuFull). The secondary structure and dynamics of VpuCyto and VpuFull have been characterized by both CD experiment and solution NMR in both aqueous media and DHPC micelles. Under both conditions, VpuCyto and VpuFull present highly helical content. In addition, ^{1}H-^{15}N HSQC spectra of VpuCyto and VpuFull in DHPC micelles

overlap to a great extent, indicating that VpuCyto is a good representation of cytoplasmic domain in Vpufull. The structure of VpuCyto in DHPC micelles was solved by solution NMR. Dihedral angles defining the peptide planes were extracted from chemical shift of ^{1}HN, ^{15}N, ^{1}Hα, ^{13}Cα and ^{13}Cβ at each amino acid site. To further refine the structure, orientational restraints obtained from RDC values, short-range distance restraints obtained from 15N edited NOESY experiment, and long-range distance restraints obtained from PRE experiments were input into the structure calculation. 20 lowest energy structures were converged to an ensemble with RMSD of 1.12Å for structured region. VpuCyto consists of two well-structured α helices connected by a interhelical loop with intermediate mobility, and highly mobile C- and N- terminal regions. The two helices adopt a U-shape structure, with all acidic and basic residues excluded to the outside of the U-shape and nonpolar residues protected in the core of the U-shape. Structure of VpuFull was solved by RA solid-state NMR in DMPC liposomes. Multidimensional spectra with single site resolution were obtained by MAS NMR experiments. Assignment experiments were performed to get 70% of assigned amino acid in structured regions and mobile regions. Motionally averaged dipolar couplings were measured and used as orientational restraints for structure calculation. In addition, PRE experiments were performed to obtain intramolecular and protein to membrane surface distances. VpuFull in DMPC liposomes consists of a TM region with tilt angle of 25^{o} with respect to bilayer normal, and a U-shape Cyto region lying on the surface of bilayer. Helix-3 in Cyto appears to be more flexible than helix-2, and closer to the membrane surface.

Vpu enhances virion release by counteracting BST2, an interferon inducible restriction factor that prevents the release of newly formed virus from infected cells by

tethering them to the cell surface. Vpu directly interacts with BST-2 through TM domain of both protein, recruits β-TrCP-containing multi-subunit ubiquitin ligase, and cause downmodulation and degradation of BST2. In addition, the W76 residue in C-terminal of Vpu is crucial for virion enhancement, which is independent of activities of BST2 downregulation and degradation. The function of W76 is correlating to the able of Vpu to displace BST2 from virion assembly site on the plasma membrane, and attributes to the interaction of W76 with the lipid bilayer. Membrane anchoring effect of W76 is proved by NMR spectroscopy on VpuCyto in DMPC liposomes and a serial of positively charged lipid liposomes. Also, PRE experiments on VpuCyto in DHPC micelles provides the evidence of membrane embedding of W76, even the majority of C-terminal residues is exposed in the aqueous media.

A well resolved, fully assigned HSQC NMR spectrum for the TM in DHPC lipid micelles were obtained. When unlabeled Vpu TM peptide was added to the ^{15}N-labeled NTB-A TM in micelles, significant chemical shift perturbation and intensity changes were observed for the resonances of NTB-A residues including Phe229, Ser232, Ile236, and Gly239, suggesting that these residues were involved in the helix-helix interaction.

On the other hand, Vpu TM employed Ile11, Ile15 and Trp22 in signals in the interaction with NTB-A. The chemical shift perturbations in Vpu TM induced by NTB-A TM is very similar to those observed for Vpu TM signals induced by interactions with the BST-2 TMD. NMR data were validated by biological experiments. Cell surface expression of NTB-A with interaction sites mutated is not effectively downmodulated. Similarly, Vpu mutant is unable to downmodulate NTB-A to the same extent as wild-type Vpu. Also, docking simulation were performed to generate a model complex of Vpu TM and NTB-A

TM. It adopts a parallel helix-helix interaction in which the AXXXAXXXA motif on Vpu acts as pocket to accept bulky residues in NTB-A. The docking simulation also suggests the hydrogen bond formed between N-term lysine and glutamine, or C-term lysine and glutamic acid favor the helix-helix interaction between the two proteins.

In summary, my thesis describes the structure and dynamics characterization of VpuCyto in DHPC micelles and VpuFull in DMPC liposomes by both solution and solid-state NMR spectroscopy. With the knowledge of structure, solution NMR experiments are employed to study the membrane attachment effect of W76 in the C-terminal of Vpu to enhance virus release. Furthermore, interaction between Vpu and NTB-A are also investigated, and key residues that involved in the interaction have been revealed.

Bibliography

1. Thompson, A. A., Liu, J. J., Chun, E., Wacker, D., Wu, H., Cherezov, V., and Stevens, R. C. (2011) GPCR stabilization using the bicelle-like architecture of mixed sterol-detergent micelles. *Methods* **55**, 310-317

2. Wallin, E., and Heijne, G. V. (1998) Genome‐wide analysis of integral membrane proteins from eubacterial, archaean, and eukaryotic organisms. *Protein Science* **7**, 1029-1038

3. Aisenbrey, C., Borowik, T., Byström, R., Bokvist, M., Lindström, F., Misiak, H., Sani, M.-A., and Gröbner, G. (2008) How is protein aggregation in amyloidogenic diseases modulated by biological membranes? *European Biophysics Journal* **37**, 247-255

4. Bkaily, G., Al-Khoury, J., and Jacques, D. (2014) Nuclear membranes GPCRs: implication in cardiovascular health and diseases. *Current vascular pharmacology* **12**, 215-222

5. Overington, J. P., Al-Lazikani, B., and Hopkins, A. L. (2006) How many drug targets are there? *Nature reviews Drug discovery* **5**, 993-996

6. Sanders, C. R., and Myers, J. K. (2004) Disease-related misassembly of membrane proteins. *Annu. Rev. Biophys. Biomol. Struct.* **33**, 25-51

7. Murray, C. W., Verdonk, M. L., and Rees, D. C. (2012) Experiences in fragment-based drug discovery. *Trends in pharmacological sciences* **33**, 224-232

8. Sahdev, S., Khattar, S. K., and Saini, K. S. (2008) Production of active eukaryotic proteins through bacterial expression systems: a review of the existing biotechnology strategies. *Molecular and cellular biochemistry* **307**, 249-264

9. Dumon-Seignovert, L., Cariot, G., and Vuillard, L. (2004) The toxicity of recombinant proteins in Escherichia coli: a comparison of overexpression in BL21 (DE3), C41 (DE3), and C43 (DE3). *Protein expression and purification* **37**, 203-206

10. Strausberg, R. L., and Strausberg, S. L. (2001) Overview of protein expression in Saccharomyces cerevisiae. *Current Protocols in Protein Science*, 5.6. 1-5.6. 7

11. Contreras‐Gómez, A., Sánchez‐Mirón, A., García‐Camacho, F., Molina‐Grima, E., and Chisti, Y. (2014) Protein production using the baculovirus‐insect cell expression system. *Biotechnology progress* **30**, 1-18

12. Khan, K. H. (2013) Gene expression in mammalian cells and its applications. *Advanced pharmaceutical bulletin* **3**, 257
13. Park, K.-H., Billon-Denis, E., Dahmane, T., Lebaupain, F., Pucci, B., Breyton, C., and Zito, F. (2011) In the cauldron of cell-free synthesis of membrane proteins: playing with new surfactants. *New biotechnology* **28**, 255-261

14. Periasamy, A., Shadiac, N., Amalraj, A., Garajova, S., Nagarajan, Y., Waters, S., Mertens, H., and Hrmova, M. (2012) Cell-free synthesis of membrane (1, 3)-β-d-glucan (curdlan) synthase: co-translational insertion in liposomes and reconstitution in nanodiscs. *Biochim Biophys Acta: Biomembr* **1828**, 743-757

15. Roos, C., Zocher, M., Müller, D., Münch, D., Schneider, T., Sahl, H.-G., Scholz, F., Wachtveitl, J., Ma, Y., and Proverbio, D. (2012) Characterization of co-translationally formed nanodisc complexes with small multidrug transporters, proteorhodopsin and with the E. coli MraY translocase. *Biochimica et Biophysica Acta (BBA)-Biomembranes* **1818**, 3098-3106

16. Sanders, C. R., and Schwonek, J. P. (1992) Characterization of magnetically orientable bilayers in mixtures of dihexanoylphosphatidylcholine and dimyristoylphosphatidylcholine by solid-state NMR. *Biochemistry* **31**, 8898-8905

17. Faham, S., and Bowie, J. U. (2002) Bicelle crystallization: a new method for crystallizing membrane proteins yields a monomeric bacteriorhodopsin structure. *Journal of molecular biology* **316**, 1-6

18. Bayburt, T. H., and Sligar, S. G. (2010) Membrane protein assembly into Nanodiscs. *FEBS letters* **584**, 1721-1727

19. Paternostre, M. T., Roux, M., and Rigaud, J. L. (1988) Mechanisms of membrane protein insertion into liposomes during reconstitution procedures involving the use of detergents. 1. Solubilization of large unilamellar liposomes (prepared by reverse-phase evaporation) by triton X-100, octyl glucoside, and sodium cholate. *Biochemistry* **27**, 2668-2677

20. Rigaud, J. L., Paternostre, M. T., and Bluzat, A. (1988) Mechanisms of membrane protein insertion into liposomes during reconstitution procedures involving the use of detergents. 2. Incorporation of the light-driven proton pump bacteriorhodopsin. *Biochemistry* **27**, 2677-2688

21. Caffrey, M., and Cherezov, V. (2009) Crystallizing membrane proteins using lipidic mesophases. *Nature protocols* **4**, 706-731

22. Chae, P. S., Rasmussen, S. G., Rana, R. R., Gotfryd, K., Chandra, R., Goren, M. A., Kruse, A. C., Nurva, S., Loland, C. J., and Pierre, Y. (2010) Maltose-neopentyl

glycol (MNG) amphiphiles for solubilization, stabilization and crystallization of membrane proteins. *Nature methods* **7**, 1003-1008

23. Zhou, Y., and Bowie, J. U. (2000) Building a thermostable membrane protein. *Journal of Biological Chemistry* **275**, 6975-6979

24. Wang, C., Wu, H., Katritch, V., Han, G. W., Huang, X.-P., Liu, W., Siu, F. Y., Roth, B. L., Cherezov, V., and Stevens, R. C. (2013) Structure of the human smoothened receptor bound to an antitumour agent. *Nature* **497**, 338-343

25. Standfuss, J., Edwards, P. C., D'Antona, A., Fransen, M., Xie, G., Oprian, D. D., and Schertler, G. F. (2011) The structural basis of agonist-induced activation in constitutively active rhodopsin. *Nature* **471**, 656-660

26. Steyaert, J., and Kobilka, B. K. (2011) Nanobody stabilization of G protein-coupled receptor conformational states. *Current opinion in structural biology* **21**, 567-572

27. Boutet, S., Lomb, L., Williams, G. J., Barends, T. R., Aquila, A., Doak, R. B., Weierstall, U., DePonte, D. P., Steinbrener, J., and Shoeman, R. L. (2012) High-resolution protein structure determination by serial femtosecond crystallography. *Science* **337**, 362-364

28. Zhang, R., Hryc, C. F., Cong, Y., Liu, X., Jakana, J., Gorchakov, R., Baker, M. L., Weaver, S. C., and Chiu, W. (2011) 4.4 Å cryo‐EM structure of an enveloped alphavirus Venezuelan equine encephalitis virus. *The EMBO journal* **30**, 3854-3863

29. Goto, N. K., Gardner, K. H., Mueller, G. A., Willis, R. C., and Kay, L. E. (1999) A robust and cost-effective method for the production of Val, Leu, Ile (δ1) methyl-protonated 15N-, 13C-, 2H-labeled proteins. *Journal of biomolecular NMR* **13**, 369-374

30. Egorova-Zachernyuk, T. A., Bosman, G. J., and DeGrip, W. J. (2011) Uniform stable-isotope labeling in mammalian cells: formulation of a cost-effective culture medium. *Applied microbiology and biotechnology* **89**, 397-406

31. Fan, Y., Shi, L., Ladizhansky, V., and Brown, L. S. (2011) Uniform isotope labeling of a eukaryotic seven-transmembrane helical protein in yeast enables high-resolution solid-state NMR studies in the lipid environment. *Journal of biomolecular NMR* **49**, 151-161

32. Hefke, F., Bagaria, A., Reckel, S., Ullrich, S. J., Dötsch, V., Glaubitz, C., and Güntert, P. (2011) Optimization of amino acid type-specific 13C and 15N labeling for the backbone assignment of membrane proteins by solution-and solid-state NMR with the UPLABEL algorithm. *Journal of biomolecular NMR* **49**, 75-84

33. Yang, D., and Kay, L. E. (1999) Improved lineshape and sensitivity in the HNCO-family of triple resonance experiments. *Journal of Biomolecular NMR* **14**, 273-276

34. Hiller, S., Garces, R. G., Malia, T. J., Orekhov, V. Y., Colombini, M., and Wagner, G. (2008) Solution structure of the integral human membrane protein VDAC-1 in detergent micelles. *Science* **321**, 1206-1210

35. Sharma, M., Yi, M., Dong, H., Qin, H., Peterson, E., Busath, D. D., Zhou, H.-X., and Cross, T. A. (2010) Insight into the mechanism of the influenza A proton channel from a structure in a lipid bilayer. *Science* **330**, 509-512

36. Park, S. H., Das, B. B., Casagrande, F., Tian, Y., Nothnagel, H. J., Chu, M., Kiefer, H., Maier, K., De Angelis, A. A., and Marassi, F. M. (2012) Structure of the chemokine receptor CXCR1 in phospholipid bilayers. *Nature* **491**, 779-783

37. Singer, S., and Nicolson, G. L. (1972) The fluid mosaic model of the structure of cell membranes. *Day and Good Membranes and viruses in immunopathology*, 7-47

38. De Angelis, A. A., and Opella, S. J. (2007) Bicelle samples for solid-state NMR of membrane proteins. *Nature protocols* **2**, 2332-2338

39. Son, W. S., Park, S. H., Nothnagel, H. J., Lu, G. J., Wang, Y., Zhang, H., Cook, G. A., Howell, S. C., and Opella, S. J. (2012) 'q-Titration'of long-chain and short-chain lipids differentiates between structured and mobile residues of membrane proteins studied in bicelles by solution NMR spectroscopy. *Journal of Magnetic Resonance* **214**, 111-118

40. Hagn, F., Etzkorn, M., Raschle, T., and Wagner, G. (2013) Optimized phospholipid bilayer nanodiscs facilitate high-resolution structure determination of membrane proteins. *Journal of the American Chemical Society* **135**, 1919-1925

41. Opella, S. J., and Marassi, F. M. (2004) Structure determination of membrane proteins by NMR spectroscopy. *Chemical reviews* **104**, 3587-3606

42. Park, S. H., Mrse, A. A., Nevzorov, A. A., De Angelis, A. A., and Opella, S. J. (2006) Rotational diffusion of membrane proteins in aligned phospholipid bilayers by solid-state NMR spectroscopy. *Journal of Magnetic Resonance* **178**, 162-165

43. Renault, M., Cukkemane, A., and Baldus, M. (2010) Solid‐State NMR Spectroscopy on Complex Biomolecules. *Angewandte Chemie International Edition* **49**, 8346-8357

44. Opella, S. J. (2013) Structure determination of membrane proteins in their native phospholipid bilayer environment by rotationally aligned solid-state NMR spectroscopy. *Accounts of chemical research* **46**, 2145-2153

45. Salzmann, M., Wider, G., Pervushin, K., and Wüthrich, K. (1999) Improved sensitivity and coherence selection for [15N, 1H]-TROSY elements in triple resonance experiments. *Journal of biomolecular NMR* **15**, 181-184

46. Wishart, D., Sykes, B., and Richards, F. (1992) The chemical shift index: a fast and simple method for the assignment of protein secondary structure through NMR spectroscopy. *Biochemistry* **31**, 1647-1651

47. Mesleh, M. F., and Opella, S. J. (2003) Dipolar waves as NMR maps of helices in proteins. *Journal of magnetic resonance* **163**, 288-299

48. Veglia, G., Zeri, A. C., Ma, C., and Opella, S. J. (2002) Deuterium/hydrogen exchange factors measured by solution nuclear magnetic resonance spectroscopy as indicators of the structure and topology of membrane proteins. *Biophysical journal* **82**, 2176-2183

49. Bogusky, M., Schiksnis, R., Leo, G., and Opella, S. (1987) Protein backbone dynamics by solid-state and solution 15 N NMR spectroscopy. *Journal of Magnetic Resonance (1969)* **72**, 186-190

50. Shen, Y., Delaglio, F., Cornilescu, G., and Bax, A. (2009) TALOS+: a hybrid method for predicting protein backbone torsion angles from NMR chemical shifts. *Journal of biomolecular NMR* **44**, 213-223

51. Schwieters, C. D., Kuszewski, J. J., Tjandra, N., and Clore, G. M. (2003) The Xplor-NIH NMR molecular structure determination package. *Journal of Magnetic Resonance* **160**, 65-73

52. Schwieters, C. D., Kuszewski, J. J., and Clore, G. M. (2006) Using Xplor–NIH for NMR molecular structure determination. *Progress in Nuclear Magnetic Resonance Spectroscopy* **48**, 47-62

53. Shen, Y., Lange, O., Delaglio, F., Rossi, P., Aramini, J. M., Liu, G., Eletsky, A., Wu, Y., Singarapu, K. K., and Lemak, A. (2008) Consistent blind protein structure generation from NMR chemical shift data. *Proceedings of the National Academy of Sciences* **105**, 4685-4690

54. Battiste, J. L., and Wagner, G. (2000) Utilization of site-directed spin labeling and high-resolution heteronuclear nuclear magnetic resonance for global fold determination of large proteins with limited nuclear overhauser effect data. *Biochemistry* **39**, 5355-5365

55. Donaldson, L. W., Skrynnikov, N. R., Choy, W.-Y., Muhandiram, D. R., Sarkar, B., Forman-Kay, J. D., and Kay, L. E. (2001) Structural characterization of proteins with an attached ATCUN motif by paramagnetic relaxation enhancement NMR spectroscopy. *Journal of the American Chemical Society* **123**, 9843-9847

56. Liang, B., Bushweller, J. H., and Tamm, L. K. (2006) Site-directed parallel spin-labeling and paramagnetic relaxation enhancement in structure determination of membrane proteins by solution NMR spectroscopy. *Journal of the American Chemical Society* **128**, 4389-4397

57. Prestegard, J., Al-Hashimi, H., and Tolman, J. (2000) NMR structures of biomolecules using field oriented media and residual dipolar couplings. *Quarterly reviews of biophysics* **33**, 371-424

58. Park, S. H., Son, W. S., Mukhopadhyay, R., Valafar, H., and Opella, S. J. (2009) Phage-induced alignment of membrane proteins enables the measurement and structural analysis of residual dipolar couplings with dipolar waves and λ-maps. *Journal of the American Chemical Society* **131**, 14140-14141

59. Sass, H.-J., Musco, G., Stahl, S. J., Wingfield, P. T., and Grzesiek, S. (2000) Solution NMR of proteins within polyacrylamide gels: diffusional properties and residual alignment by mechanical stress or embedding of oriented purple membranes. *Journal of biomolecular NMR* **18**, 303-309

60. Chou, J. J., Gaemers, S., Howder, B., Louis, J. M., and Bax, A. (2001) A simple apparatus for generating stretched polyacrylamide gels, yielding uniform alignment of proteins and detergent micelles*. *Journal of biomolecular NMR* **21**, 377-382

61. Douglas, S. M., Chou, J. J., and Shih, W. M. (2007) DNA-nanotube-induced alignment of membrane proteins for NMR structure determination. *Proceedings of the National Academy of Sciences* **104**, 6644-6648

62. Veglia, G., and Opella, S. J. (2000) Lanthanide ion binding to adventitious sites aligns membrane proteins in micelles for solution NMR spectroscopy. *Journal of the American Chemical Society* **122**, 11733-11734

63. Gaemers, S., and Bax, A. (2001) Morphology of three lyotropic liquid crystalline biological NMR media studied by translational diffusion anisotropy. *Journal of the American Chemical Society* **123**, 12343-12352

64. Marassi, F. M., Das, B. B., Lu, G. J., Nothnagel, H. J., Park, S. H., Son, W. S., Tian, Y., and Opella, S. J. (2011) Structure determination of membrane proteins in five easy pieces. *Methods* **55**, 363-369

65. Lewis, B., Harbison, G., Herzfeld, J., and Griffin, R. G. (1985) NMR structural analysis of a membrane protein: bacteriorhodopsin peptide backbone orientation and motion. *Biochemistry* **24**, 4671-4679

66. Hong, M., and Doherty, T. (2006) Orientation determination of membrane-disruptive proteins using powder samples and rotational diffusion: a simple solid-state NMR approach. *Chemical physics letters* **432**, 296-300

67. Das, B. B., Nothnagel, H. J., Lu, G. J., Son, W. S., Tian, Y., Marassi, F. M., and Opella, S. J. (2012) Structure determination of a membrane protein in proteoliposomes. *Journal of the American Chemical Society* **134**, 2047-2056

68. Williamson, R. A., Carr, M. D., Frenkiel, T. A., Feeney, J., and Freedman, R. B. (1997) Mapping the binding site for matrix metalloproteinase on the N-terminal domain of the tissue inhibitor of metalloproteinases-2 by NMR chemical shift perturbation. *Biochemistry* **36**, 13882-13889

69. Williamson, M. P. (2013) Using chemical shift perturbation to characterise ligand binding. *Progress in nuclear magnetic resonance spectroscopy* **73**, 1-16

70. Mahoney, N. M., Rastogi, V. K., Cahill, S. M., Girvin, M. E., and Almo, S. C. (2000) Binding orientation of proline-rich peptides in solution: polarity of the profilin-ligand interaction. *Journal of the American Chemical Society* **122**, 7851-7852

71. Ramos, A., and Varani, G. (1998) A new method to detect long-range protein-RNA contacts: NMR detection of electron-proton relaxation induced by nitroxide spin-labeled RNA. *Journal of the American Chemical Society* **120**, 10992-10993

72. Mayer, M., and Meyer, B. (1999) Characterization of ligand binding by saturation transfer difference NMR spectroscopy. *Angewandte Chemie International Edition* **38**, 1784-1788

73. Lepre, C. A., Moore, J. M., and Peng, J. W. (2004) Theory and applications of NMR-based screening in pharmaceutical research. *Chemical reviews* **104**, 3641-3676

74. Cohen, E. A., Terwilliger, E. F., Sodroski, J. G., and Haseltine, W. A. (1988) Identification of a protein encoded by the vpu gene of HIV-1.

75. Strebel, K., Klimkait, T., and Martin, M. A. (1988) A novel gene of HIV-1, vpu, and its 16-kilodalton product. *Science* **241**, 1221-1223

76. Maldarelli, F., Chen, M., Willey, R. L., and Strebel, K. (1993) Human immunodeficiency virus type 1 Vpu protein is an oligomeric type I integral membrane protein. *Journal of virology* **67**, 5056-5061

77. Courgnaud, V., Salemi, M., Pourrut, X., Mpoudi-Ngole, E., Abela, B., Auzel, P., Bibollet-Ruche, F., Hahn, B., Vandamme, A.-M., and Delaporte, E. (2002) Characterization of a novel simian immunodeficiency virus with a vpu gene from

greater spot-nosed monkeys (Cercopithecus nictitans) provides new insights into simian/human immunodeficiency virus phylogeny. *Journal of virology* **76**, 8298-8309

78. Barlow, K. L., Ajao, A. O., and Clewley, J. P. (2003) Characterization of a novel simian immunodeficiency virus (SIVmonNG1) genome sequence from a mona monkey (Cercopithecus mona). *Journal of virology* **77**, 6879-6888

79. SCHUBERT, U., SCHNEIDER, T., HENKLEIN, P., HOFFMANN, K., BERTHOLD, E., HAUSER, H., PAULI, G., and PORSTMANN, T. (1992) Human ‐ immundeficiency ‐ virus ‐ type ‐ 1 ‐ encoded Vpu protein is phosphorylated by casein kinase II. *European Journal of Biochemistry* **204**, 875-883

80. Ruiz, A., Guatelli, J. C., and Stephens, E. B. (2010) The Vpu protein: new concepts in virus release and CD4 down-modulation. *Current HIV research* **8**, 240

81. Richard, J., and Cohen, É. A. (2010) HIV-1 Vpu disarms natural killer cells. *Cell host & microbe* **8**, 389-391

82. Willey, R., Maldarelli, F., Martin, M., and Strebel, K. (1992) Human immunodeficiency virus type 1 Vpu protein induces rapid degradation of CD4. *Journal of virology* **66**, 7193-7200

83. Crise, B., Buonocore, L., and Rose, J. (1990) CD4 is retained in the endoplasmic reticulum by the human immunodeficiency virus type 1 glycoprotein precursor. *Journal of virology* **64**, 5585-5593

84. Jabbar, M. A., and Nayak, D. P. (1990) Intracellular interaction of human immunodeficiency virus type 1 (ARV-2) envelope glycoprotein gp160 with CD4 blocks the movement and maturation of CD4 to the plasma membrane. *Journal of virology* **64**, 6297-6304

85. Tanaka, M., Ueno, T., Nakahara, T., Sasaki, K., Ishimoto, A., and Sakai, H. (2003) Downregulation of CD4 is required for maintenance of viral infectivity of HIV-1. *Virology* **311**, 316-325

86. Wildum, S., Schindler, M., Münch, J., and Kirchhoff, F. (2006) Contribution of Vpu, Env, and Nef to CD4 down-modulation and resistance of human immunodeficiency virus type 1-infected T cells to superinfection. *Journal of virology* **80**, 8047-8059

87. Margottin, F., Bour, S., Durand, H., Selig, L., Benichou, S., Richard, V., Thomas, D., and Strebel, K. 440 and R. Benarous. 1998. A novel human WD protein, h-beta TrCp, that interacts with HIV-1 Vpu 441 connects CD4 to the ER degradation pathway through an F-box motif. *Mol Cell* **1**, 565-574

88. Tiganos, E., Yao, X.-J., Friborg, J., Daniel, N., and Cohen, E. A. (1997) Putative alpha-helical structures in the human immunodeficiency virus type 1 Vpu protein and CD4 are involved in binding and degradation of the CD4 molecule. *Journal of virology* **71**, 4452-4460

89. Pacyniak, E., Gomez, M. L., Gomez, L. M., Mulcahy, E. R., Jackson, M., Hout, D. R., Wisdom, B. J., and Stephens, E. B. (2005) Identification of a region within the cytoplasmic domain of the subtype B Vpu protein of human immunodeficiency virus type 1 (HIV-1) that is responsible for retention in the golgi complex and its absence in the Vpu protein from a subtype C HIV-1. *AIDS Research & Human Retroviruses* **21**, 379-394

90. Hill, M. S., Ruiz, A., Schmitt, K., and Stephens, E. B. (2010) Identification of amino acids within the second alpha helical domain of the human immunodeficiency virus type 1 Vpu that are critical for preventing CD4 cell surface expression. *Virology* **397**, 104-112

91. Neil, S. J., Zang, T., and Bieniasz, P. D. (2008) Tetherin inhibits retrovirus release and is antagonized by HIV-1 Vpu. *Nature* **451**, 425-430

92. Van Damme, N., Goff, D., Katsura, C., Jorgenson, R. L., Mitchell, R., Johnson, M. C., Stephens, E. B., and Guatelli, J. (2008) The interferon-induced protein BST-2 restricts HIV-1 release and is downregulated from the cell surface by the viral Vpu protein. *Cell host & microbe* **3**, 245-252

93. McNatt, M. W., Zang, T., Hatziioannou, T., Bartlett, M., Fofana, I. B., Johnson, W. E., Neil, S. J., and Bieniasz, P. D. (2009) Species-specific activity of HIV-1 Vpu and positive selection of tetherin transmembrane domain variants. *PLoS pathogens* **5**, e1000300

94. Skasko, M., Wang, Y., Tian, Y., Tokarev, A., Munguia, J., Ruiz, A., Stephens, E. B., Opella, S. J., and Guatelli, J. (2012) HIV-1 Vpu protein antagonizes innate restriction factor BST-2 via lipid-embedded helix-helix interactions. *Journal of Biological Chemistry* **287**, 58-67

95. Iwabu, Y., Fujita, H., Kinomoto, M., Kaneko, K., Ishizaka, Y., Tanaka, Y., Sata, T., and Tokunaga, K. (2009) HIV-1 accessory protein Vpu internalizes cell-surface BST-2/tetherin through transmembrane interactions leading to lysosomes. *Journal of Biological Chemistry* **284**, 35060-35072

96. Mitchell, R. S., Katsura, C., Skasko, M. A., Fitzpatrick, K., Lau, D., Ruiz, A., Stephens, E. B., Margottin-Goguet, F., Benarous, R., and Guatelli, J. C. (2009) Vpu antagonizes BST-2–mediated restriction of HIV-1 release via β-TrCP and endo-lysosomal trafficking. *PLoS pathogens* **5**, e1000450

97. McNatt, M. W., Zang, T., and Bieniasz, P. D. (2013) Vpu binds directly to tetherin and displaces it from nascent virions. *PLoS pathogens* **9**, e1003299

98. Jafari, M., Guatelli, J., and Lewinski, M. K. (2014) Activities of transmitted/founder and chronic clade B HIV-1 Vpu and a C-terminal polymorphism specifically affecting virion release. *Journal of virology* **88**, 5062-5078

99. Shah, A. H., Sowrirajan, B., Davis, Z. B., Ward, J. P., Campbell, E. M., Planelles, V., and Barker, E. (2010) Degranulation of natural killer cells following interaction with HIV-1-infected cells is hindered by downmodulation of NTB-A by Vpu. *Cell host & microbe* **8**, 397-409

100. Moll, M., Andersson, S. K., Smed-Sörensen, A., and Sandberg, J. K. (2010) Inhibition of lipid antigen presentation in dendritic cells by HIV-1 Vpu interference with CD1d recycling from endosomal compartments. *Blood* **116**, 1876-1884

101. Ramirez, P. W., Famiglietti, M., Sowrirajan, B., DePaula-Silva, A. B., Rodesch, C., Barker, E., Bosque, A., and Planelles, V. (2014) Downmodulation of CCR7 by HIV-1 Vpu Results in Impaired Migration and Chemotactic Signaling within CD4+ T Cells. *Cell reports* **7**, 2019-2030

102. Bolduan, S., Reif, T., Schindler, M., and Schubert, U. (2014) HIV-1 Vpu mediated downregulation of CD155 requires alanine residues 10, 14 and 18 of the transmembrane domain. *Virology* **464**, 375-384

103. Dubé, M., Bego, M. G., Paquay, C., and Cohen, É. A. (2010) Modulation of HIV-1-host interaction: role of the Vpu accessory protein. *Retrovirology* **7**, 114

104. Roy, N., Pacini, G., Berlioz-Torrent, C., and Janvier, K. (2014) Mechanisms underlying HIV-1 Vpu-mediated viral egress. *Frontiers in microbiology* **5**

105. Sowrirajan, B., and Barker, E. (2011) The natural killer cell cytotoxic function is modulated by HIV-1 accessory proteins. *Viruses* **3**, 1091-1111

106. Magadán, J. G., and Bonifacino, J. S. (2012) Transmembrane domain determinants of CD4 Downregulation by HIV-1 Vpu. *Journal of virology* **86**, 757-772

107. Kerkau, T., Bacik, I., Bennink, J. R., Yewdell, J. W., Hünig, T., Schimpl, A., and Schubert, U. (1997) The human immunodeficiency virus type 1 (HIV-1) Vpu protein interferes with an early step in the biosynthesis of major histocompatibility complex (MHC) class I molecules. *The Journal of experimental medicine* **185**, 1295-1306

108. Hart, M., Concordet, J., Lassot, I., Albert, I., Del los Santos, R., Durand, H., Perret, C., Rubinfeld, B., Margottin, F., and Benarous, R. (1999) The F-box protein β-TrCP associates with phosphorylated β-catenin and regulates its activity in the cell. *Current biology* **9**, 207-211

109. Miyagi, E., Andrew, A. J., Kao, S., and Strebel, K. (2009) Vpu enhances HIV-1 virus release in the absence of Bst-2 cell surface down-modulation and intracellular depletion. *Proceedings of the National Academy of Sciences* **106**, 2868-2873

110. Goffinet, C., Homann, S., Ambiel, I., Tibroni, N., Rupp, D., Keppler, O. T., and Fackler, O. T. (2010) Antagonism of CD317 restriction of human immunodeficiency virus type 1 (HIV-1) particle release and depletion of CD317 are separable activities of HIV-1 Vpu. *Journal of virology* **84**, 4089-4094

111. Tervo, H.-M., Homann, S., Ambiel, I., Fritz, J. V., Fackler, O. T., and Keppler, O. T. (2011) b-TrCP is dispensable for Vpu's ability to overcome the CD317/Tetherin-imposed restriction to HIV-1 release. *Retrovirology* **8**

112. Tokarev, A. A., Munguia, J., and Guatelli, J. C. (2011) Serine-threonine ubiquitination mediates downregulation of BST-2/tetherin and relief of restricted virion release by HIV-1 Vpu. *Journal of virology* **85**, 51-63

113. Lewinski, M. K., Jafari, M., Zhang, H., Opella, S. J., and Guatelli, J. (2015) Membrane Anchoring by a C-terminal Tryptophan Enables HIV-1 Vpu to Displace Bone Marrow Stromal Antigen 2 (BST2) from Sites of Viral Assembly. *Journal of Biological Chemistry* **290**, 10919-10933

114. Campbell, R., Meirovitch, E., and Freed, J. (1979) Slow-motional NMR line shapes for very anisotropic rotational diffusion. Phosphorus-31 NMR of phospholipids. *Journal of Physical Chemistry* **83**, 525-533

115. Park, S. H., Mrse, A. A., Nevzorov, A. A., Mesleh, M. F., Oblatt-Montal, M., Montal, M., and Opella, S. J. (2003) Three-dimensional structure of the channel-forming trans-membrane domain of virus protein "u"(Vpu) from HIV-1. *Journal of molecular biology* **333**, 409-424

116. Park, S. H., De Angelis, A. A., Nevzorov, A. A., Wu, C. H., and Opella, S. J. (2006) Three-dimensional structure of the transmembrane domain of Vpu from HIV-1 in aligned phospholipid bicelles. *Biophysical journal* **91**, 3032-3042

117. Willbold, D., Hoffmann, S., and Rösch, P. (1997) Secondary structure and tertiary fold of the human immunodeficiency virus protein U (Vpu) cytoplasmic domain in solution. *European Journal of Biochemistry* **245**, 581-588

118. Wittlich, M., Koenig, B. W., Stoldt, M., Schmidt, H., and Willbold, D. (2009) NMR structural characterization of HIV‐1 virus protein U cytoplasmic domain in the presence of dodecylphosphatidylcholine micelles. *Febs Journal* **276**, 6560-6575

119. Lesage, A., Bardet, M., and Emsley, L. (1999) Through-bond carbon-carbon connectivities in disordered solids by NMR. *Journal of the American Chemical Society* **121**, 10987-10993

120. Leppert, J., Ohlenschläger, O., Görlach, M., and Ramachandran, R. (2004) Adiabatic TOBSY in rotating solids. *Journal of biomolecular NMR* **29**, 167-173

121. Zweckstetter, M., and Bax, A. (2000) Prediction of sterically induced alignment in a dilute liquid crystalline phase: aid to protein structure determination by NMR. *Journal of the American Chemical Society* **122**, 3791-3792

122. Kay, L. E., Torchia, D. A., and Bax, A. (1989) Backbone dynamics of proteins as studied by nitrogen-15 inverse detected heteronuclear NMR spectroscopy: application to staphylococcal nuclease. *Biochemistry* **28**, 8972-8979

123. Farrow, N. A., Muhandiram, R., Singer, A. U., Pascal, S. M., Kay, C. M., Gish, G., Shoelson, S. E., Pawson, T., Forman-Kay, J. D., and Kay, L. E. (1994) Backbone dynamics of a free and a phosphopeptide-complexed Src homology 2 domain studied by 15N NMR relaxation. *Biochemistry* **33**, 5984-6003

124. Wittlich, M., Koenig, B. W., and Willbold, D. (2008) Structural consequences of phosphorylation of two serine residues in the cytoplasmic domain of HIV‐1 VpU. *Journal of Peptide Science* **14**, 804-810

125. Coadou, G., Evrard-Todeschi, N., Gharbi-Benarous, J., Benarous, R., and Girault, J.-P. (2002) HIV-1 encoded virus protein U (Vpu) solution structure of the 41–62 hydrophilic region containing the phosphorylated sites Ser 52 and Ser 56. *International journal of biological macromolecules* **30**, 23-40

126. Coadou, G., Gharbi-Benarous, J., Megy, S., Bertho, G., Evrard-Todeschi, N., Segeral, E., Benarous, R., and Girault, J.-P. (2003) NMR studies of the phosphorylation motif of the HIV-1 protein Vpu bound to the F-box protein β-TrCP. *Biochemistry* **42**, 14741-14751

127. Evrard-Todeschi, N., Gharbi-Benarous, J., Bertho, G., Coadou, G., Megy, S., Benarous, R., and Girault, J.-P. (2006) NMR studies for identifying phosphopeptide ligands of the HIV-1 protein Vpu binding to the F-box protein β-TrCP. *peptides* **27**, 194-210

128. Ma, C., Marassi, F. M., Jones, D. H., Straus, S. K., Bour, S., Strebel, K., Schubert, U., Oblatt‐Montal, M., Montal, M., and Opella, S. J. (2002) Expression,

purification, and activities of full‐length and truncated versions of the integral membrane protein Vpu from HIV‐1. *Protein science* **11**, 546-557

129. Marassi, F., Ma, C., Gratkowski, H., Straus, S., Strebel, K., Oblatt-Montal, M., Montal, M., and Opella, S. (1999) Correlation of the structural and functional domains in the membrane protein Vpu from HIV-1. *Proceedings of the National Academy of Sciences* **96**, 14336-14341

130. Jones, D. H., and Opella, S. J. (2004) Weak alignment of membrane proteins in stressed polyacrylamide gels. *Journal of Magnetic Resonance* **171**, 258-269

131. Whitmore, L., and Wallace, B. (2004) DICHROWEB, an online server for protein secondary structure analyses from circular dichroism spectroscopic data. *Nucleic acids research* **32**, W668-W673

132. Whitmore, L., and Wallace, B. A. (2008) Protein secondary structure analyses from circular dichroism spectroscopy: methods and reference databases. *Biopolymers* **89**, 392-400

133. Bloembergen, N. (1949) On the interaction of nuclear spins in a crystalline lattice. *Physica* **15**, 386-426

134. Takegoshi, K., Nakamura, S., and Terao, T. (2001) 13C–1H dipolar-assisted rotational resonance in magic-angle spinning NMR. *Chemical Physics Letters* **344**, 631-637

135. Takegoshi, K., Nakamura, S., and Terao, T. (2003) 13C-1H dipolar-driven 13C-13C recoupling without 13C rf irradiation in nuclear magnetic resonance of rotating solids. *Journal of Chemical Physics* **118**, 2325-2341

136. Baldus, M., Petkova, A. T., Herzfeld, J., and Griffin, R. G. (1998) Cross polarization in the tilted frame: assignment and spectral simplification in heteronuclear spin systems. *Molecular Physics* **95**, 1197-1207

137. Zhao, X., Edén, M., and Levitt, M. H. (2001) Recoupling of heteronuclear dipolar interactions in solid-state NMR using symmetry-based pulse sequences. *Chemical physics letters* **342**, 353-361

138. Delaglio, F., Grzesiek, S., Vuister, G. W., Zhu, G., Pfeifer, J., and Bax, A. (1995) NMRPipe: a multidimensional spectral processing system based on UNIX pipes. *Journal of biomolecular NMR* **6**, 277-293

139. Gong, X.-M., Ding, Y., Yu, J., Yao, Y., and Marassi, F. M. (2015) Structure of the Na, K-ATPase regulatory protein FXYD2b in micelles: Implications for membrane–water interfacial arginines. *Biochimica et Biophysica Acta (BBA)-Biomembranes* **1848**, 299-306

140. Neil, S. J., Zang, T., and Bieniasz, P. D. (2008) Tetherin inhibits retrovirus release and is antagonized by HIV-1 Vpu. *Nature* **451**, 425-430

141. Van Damme, N., Goff, D., Katsura, C., Jorgenson, R. L., Mitchell, R., Johnson, M. C., Stephens, E. B., and Guatelli, J. (2008) The interferon-induced protein BST-2 restricts HIV-1 release and is downregulated from the cell surface by the viral Vpu protein. *Cell Host Microbe* **3**, 245-252

142. Park, S. H., De Angelis, A. A., Nevzorov, A. A., Wu, C. H., and Opella, S. J. (2006) Three-dimensional structure of the transmembrane domain of Vpu from HIV-1 in aligned phospholipid bicelles. *Biophys J* **91**, 3032-3042

143. Kupzig, S., Korolchuk, V., Rollason, R., Sugden, A., Wilde, A., and Banting, G. (2003) Bst-2/HM1.24 is a raft-associated apical membrane protein with an unusual topology. *Traffic* **4**, 694-709

144. McNatt, M. W., Zang, T., Hatziioannou, T., Bartlett, M., Fofana, I. B., Johnson, W. E., Neil, S. J., and Bieniasz, P. D. (2009) Species-specific activity of HIV-1 Vpu and positive selection of tetherin transmembrane domain variants. *PLoS Pathog* **5**, e1000300

145. Skasko, M., Wang, Y., Tian, Y., Tokarev, A., Munguia, J., Ruiz, A., Stephens, E. B., Opella, S. J., and Guatelli, J. (2012) HIV-1 Vpu protein antagonizes innate restriction factor BST-2 via lipid-embedded helix-helix interactions. *J Biol Chem* **287**, 58-67

146. Dube, M., Roy, B. B., Guiot-Guillain, P., Binette, J., Mercier, J., Chiasson, A., and Cohen, E. A. (2010) Antagonism of tetherin restriction of HIV-1 release by Vpu involves binding and sequestration of the restriction factor in a perinuclear compartment. *PLoS Pathog* **6**, e1000856

147. Iwabu, Y., Fujita, H., Kinomoto, M., Kaneko, K., Ishizaka, Y., Tanaka, Y., Sata, T., and Tokunaga, K. (2009) HIV-1 accessory protein Vpu internalizes cell-surface BST-2/tetherin through transmembrane interactions leading to lysosomes. *J Biol Chem* **284**, 35060-35072

148. Goffinet, C., Allespach, I., Homann, S., Tervo, H. M., Habermann, A., Rupp, D., Oberbremer, L., Kern, C., Tibroni, N., Welsch, S., Krijnse-Locker, J., Banting, G., Krausslich, H. G., Fackler, O. T., and Keppler, O. T. (2009) HIV-1 antagonism of CD317 is species specific and involves Vpu-mediated proteasomal degradation of the restriction factor. *Cell Host Microbe* **5**, 285-297

149. Mitchell, R. S., Katsura, C., Skasko, M. A., Fitzpatrick, K., Lau, D., Ruiz, A., Stephens, E. B., Margottin-Goguet, F., Benarous, R., and Guatelli, J. C. (2009) Vpu

antagonizes BST-2-mediated restriction of HIV-1 release via beta-TrCP and endo-lysosomal trafficking. *PLoS Pathog* **5**, e1000450

150. Douglas, J. L., Viswanathan, K., McCarroll, M. N., Gustin, J. K., Fruh, K., and Moses, A. V. (2009) Vpu directs the degradation of the human immunodeficiency virus restriction factor BST-2/Tetherin via a {beta}TrCP-dependent mechanism. *J Virol* **83**, 7931-7947

151. Tokarev, A. A., Munguia, J., and Guatelli, J. C. (2011) Serine-threonine ubiquitination mediates downregulation of BST-2/tetherin and relief of restricted virion release by HIV-1 Vpu. *J Virol* **85**, 51-63

152. Janvier, K., Pelchen-Matthews, A., Renaud, J. B., Caillet, M., Marsh, M., and Berlioz-Torrent, C. (2011) The ESCRT-0 component HRS is required for HIV-1 Vpu-mediated BST-2/tetherin down-regulation. *PLoS Pathog* **7**, e1001265

153. Mangeat, B., Gers-Huber, G., Lehmann, M., Zufferey, M., Luban, J., and Piguet, V. (2009) HIV-1 Vpu neutralizes the antiviral factor Tetherin/BST-2 by binding it and directing its beta-TrCP2-dependent degradation. *PLoS Pathog* **5**, e1000574

154. Miyagi, E., Andrew, A. J., Kao, S., and Strebel, K. (2009) Vpu enhances HIV-1 virus release in the absence of Bst-2 cell surface down-modulation and intracellular depletion. *Proc Natl Acad Sci U S A* **106**, 2868-2873

155. McNatt, M. W., Zang, T., and Bieniasz, P. D. (2013) Vpu Binds Directly to Tetherin and Displaces It from Nascent Virions. *PLoS Pathog* **9**, e1003299

156. Jafari, M., Guatelli, J., and Lewinski, M. K. (2014) Activities of Transmitted/Founder and Chronic Clade B HIV-1 Vpu and a C-terminal Polymorphism Specifically Affecting Virion Release. *J Virol*

157. Rollason, R., Korolchuk, V., Hamilton, C., Schu, P., and Banting, G. (2007) Clathrin-mediated endocytosis of a lipid-raft-associated protein is mediated through a dual tyrosine motif. *Journal of cell science* **120**, 3850-3858

158. Rollason, R., Korolchuk, V., Hamilton, C., Jepson, M., and Banting, G. (2009) A CD317/tetherin-RICH2 complex plays a critical role in the organization of the subapical actin cytoskeleton in polarized epithelial cells. *J Cell Biol* **184**, 721-736

159. Nydegger, S., Khurana, S., Krementsov, D. N., Foti, M., and Thali, M. (2006) Mapping of tetraspanin-enriched microdomains that can function as gateways for HIV-1. *J Cell Biol* **173**, 795-807

160. Thali, M. (2011) Tetraspanin functions during HIV-1 and influenza virus replication. *Biochemical Society transactions* **39**, 529-531

161. Krementsov, D. N., Rassam, P., Margeat, E., Roy, N. H., Schneider-Schaulies, J., Milhiet, P. E., and Thali, M. (2010) HIV-1 assembly differentially alters dynamics and partitioning of tetraspanins and raft components. *Traffic* **11**, 1401-1414

162. Klimkait, T., Strebel, K., Hoggan, M. D., Martin, M. A., and Orenstein, J. M. (1990) The human immunodeficiency virus type 1-specific protein vpu is required for efficient virus maturation and release. *J Virol* **64**, 621-629

163. Schubert, U., Bour, S., Ferrer-Montiel, A. V., Montal, M., Maldarell, F., and Strebel, K. (1996) The two biological activities of human immunodeficiency virus type 1 Vpu protein involve two separable structural domains. *J Virol* **70**, 809-819

164. Tokarev, A., Suarez, M., Kwan, W., Fitzpatrick, K., Singh, R., and Guatelli, J. (2013) Stimulation of NF-kappaB activity by the HIV restriction factor BST2. *J Virol* **87**, 2046-2057

165. Deng, H., Liu, R., Ellmeier, W., Choe, S., Unutmaz, D., Burkhart, M., Di Marzio, P., Marmon, S., Sutton, R. E., Hill, C. M., Davis, C. B., Peiper, S. C., Schall, T. J., Littman, D. R., and Landau, N. R. (1996) Identification of a major co-receptor for primary isolates of HIV-1. *Nature* **381**, 661-666

166. Morgenstern, J. P., and Land, H. (1990) Advanced mammalian gene transfer: high titre retroviral vectors with multiple drug selection markers and a complementary helper-free packaging cell line. *Nucleic Acids Res* **18**, 3587-3596

167. Charneau, P., Mirambeau, G., Roux, P., Paulous, S., Buc, H., and Clavel, F. (1994) HIV-1 reverse transcription. A termination step at the center of the genome. *J Mol Biol* **241**, 651-662

168. Tokarev, A., Suarez, M., Kwan, W., Fitzpatrick, K., Singh, R., and Guatelli, J. (2012) STIMULATION OF NF-kappaB ACTIVITY BY THE HIV RESTRICTION FACTOR BST2. *J Virol*

169. Ma, C., Marassi, F. M., Jones, D. H., Straus, S. K., Bour, S., Strebel, K., Schubert, U., Oblatt-Montal, M., Montal, M., and Opella, S. J. (2002) Expression, purification, and activities of full-length and truncated versions of the integral membrane protein Vpu from HIV-1. *Protein Sci* **11**, 546-557

170. Delaglio, F., Grzesiek, S., Vuister, G. W., Zhu, G., Pfeifer, J., and Bax, A. (1995) NMRPipe: a multidimensional spectral processing system based on UNIX pipes. *Journal of biomolecular NMR* **6**, 277-293

171. Homann, S., Smith, D., Little, S., Richman, D., and Guatelli, J. (2011) Upregulation of BST-2/Tetherin by HIV infection in vivo. *J Virol* **85**, 10659-10668

172. Perez-Caballero, D., Zang, T., Ebrahimi, A., McNatt, M. W., Gregory, D. A., Johnson, M. C., and Bieniasz, P. D. (2009) Tetherin inhibits HIV-1 release by directly tethering virions to cells. *Cell* **139**, 499-511

173. Kuhl, A., Banning, C., Marzi, A., Votteler, J., Steffen, I., Bertram, S., Glowacka, I., Konrad, A., Sturzl, M., Guo, J. T., Schubert, U., Feldmann, H., Behrens, G., Schindler, M., and Pohlmann, S. (2011) The Ebola virus glycoprotein and HIV-1 Vpu employ different strategies to counteract the antiviral factor tetherin. *J Infect Dis* **204 Suppl 3**, S850-860

174. Lau, D., Kwan, W., and Guatelli, J. (2011) Role of the endocytic pathway in the counteraction of BST-2 by human lentiviral pathogens. *J Virol* **85**, 9834-9846

175. Dube, M., Roy, B. B., Guiot-Guillain, P., Mercier, J., Binette, J., Leung, G., and Cohen, E. A. (2009) Suppression of Tetherin-restricting activity upon human immunodeficiency virus type 1 particle release correlates with localization of Vpu in the trans-Golgi network. *J Virol* **83**, 4574-4590

176. Hauser, H., Lopez, L. A., Yang, S. J., Oldenburg, J. E., Exline, C. M., Guatelli, J. C., and Cannon, P. M. (2011) HIV-1 Vpu and HIV-2 Env counteract BST-2/tetherin by sequestration in a perinuclear compartment. *Retrovirology* **8**, 85

177. Petit, S. J., Blondeau, C., and Towers, G. J. (2011) Analysis of the human immunodeficiency virus type 1 M group Vpu domains involved in antagonizing tetherin. *J Gen Virol* **92**, 2937-2948

178. Bour, S., Perrin, C., and Strebel, K. (1999) Cell surface CD4 inhibits HIV-1 particle release by interfering with Vpu activity. *J Biol Chem* **274**, 33800-33806

179. Billcliff, P. G., Rollason, R., Prior, I., Owen, D. M., Gaus, K., and Banting, G. (2013) CD317/tetherin is an organiser of membrane microdomains. *Journal of cell science* **126**, 1553-1564

180. Wittlich, M., Koenig, B. W., Stoldt, M., Schmidt, H., and Willbold, D. (2009) NMR structural characterization of HIV-1 virus protein U cytoplasmic domain in the presence of dodecylphosphatidylcholine micelles. *FEBS J* **276**, 6560-6575

181. Jia, X., Weber, E., Tokarev, A., Lewinski, M., Rizk, M., Suarez, M., Guatelli, J., and Xiong, Y. (2014) Structural basis of HIV-1 Vpu-mediated BST2 antagonism via hijacking of the clathrin adaptor protein complex 1. *Elife* **3**, e02362

182. Kobayashi, T., Ode, H., Yoshida, T., Sato, K., Gee, P., Yamamoto, S. P., Ebina, H., Strebel, K., Sato, H., and Koyanagi, Y. (2011) Identification of amino acids in the

human tetherin transmembrane domain responsible for HIV-1 Vpu interaction and susceptibility. *J Virol* **85**, 932-945

183. Vigan, R., and Neil, S. J. (2010) Determinants of tetherin antagonism in the transmembrane domain of the human immunodeficiency virus type 1 Vpu protein. *J Virol* **84**, 12958-12970

184. Bakolitsa, C., de Pereda, J. M., Bagshaw, C. R., Critchley, D. R., and Liddington, R. C. (1999) Crystal structure of the vinculin tail suggests a pathway for activation. *Cell* **99**, 603-613

185. Campos, B., Mo, Y. D., Mealy, T. R., Li, C. W., Swairjo, M. A., Balch, C., Head, J. F., Retzinger, G., Dedman, J. R., and Seaton, B. A. (1998) Mutational and crystallographic analyses of interfacial residues in annexin V suggest direct interactions with phospholipid membrane components. *Biochemistry* **37**, 8004-8010

186. Lanier, L. L. (2008) Evolutionary struggles between NK cells and viruses. *Nature Reviews Immunology* **8**, 259-268

187. Moretta, A., Bottino, C., Vitale, M., Pende, D., Cantoni, C., Mingari, M. C., Biassoni, R., and Moretta, L. (2001) Activating receptors and coreceptors involved in human natural killer cell-mediated cytolysis. *Annual review of immunology* **19**, 197-223

188. Bryceson, Y. T., March, M. E., Ljunggren, H. G., and Long, E. O. (2006) Activation, coactivation, and costimulation of resting human natural killer cells. *Immunological reviews* **214**, 73-91

189. Lanier, L. L. (2008) Up on the tightrope: natural killer cell activation and inhibition. *Nature immunology* **9**, 495-502

190. Borrego, F., Kabat, J., Kim, D.-K., Lieto, L., Maasho, K., Peña, J., Solana, R., and Coligan, J. E. (2002) Structure and function of major histocompatibility complex (MHC) class I specific receptors expressed on human natural killer (NK) cells. *Molecular immunology* **38**, 637-660

191. Bottino, C., Falco, M., Parolini, S., Marcenaro, E., Augugliaro, R., Sivori, S., Landi, E., Biassoni, R., Notarangelo, L. D., and Moretta, L. (2001) Gntb-A, a Novel Sh2d1a-Associated Surface Molecule Contributing to the Inability of Natural Killer Cells to Kill Epstein-Barr Virus–Infected B Cells in X-Linked Lymphoproliferative Disease. *The Journal of experimental medicine* **194**, 235-246

192. Flaig, R. M., Stark, S., and Watzl, C. (2004) Cutting edge: NTB-A activates NK cells via homophilic interaction. *The Journal of Immunology* **172**, 6524-6527

193. Falco, M., Marcenaro, E., Romeo, E., Bellora, F., Marras, D., Vély, F., Ferracci, G., Moretta, L., Moretta, A., and Bottino, C. (2004) Homophilic interaction of NTBA, a member of the CD2 molecular family: induction of cytotoxicity and cytokine release in human NK cells. *European journal of immunology* **34**, 1663-1672

194. Cao, E., Ramagopal, U. A., Fedorov, A., Fedorov, E., Yan, Q., Lary, J. W., Cole, J. L., Nathenson, S. G., and Almo, S. C. (2006) NTB-A receptor crystal structure: insights into homophilic interactions in the signaling lymphocytic activation molecule receptor family. *Immunity* **25**, 559-570

195. Cohen, G. B., Gandhi, R. T., Davis, D. M., Mandelboim, O., Chen, B. K., Strominger, J. L., and Baltimore, D. (1999) The selective downregulation of class I major histocompatibility complex proteins by HIV-1 protects HIV-infected cells from NK cells. *Immunity* **10**, 661-671